

**ROBUST CONTROLLER DESIGN FOR VOLTAGE SOURCE INVERTERS IN
MICROGRIDS**

BY

SYED ASIM HUSSAIN

A Dissertation Presented to the
DEANSHIP OF GRADUATE STUDIES

KING FAHD UNIVERSITY OF PETROLEUM & MINERALS

DHAHRAN, SAUDI ARABIA

In Partial Fulfillment of the
Requirements for the Degree of

DOCTOR OF PHILOSOPHY

In

ELECTRICAL ENGINEERING

May 2015

KING FAHD UNIVERSITY OF PETROLEUM & MINERALS

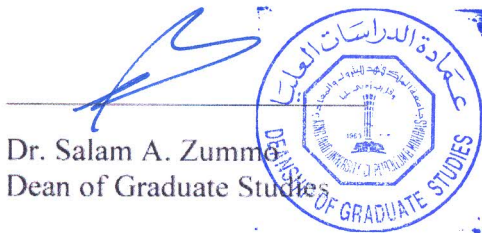
DHAHRAN- 31261, SAUDI ARABIA

DEANSHIP OF GRADUATE STUDIES

This thesis, written by Syed Asim Hussain under the direction his thesis advisor and approved by his thesis committee, has been presented and accepted by the Dean of Graduate Studies, in partial fulfillment of the requirements for the degree of **DOCTOR OF PHILOSOPHY IN ELECTRICAL ENGINEERING.**



Dr. Ali Ahmed Al-Shaikhi
Department Chairman



Dr. Salam A. Zummeh
Dean of Graduate Studies

19/1/15
Date



Dr. Mohammad Ali Abido
(Advisor)



Dr. Ibrahim Mohamed ElAmin
(Member)



Dr. Ralph Kennel
(Member)



Dr. Ibrahim Omar Habiballah
(Member)



Dr. Salim Ibrir
(Member)

© Syed Asim Hussain

2015

Dedicated to my father *Professor Syed Rafat Husain*

ACKNOWLEDGMENTS

بِسْمِ اللَّهِ الرَّحْمَنِ الرَّحِيمِ

In the name of Allah, the Beneficent, the Merciful.

Praise be to Allah the almighty who has given me the strength to complete this thesis.

Without His support this thesis was not possible.

Supplications and blessings be upon the beloved Prophet Muhammad (Peace be upon Him), who is the teacher of whole mankind.

I would like to express my gratitude towards my advisor Dr. Abido whose mentorship has always guided us in the right path and who has helped us stand up back on our feet whenever we fell. The work in this thesis was not possible without him.

I would also like to thank my parents, who made me whatever I am today, my wife for her full support during all these years, my son Aneeq who has come as a blessing in my life and my brothers and my sister for their encouragement and affection.

I am also grateful to my friends, Dr. Uneb Gazdar, Saad Khan, Saad Sadiq, Danish Ahmed, Usama Siddiqui, Shoieb Arshad, Humayun Kathuria, Zahid Saleem and Dr. Haris Khalid who helped me in every possible way.

I am also very thankful to all my professors who taught me during this program, especially Dr. Magdi Mahmoud and Dr. Sami Elferik.

TABLE OF CONTENTS

ACKNOWLEDGMENTS	IV
TABLE OF CONTENTS	V
LIST OF TABLES	X
LIST OF FIGURES	XI
LIST OF ABBREVIATIONS	XVI
NOMENCLATURE	XVII
ABSTRACT	XX
ARABIC ABSTRACT	XXII
CHAPTER 1 INTRODUCTION	1
1.1 Thesis motivation	1
1.2 Problem statement	3
1.3 Thesis objectives	3
1.4 Outline of the contributions	4
1.5 Thesis organization	4
CHAPTER 2 LITERATURE REVIEW	6
2.1 Voltage source inverters (VSIs)	6
2.1.1 Definition	6
2.1.2 Applications	7
2.1.3 Recent research areas related to VSIs	7

2.2	Control of voltage source inverters	8
2.3	Robust control for voltage Source Inverters.....	11
2.4	Proposed work in comparison to the literature.....	15
CHAPTER 3 STANDALONE VSI: MODELING AND CONTROL DESIGN		18
3.1	Preliminaries.....	18
3.2	Derivation of mathematical model of the standalone system.....	19
3.3	Controller Design for the standalone system	21
3.3.1	Controller for robust stabilization	23
3.3.2	Robust stability analysis and limits of parameter variations	28
3.3.3	Analysis of the derived theorems.....	31
3.3.4	Integral control for set-point tracking	32
3.4	Conclusion	34
CHAPTER 4 GRID-CONNECTED VSI: MODELING AND CONTROL DESIGN		36
4.1	Derivation of mathematical model of the grid connected system	36
4.2	Controller Design for the grid-connected system	38
4.2.1	Controller for robust stabilization	40
4.2.2	Robust stability analysis and limits of parameter variations	45
4.2.3	Integral control for set-point tracking	47
4.3	Conclusion	50
CHAPTER 5 CONTROLLER OPTIMIZATION ALGORITHMS		52
5.1	Differential Evolution.....	52

5.1.1 Initialization	53
5.1.2 Cost evaluation and search for best solution	53
5.1.3 Mutation.....	54
5.1.4 Crossover	54
5.1.5 Selection	55
5.1.6 Termination and its Criterion	55
5.2 Control design algorithms for standalone system	55
5.2.1 Phase I: Initialization.....	57
5.2.2 Phase II: The IRSD algorithm	57
5.2.3 Phase III: The IRTD algorithm	59
5.3 Control design algorithms for grid-connected system	61
5.3.1 Phase I: Initialization.....	63
5.3.2 Phase II: The IRSD algorithm	63
5.3.3 Phase III: The IRTD algorithm	65
5.4 Conclusion	67
CHAPTER 6 PROPOSED CONTROLLER IMPLEMENTATION	68
6.1 MATLAB Implementations	68
6.1.1 Implementation of algorithms	68
6.1.2 Implementation of the standalone system	69
6.1.3 Implementation of the grid-connected system	77
6.2 RTDS plus DS1103 Implementation	84

6.2.1 Schematics of standalone VSI system in RSCAD	86
6.2.2 Schematics of grid-connected VSI system in RSCAD	89
6.2.3 Schematics of controller for standalone and grid-connected VSI on DS1103 controller board	92
CHAPTER 7 RESULTS AND ANALYSIS: STANDALONE VSI	95
7.1 Results of the algorithms	95
7.1.1 IRSD results	95
7.1.2 IRTD results	98
7.2 Simulation results	99
7.3 Experimental results	105
7.4 Comparison of Simulation and Experimental Results	109
7.5 Performance comparison of the proposed controller to existing methods in literature	111
7.5.1 Comparison of transient behavior	111
7.5.2 Steady-state performance	114
7.6 Conclusion	115
CHAPTER 8 RESULTS AND ANALYSIS: GRID-CONNECTED VSI	116
8.1 Results of the algorithms	116
8.1.1 IRSD results	116
8.1.2 IRTD results	119
8.2 Simulation results	119
8.3 Experimental results	128
8.4 Comparison of Simulation and Experimental Results	134

8.5	Performance comparison of the proposed controller to existing methods in literature	136
8.5.1	Comparison of transient behavior.....	136
8.5.2	Comparison of steady-state performance	139
8.6	Conclusion	141
CHAPTER 9 CONCLUSIONS AND FUTURE WORK.....		142
9.1	Standalone VSI: Conclusions	142
9.2	Grid-connected VSI: Conclusions.....	144
9.3	Future Work.....	146
APPENDIX DSPACE DS1103 CONTROLLER BOARD: UTILITY AND APPLICATIONS		148
1.	Prominent features.....	148
2.	Major applications	149
3.	Input/output interfaces	149
4.	Controller programming with RTI Simulink blocks library.	150
REFERENCES.....		152
VITAE.....		160

LIST OF TABLES

TABLE 2-1: PROS AND CONS OF SOME COMMONLY APPLIED CONTROL METHODS OVER THE VSIS.	10
TABLE 2-2: SOME STATE-OF-THE-ART ROBUST CONTROL METHODS.....	14
TABLE 3-1: A MATRICES FOR ALL UNCERTAINTY EXTREMA COMBINATIONS.....	34
TABLE 4-1: A MATRICES FOR ALL UNCERTAINTY EXTREMA COMBINATIONS.....	49
TABLE 7-1: SYSTEM CONSTANTS FOR STANDALONE VSI.	96
TABLE 7-2: DE PARAMETERS OF IRSD ALGORITHM FOR STANDALONE MODE.	96
TABLE 7-3: RESULTS OF IRSD ALGORITHM FOR STANDALONE CASE.	97
TABLE 7-4: DE PARAMETERS AND RESULTS OF IRTD ALGORITHM FOR STANDALONE MODE.....	98
TABLE 7-5: SIMULATION AND EXPERIMENTAL TESTS VARIATIONS.	100
TABLE 7-6: COMPARISON OF STEADY-STATE PERFORMANCE OF THE PROPOSED CONTROLLER WITH [48].	115
TABLE 8-1: SYSTEM CONSTANTS FOR GRID-CONNECTED VSI.	117
TABLE 8-2: DE PARAMETERS OF IRSD ALGORITHM FOR GRID-CONNECTED MODE.	117
TABLE 8-3: RESULTS OF IRSD ALGORITHM FOR GRID-CONNECTED CASE.....	118
TABLE 8-4: DE PARAMETERS AND RESULTS OF IRTD ALGORITHM FOR GRID-CONNECTED MODE.	120
TABLE 8-5: SIMULATION AND EXPERIMENTAL TESTS VARIATIONS.	121
TABLE 8-6: THD VALUES OF THE H^∞ CONTROLLER IN REFERENCE [30] AND THE PROPOSED CONTROLLER.	140

LIST OF FIGURES

FIGURE 3.1 THREE PHASE VOLTAGE SOURCE INVERTER WITH OUTPUT LC FILTER FOR STANDALONE OPERATION.....	20
FIGURE 4.1 THE GRID CONNECTED VSI PLUS LC FILTER SYSTEM.	36
FIGURE 5.1 OVERALL CONTROL DESIGN ALGORITHM FOR STANDALONE SYSTEM.....	56
FIGURE 5.2 INITIALIZATION OF CONTROL DESIGN ALGORITHM FOR STANDALONE CASE.	57
FIGURE 5.3 IRSD ALGORITHM FOR STANDALONE CASE.....	58
FIGURE 5.4 IRTD ALGORITHM FOR STANDALONE CASE.....	60
FIGURE 5.5 OVERALL CONTROL DESIGN ALGORITHM FOR GRID-CONNECTED SYSTEM.....	62
FIGURE 5.6 INITIALIZATION OF CONTROL DESIGN ALGORITHM FOR GRID-CONNECTED CASE.	63
FIGURE 5.7 IRSD ALGORITHM FOR GRID-CONNECTED CASE.....	64
FIGURE 5.8 IRTD ALGORITHM FOR GRID-CONNECTED CASE.....	66
FIGURE 6.1 SCHEMATIC OF THE STANDALONE VSI SYSTEM WITH PROPOSED CONTROLLER.	70
FIGURE 6.2 MATLAB IMPLEMENTATION OF STANDALONE VSI SYSTEM.....	73
FIGURE 6.3 STANDALONE VSI: SCHEMATIC OF SUBSYSTEM 'ALL MEASUREMENTS.'	74
FIGURE 6.4 STANDALONE VSI: SCHEMATIC OF SUBSYSTEM 'ROBUST CONTROLLER.'	75
FIGURE 6.5 STANDALONE VSI: SCHEMATIC OF SIMULINK FILE FOR IRTD ALGORITHM.	76
FIGURE 6.6 CONTROLLER IMPLEMENTATION FOR GRID CONNECTED VSI.....	78
FIGURE 6.7 GRID-CONNECTED VSI: THE 'P TO I' SUBSYSTEM	79
FIGURE 6.8 MATLAB IMPLEMENTATION OF GRID-CONNECTED VSI SYSTEM.....	80
FIGURE 6.9 GRID-CONNECTED VSI: SCHEMATIC OF SUBSYSTEM 'ALL MEASUREMENTS.'	81
FIGURE 6.10 GRID-CONNECTED VSI: SCHEMATIC OF SUBSYSTEM ROBUST CONTROLLER.'	82

FIGURE 6.11 GRID-CONNECTED VSI: SCHEMATIC OF SIMULINK FILE FOR IRTD ALGORITHM.	83
FIGURE 6.12 HARDWARE ARRANGEMENT.	84
FIGURE 6.13 INTERCONNECTION OF HARDWARE COMPONENTS.	85
FIGURE 6.14 STANDALONE VSI: LARGE-TIME-STEP SCHEMATIC IN RSCAD.	87
FIGURE 6.15 STANDALONE VSI: SMALL-TIME-STEP SCHEMATIC IN RSCAD.	88
FIGURE 6.16 GRID-CONNECTED VSI: LARGE-TIME-STEP SCHEMATIC IN RSCAD	90
FIGURE 6.17 GRID-CONNECTED VSI: SMALL-TIME-STEP SCHEMATIC IN RSCAD.	91
FIGURE 6.18 STANDALONE VSI: CONTROLLER SCHEMATIC FOR DS1103.	93
FIGURE 6.19 GRID-CONNECTED VSI: CONTROLLER SCHEMATIC FOR DS1103.	94
FIGURE 7.1 COST MINIMIZATION IN STANDALONE IRSD ALGORITHM.	97
FIGURE 7.2 COST FUNCTION PLOT OF IRTD ALGORITHM FOR STANDALONE MODE.	99
FIGURE 7.3 STANDALONE VSI: OUTPUT/LOAD VOLTAGE IN ROBUSTNESS TEST SIMULATION.	102
FIGURE 7.4 STANDALONE VSI: OUTPUT/LOAD CURRENT IN ROBUSTNESS TEST SIMULATION.	102
FIGURE 7.5 STANDALONE VSI: OUTPUT/LOAD VOLTAGE IN DISTURBANCE TEST SIMULATION.	103
FIGURE 7.6 STANDALONE VSI: OUTPUT/LOAD CURRENT IN DISTURBANCE TEST SIMULATION.	103
FIGURE 7.7 STANDALONE VSI: OUTPUT/LOAD VOLTAGE IN TRACKING PERFORMANCE TEST SIMULATION.	104
FIGURE 7.8 STANDALONE VSI: OUTPUT/LOAD CURRENT IN TRACKING PERFORMANCE TEST SIMULATION.	104
FIGURE 7.9 STANDALONE VSI: OUTPUT/LOAD VOLTAGE IN ROBUSTNESS TEST EXPERIMENT.	106
FIGURE 7.10 STANDALONE VSI: OUTPUT/LOAD CURRENT IN ROBUSTNESS TEST EXPERIMENT.	106
FIGURE 7.11 STANDALONE VSI: OUTPUT/LOAD VOLTAGE IN DISTURBANCE TEST EXPERIMENT.	107

FIGURE 7.12 STANDALONE VSI: OUTPUT/LOAD CURRENT IN DISTURBANCE TEST EXPERIMENT.....	107
FIGURE 7.13 STANDALONE VSI: OUTPUT/LOAD VOLTAGE IN TRACKING PERFORMANCE TEST EXPERIMENT.	108
FIGURE 7.14 STANDALONE VSI: OUTPUT/LOAD CURRENT IN TRACKING PERFORMANCE TEST EXPERIMENT.	109
FIGURE 7.15 ROBUSTNESS TEST: COMPARISON OF OUTPUT VOLTAGE IN SIMULATIONS AND EXPERIMENTS.	110
FIGURE 7.16 DISTURBANCE TEST: COMPARISON OF OUTPUT VOLTAGE IN SIMULATIONS AND EXPERIMENTS.....	110
FIGURE 7.17 TRACKING PERFORMANCE TEST: COMPARISON OF OUTPUT VOLTAGE IN SIMULATIONS AND EXPERIMENTS.....	111
FIGURE 7.18 ON-LOAD RESPONSE OF THE CONTROLLER IN [48]. THE VOLTAGE AND CURRENT WAVEFORMS.....	112
FIGURE 7.19 ON-LOAD PERFORMANCE OF THE PROPOSED CONTROLLER.	113
FIGURE 7.20 OFF-LOAD RESPONSE OF THE CONTROLLER IN [48]. THE VOLTAGE AND CURRENT WAVEFORMS.....	113
FIGURE 7.21 OFF-LOAD PERFORMANCE OF THE PROPOSED CONTROLLER.....	114
FIGURE 8.1 COST MINIMIZATION IN GRID-CONNECTED IRSD ALGORITHM.	118
FIGURE 8.2 COST FUNCTION PLOT OF IRTD ALGORITHM FOR GRID-CONNECTED MODE.	120
FIGURE 8.3 GRID-CONNECTED VSI: OUTPUT REAL AND REACTIVE POWER IN ROBUSTNESS TEST SIMULATION.	123
FIGURE 8.4 GRID-CONNECTED VSI: OUTPUT/LOAD CURRENT IN ROBUSTNESS TEST SIMULATION.....	123

FIGURE 8.5 GRID-CONNECTED VSI: CAPACITOR VOLTAGE IN ROBUSTNESS TEST SIMULATION.	124
FIGURE 8.6 GRID-CONNECTED VSI: OUTPUT REAL AND REACTIVE POWER IN DISTURBANCE TEST SIMULATION.	124
FIGURE 8.7 GRID-CONNECTED VSI: OUTPUT/LOAD CURRENT IN DISTURBANCE TEST SIMULATION.	125
FIGURE 8.8 GRID-CONNECTED VSI: CAPACITOR VOLTAGE IN DISTURBANCE TEST SIMULATION.....	125
FIGURE 8.9 GRID-CONNECTED VSI: OUTPUT REAL AND REACTIVE POWER IN TRACKING PERFORMANCE TEST SIMULATION.	126
FIGURE 8.10 GRID-CONNECTED VSI: OUTPUT/LOAD CURRENT IN TRACKING PERFORMANCE TEST SIMULATION.	127
FIGURE 8.11 GRID-CONNECTED VSI: CAPACITOR VOLTAGE IN DISTURBANCE TEST SIMULATION.....	127
FIGURE 8.12 GRID-CONNECTED VSI: OUTPUT REAL AND REACTIVE POWER IN ROBUSTNESS TEST EXPERIMENT.	128
FIGURE 8.13 GRID-CONNECTED VSI: OUTPUT/LOAD CURRENT IN ROBUSTNESS TEST EXPERIMENT.....	129
FIGURE 8.14 GRID-CONNECTED VSI: CAPACITOR VOLTAGE IN ROBUSTNESS TEST EXPERIMENT.....	129
FIGURE 8.15 GRID-CONNECTED VSI: OUTPUT REAL AND REACTIVE POWER IN DISTURBANCE TEST EXPERIMENT.	130
FIGURE 8.16 GRID-CONNECTED VSI: OUTPUT/LOAD CURRENT IN DISTURBANCE TEST EXPERIMENT. ..	131
FIGURE 8.17 GRID-CONNECTED VSI: CAPACITOR VOLTAGE IN DISTURBANCE TEST EXPERIMENT.....	131
FIGURE 8.18 GRID-CONNECTED VSI: OUTPUT REAL AND REACTIVE POWER IN TRACKING PERFORMANCE TEST EXPERIMENT.	132
FIGURE 8.19 GRID-CONNECTED VSI: OUTPUT/LOAD CURRENT IN TRACKING PERFORMANCE TEST EXPERIMENT.	133

FIGURE 8.20 GRID-CONNECTED VSI: CAPACITOR VOLTAGE IN TRACKING PERFORMANCE TEST	
EXPERIMENT.	133
FIGURE 8.21 ROBUSTNESS TEST: COMPARISON OF OUTPUT VOLTAGE IN SIMULATIONS AND EXPERIMENTS.	
.....	134
FIGURE 8.22 DISTURBANCE TEST: COMPARISON OF OUTPUT VOLTAGE IN SIMULATIONS AND	
EXPERIMENTS.	135
FIGURE 8.23 TRACKING PERFORMANCE TEST: COMPARISON OF OUTPUT VOLTAGE IN SIMULATIONS AND	
EXPERIMENTS.	135
FIGURE 8.24 TRANSIENT PERFORMANCE OF THE CONTROLLER PROPOSED IN [30].	136
FIGURE 8.25 SIMULATION RESULTS OF THE PROPOSED CONTROLLER FOR GRID-CONNECTED VSI, WHEN	
r_g, l_g CHANGE FROM $[0.2\Omega, 0.1\mu H]$ TO $[0.4\Omega, 10\mu H]$	137
FIGURE 8.26 TRANSIENT PERFORMANCE OF THE PROPOSED CONTROLLER WHEN l_g IS CHANGED FROM	
0.05 mH TO 0.3 mH	138
FIGURE 1 RTI SIMULINK LIBRARY.	150
FIGURE 2 VIEW OF THE RTI MASTER PPC LIBRARY.	151

LIST OF ABBREVIATIONS

CLF	:	Control Lyapunov Function
DE	:	Differential Evolution
DG	:	Distributed Generation
DPC	:	Direct Power Control
IRSD	:	Intelligent Robust Stabilizer Design
IRTD	:	Intelligent Robust Tracker Design
LMI	:	Linear Matrix Inequality
MPC	:	Model Predictive Control
MRC	:	Multi Resonant Control
PI	:	Proportional Integral
PR	:	Proportional Resonant
PWM	:	Pulse Width Modulation
RTDS	:	Real Time Digital Simulator
SVM	:	Space Vector Modulation
SF	:	State Feedback
THD	:	Total Harmonic Distortion
VSC	:	Voltage Source Converter

VSI : Voltage Source Inverter

NOMENCLATURE

x_{abc} : A balanced three phase sinusoidal function with components x_a, x_b, x_c

\vec{x} : Space phasor of x_{abc}

x_p : Amplitude of x_{abc}

ω' : Time varying frequency of x_{abc} (rad/s)

ω : Constant frequency of x_{abc} (rad/s)

θ : Initial phase angle of x_{abc} (rad)

ρ : Angle of the dq rotating reference frame (rad)

v_d : d -axis component of the three phase inverter output voltage (V)

v_q : q -axis component of the three phase inverter output voltage (V)

i_d : d -axis component of the three phase inverter output current (A)

i_q : q -axis component of the three phase inverter output current (A)

v_{cd} : d -axis component of the three phase filter capacitor voltage (V)

v_{cq} : q -axis component of the three phase filter capacitor voltage (V)

i_{ld} : d -axis component of the three phase load current (A)

i_{lq} : q -axis component of the three phase load current (A)

\vec{v}	:	Space phasor of three phase inverter output voltage \mathbf{v}_{abc} (V)
\vec{i}	:	Space phasor of three phase inverter output current \mathbf{i}_{abc} (A)
\vec{v}_c	:	Space phasor of three phase filter capacitor voltage \mathbf{v}_{cab} (V)
\vec{i}_c	:	Space phasor of three phase filter capacitor current \mathbf{i}_{cab} (A)
\vec{i}_l	:	Space phasor of three phase load current \mathbf{i}_{lab} (A)
L_f	:	Inductance in the LC filter (H)
C_f	:	Capacitance in the LC filter (F)
R	:	Total load resistance (Ω)
L	:	Total load inductance (H)
R_0	:	Nominal load resistance (Ω)
L_0	:	Nominal load inductance (H)
ΔR	:	Uncertainty in load resistance (Ω)
ΔL	:	Uncertainty in load inductance (H)
λ_R	:	Magnitude upper bound of load/line resistance uncertainty (Ω)
λ_L	:	Magnitude upper bound of load/line inductance uncertainty (H)
\mathbf{K}	:	Robust stabilizing controller gain
\mathbf{L}	:	Observer gain

h	:	Convergence rate of closed loop system
$\bar{\lambda}_R$:	Magnitude upper bound of load/line resistance uncertainty for guaranteed convergence rate h (Ω)
$\bar{\lambda}_L$:	Magnitude upper bound of load/line inductance uncertainty for guaranteed convergence rate h (H)
K_I	:	Integral controller gain
r_g	:	Total line resistance of the grid (Ω)
l_g	:	Total line inductance of the grid (H)
r_{g0}	:	Nominal line resistance (Ω)
l_{g0}	:	Nominal line inductance (H)
Δr_g	:	Uncertainty in line resistance (Ω)
Δl_g	:	Uncertainty in line inductance (H)
v_{gd}	:	d -axis component of the three phase grid voltage (V)
v_{gq}	:	q -axis component of the three phase grid voltage (V)
\vec{v}_g	:	Space phasor of three phase filter grid voltage \mathbf{v}_{gabc} (V)
J	:	Cost function used in optimization algorithms
V_{DC}	:	Voltage of the DC source (V)

ABSTRACT

Full Name : Syed Asim Hussain
Thesis Title : Robust Controller Design for Voltage Source Inverters in Microgrids
Major Field : Electrical Engineering
Date of Degree : May 2015

The renewable energy sources have gained a lot of interest in recent years to tackle the issue of rapidly increasing electricity demand, as the fossil fuel based plants continue to adversely affect the environment. Most popular of them, the solar and wind energy systems can provide electric power on a large scale and are environment friendly. Naturally the technological advancement of these renewable energy sources has been investigated with a lot of interest. An integral component of the power electronics system that interfaces a renewable energy source to the main power grid by converting DC to AC, is the voltage source inverter (VSI). A controller for the VSI is crucial to regulate its output voltage and/or output power. A lot of work exists in literature in this regard. Several issues relevant to the control design have been addressed including the problem of vulnerability of the system to parameter variation and uncertainty.

In this thesis work the issue of robust control design for VSIs is considered. VSIs are considered for applications in standalone and grid-connected modes of the microgrid. For the standalone case VSI is connected to an uncertain RL load. For the grid-connected case, the uncertainty is considered in the line impedance of the grid. New robust control design methods are developed using the condition of bounds on uncertainty radius of the system. Using Sylvester's criterion some relations are derived to determine the uncertainty coefficient matrices of the system. These relations also involved some tuning parameters

which can be optimized to achieve an improved robustness and stability tradeoff. The proposed methods for the standalone and grid-connected cases, result in controllers that robustly stabilize the VSI systems with guaranteed convergence rates for certain bounds of uncertainties. It is also required that the system output tracks the specified reference. For this integral controllers are augmented in the control law. Optimization schemes to design the integral controller gains and to test their robustness are also presented. The controller designed is implemented and tested on simulations and real-time hardware-in-the-loop experimental setup and its effectiveness is proven by the results. Also a comparison is performed to show the improvement in performance of the proposed method over some relevant works in the literature, in terms of deviations caused by a certain amount of uncertainties and the settling time.]

ملخص الرسالة

الاسم الكامل: سيد عاصم حسين

عنوان الرسالة: تصميم المتحكمات المتينة لقلابات مصدر الجهد في الشبكات الصغيرة

التخصص: الهندسة الكهربائية

تاريخ الدرجة العلمية: مايو/ 2015

اكتسبت مصادر الطاقة المتجددة كثيرا من الاهتمام في السنوات الأخيرة لمعالجة مسألة زيادة الطلب المتسارع على الكهرباء، وحيث أن المصانع تستند على الوقود الأحفوري فيستمر تأثيرها على البيئة بشكل عكسي. أكثر مصادر الطاقة المتجددة شهرة هي أنظمة الطاقة الشمسية وطاقة الرياح اللتان تستطيعان تزويد الطاقة الكهربائية على نطاق واسع وهما صديقتان للبيئة. وبطبيعة الحال فالتقدم التكنولوجي لمصادر الطاقة الطبيعية تم التحقق منها بكثير من الاهتمام. وأما مصادر الطاقة الطبيعية فيتم تكاملها مع شبكات الطاقة الرئيسية باستخدام الكترنيات القدرة والتي منها قلاب مصدر الجهد والمسمى اخصارا (VSI). يتم ذلك عن طريق تحويل فولتية الخرج لمصدر الطاقة الكهربائية ذات التيار الثابت (DC) الى تيار اخر متردد (AC). أما المتحكمات المستخدمة في هذا المجال فهي ذو أهمية كبيرة كونها تستخدم للمحافظة على خرج ثابت سواء كان للفولتية والقدرة معا أو احدهما. كثيرة هي الأعمال البحثية في هذا المجال، عديدة هي القضايا ذات الصلة والمتعلقة بتصميم المتحكمات والتي تم تناولها متضمنة مشكلة حساسية النظام لتغير قيم المعاملات وعدم التأكد منها.

في هذا العمل البحثي تم الاخذ بعين الاعتبار مشكلة تصميم المتحكمات المتينة لقلابات مصدر الجهد. تستخدم هذه القلابات في تطبيقات الشبكات الصغيرة سواء كانت قائمة بذاتها أو موصولة بالشبكة الكهربائية. ففي الشبكات القائمة بذاتها فان القلابات يتم وصلها بالاحمال غير التأكدية. وأما في حالة القلابات المتصلة بالشبكة فان عدم التأكدية تكون في قيم مقاومة خط الشبكة الكهربائية. تم تطوير طريقة تصميم جديدة للمتحكمات المتينة عندما تكون قيم النظام غير التأكدية تتغير في مدى معين. تم اشتقاق بعض العلاقات باستعمال معيار سلفستر (Sylvester's criterion) لتحديد مصفوفات العوامل غير التأكدية للنظام. تضمنت هذه العلاقات أيضا بعض معاملات الضبط والتي يمكن أن تحسن لتحقيق مزيد من المتانة والاستقرارية للنظام بشكل تفاضلي. فالطرق المقترحة لحالة الشبكة القائمة بذاتها أو تلك المتصلة بالشبكة الكهربائية تعطي متحكمات قادرة وبقوة على المحافظة على استقرارية أنظمة قلابات الجهد بمعدلات تقارب مضمونة لمدى معين من عدم التأكدية. كما هو مطلوب أيضا من خرج النظام أن يتبع مرجعيات محددة. تم اضافة المتحكمات المتكاملة على قانون التحكم. تم أيضا عرض

نظم التحسين لتصميم معاملات المتحكمات المتكاملة وفحص متانتها. تم بناء المتحكمات المصممة وفحصها باستخدام المحاكاة وباستخدام التجربة العملية للأجهزة العاملة في الزمن الحقيقي والمركبة على شكل حلقة والتي تم اثبات فعاليتها عن طريق النتائج المأخوذة. تم أيضا اجراء مقارنة لاطهار التحسن في الأداء للطريقة المقترحة مقارنة بالأعمال ذات الصلة في هذا المجال باستخدام قيم الانحرافات الناتجة عن قدر معين من عدم التأكدية وعن طريق زمن الاستقرار.

CHAPTER 1

INTRODUCTION

The demand of electric power is predicted to rise significantly in the near future. Having foreseen this challenge, advancement in the technology for efficient and environment friendly power generation has attained a great deal of interest in the recent years. Hence renewable energy sources and Microgrids are rapidly populating the modern power generation network [1],[2],[3], [4]. The work proposed here is on a specific topic in the domain of renewable energy, which is control system design for the voltage source inverter (VSI). VSI is the power electronics interface between renewable energy source or any distributed generation (DG) unit and the ac load or the main utility grid[5], [6]. In the subsections to follow the motivation behind working in this area is described. Also a discussion is presented on the current state of the technology in the area of VSI control design and applications.

1.1 Thesis motivation

The voltage source inverters (VSI) or the voltage source converters (VSC) have gained a lot of interest for its control design with an output filter. Being an integral part of power electronics system that enables the energy transfer from these sources to the utility grid, control and applications of VSIs is an important research area. VSIs convert the DC power output of the renewable energy source to AC. Due to the inherent fluctuation in the power generation of the renewable energy sources, their output electrical power is converted to

DC. In this way the electrical power can be stored in batteries or other energy storage units. To supply power to main utility grids, it is converted back to AC by using VSIs and thus it becomes possible to supply uninterrupted power from these sources to a load according to their capacity [7].

The VSI needs to be controlled for either its output voltage or its output power, which will be transferred to the main grid, depending on which mode of operation it is working in. There are two possible modes, the standalone mode and the grid-connected mode. In the standalone mode a reference tracking controller for the output voltage of the inverter is to be designed. While in the grid-connected mode the output voltage is dictated by the main grid, thus the power output of the inverter is controlled on the basis of demand and capacity[8]–[11].

A lot of literature exists for the control of VSIs [12]. Details of which are covered in the following section. The conventional methods, like the proportional resonant (PR) controller [13], [14], deadbeat predictive controller [15]–[21], active damping algorithm with LCL filter [22], [23] and feedback linearization [12], [24]–[27] have been extensively applied, but are reported to be vulnerable in systems with parameter variations. Therefore robust controller design methods have been proposed in literature to address this issue. A discussion of these methods is presented in section 2.3. The focus of the recent research on robust control design for VSIs has been on how to improve the performance and stability tradeoff [28]. Hence in this research work it is proposed to design an intelligently optimized robust controller for the VSI, which can provide improved performance for all the admissible uncertainties. A comparison with the literature will be shown to demonstrate the improved performance of the proposed controller.

1.2 Problem statement

Robust controller is to be designed for the VSI and filter system. The control objective will be to drive the VSI for application in both modes of operation of the micro-grid, standalone and grid-connected. In the standalone mode, the output voltage will be regulated. In the grid-connected mode the power injection to the main grid will be controlled by regulating the output current at the required reference levels. The controller should be designed such that it enables the system to be less sensitive to system uncertainties. The efficiency of the designed controllers will be verified by showing improvement in contrast to other existing related works. To verify the performance of the proposed controllers, simulations and experimental work will be carried out. MATLAB/SIMULINK will be used for the simulation work. Real-time hardware-in-the-loop (RTHIL) experimental setup based on RTDS and dSPACE DS1103 board, will be used for the experimental results.

1.3 Thesis objectives

Now the objectives of this thesis are listed.

- 1- To develop a novel control methodology for robust controller design of VSI in autonomous and grid connected modes.
- 2- To design new algorithms based on heuristic methods to optimize the robust controller by enhancing the system performance for a certain range of uncertainties.
- 3- To perform simulations in MATLAB with the proposed controller to determine its effectiveness.
- 4- To perform RTHIL experimental tests using RTDS and DS1103 controller board, with the proposed controller to determine its effectiveness.

- 5- To analyze the improvement in the performance of the system in comparison to existing methods.

1.4 Outline of the contributions

The major contributions of this thesis are listed as following:

- 1- Development of a novel optimized robust control design strategy for VSI applications in standalone and grid connected modes that provides enhanced performance of the system in presence of uncertainties.
- 2- Development of a new efficient and systematic scheme to apply any robust control design theory for linear systems with norm-bounded time varying uncertainties, for the control of standalone and grid-connected VSIs.
- 3- Development of a new systematic way to design robust controller with guaranteed convergence rate for a certain uncertainty range.
- 4- Simulation work in MATLAB/SIMULINK, to illustrate the effectiveness of the proposed controller design methodology for standalone VSI and grid-connected VSI.
- 5- RTHIL experimental work using RTDS and DS1103 controller board, to demonstrate the efficacy of the proposed controller for standalone VSI and grid-connected VSI.

1.5 Thesis organization

The organization of the thesis is as following. In the first chapter an introduction of this work is provided which includes the motivation behind working on this topic, the problem

statement and an outline of objectives and the contributions. In chapter 2, a literature review is presented. A discussion of current research on VSIs, their popular control methods and robust control methods and a comparison of this work to the literature is provided in this chapter. In chapter 3, the details of the proposed robust control design scheme is presented for standalone VSIs in the form of two novel theorems. In chapter 4, the same is presented for the grid-connected VSIs in details. After this, some intelligent optimization algorithms for control design are presented for the two modes in chapter 5. Next, the details of controller implementation for the two systems are mentioned in chapter 6, which includes the implementations on MATLAB/SIMULINK and the RTHIL setup. In chapter 7 and chapter 8, the MATLAB simulations and RTHIL results are presented and analyzed for the standalone and grid-connected cases respectively. In chapter 9, the conclusions and future directions of this work are discussed. There are two appendices at the end. In appendix A, the schematics of the systems developed for MATLAB simulations are presented. In Appendix B, the RTHIL schematics are provided, which includes the schematics of plant implementations on RSCAD, the software package for RTDS simulator, and controller implementation for DS1103 controller board. |

CHAPTER 2

LITERATURE REVIEW

In this chapter a literature review related to the proposed work is presented. This mainly includes the discussion of VSIs, their functionality, applications, control and the current trends in research related to them. Some hot research topics relevant to the VSIs in general are described and a discussion of some of the latest control techniques being used for the inverter is presented. In particular some recent papers which have addressed the issue of robust control design problem for VSIs are discussed.

2.1 Voltage source inverters (VSIs)

2.1.1 Definition

The term voltage source inverters (VSIs) usually refers to a type of power electronic converter which is used to convert DC power to AC. It is also sometimes referred to as the voltage source converter (VSC). A VSI basically is a bridge of power electronic switches. At the input of the bridge is connected a constant DC voltage source and at the output an AC voltage/current is obtained. The amplitude of the AC voltage/current is controlled by the switching pattern and frequency of the bridge, generally using the pulse width modulation (PWM) method [29].

2.1.2 Applications

There is a wide range of applications of VSI. Most popular among these applications are;

- 1- its application in distributed generation (DG) systems [30]–[36] where it usually serve the purpose of controlling real and reactive power injection to the main grid and aid in complying with the regulatory standards [37],
- 2- active power filtering [38]–[42] where it serves the purpose of absorbing or inject certain voltage and current components in order to enhance the power quality of the system,
- 3- power electronic variable speed motor drives [43]–[45] where it provides a convenient and efficient way of control of speed of AC motors and
- 4- the uninterruptable electric power supply systems [12], [13], [24], [31], [34], [46]–[48], where it converts DC power from a battery storage system to AC to supply to local loads in the event of utility power outage.

2.1.3 Recent research areas related to VSIs

There is a lot of research going on over VSIs in various directions. In [10], the problem of fault detection is discussed. It has been pointed out the IEEE std. 1547 lacks completeness in providing solution to calculate fault currents and that with power electronic inverter the DGs are unable to provide sufficient fault currents. Also the effect of voltage and current controllers on the protection schemes of commercial and industrial distribution networks is discussed. A solution is provided to the fault detection problem by an adaptive relaying algorithm.

The output filter which is used for harmonics attenuations and smoothing the inverter output, is under study in [49]. An LCL output filter is used instead of the usual LC filter for better performance and simplicity of design. This LCL filter, however, has a disadvantage which is oscillations between the inductor and capacitor, which requires a separate active or passive damping algorithm. The passive algorithm is not preferable as it increases the power losses. Thus active damping is required, which can complicate the control design and increase computational cost. To address this issue, two-cascaded Model Predictive Control (MPC) controller scheme is provided which controls the VSI and accomplishes the active damping as well, so no separate algorithm is required.

Another similar work [22], provides the idea of using current in the feedback loop as it possesses some natural damping terms. Design method of the LCL filter is provided to achieve optimum damping for a given bandwidth. In case of presence of uncertainty in the system, the filter could deviate from the targeted performance. For this case a simple method is provided to estimate the filter capacitor current.

2.2 Control of voltage source inverters

Various methods exist in literature for the control of VSIs. Three direct power control algorithms (DPC) are compared in [50]. The space vector modulation (SVM) DPC is shown to give better performance in terms of lower tracking error and lower THD. A disadvantage however is the rise in computational difficulty and cost. In [37], again VSI with LCL filter is considered. A new control method using control Lyapunov function (CLF) is presented and its performance is compared to the commonly used proportional

resonant plus state feedback controller (PR+SF). A major drawback of the PR+SF controller is the reduction in bandwidth which greatly deteriorates the transient behavior of the system. Also the disturbance rejection capability is very poor. The CLF based controller alleviates these problems. An integral control approach is adopted to provide disturbance rejection and deal with parameter uncertainties. However the controller is designed for single phase inverter and the results presented are limited. The results on transient behavior of the system in presence of uncertainties are not shown.

A two level fault tolerant VSI is designed for a PM (Permanent Magnet) drive which consist of 3 legs in [44]. A redundant leg is added for the fault tolerant inverter. In the event of fault, the faulted leg is isolated and the redundant leg is inserted. This enables the VSI to tolerate open and short circuit fault due to the switching devices. A similar issue is addressed in [51], where an open circuit fault detection method is presented. Detection method is based on system identification techniques which is fast and robust and can detect multiple faults.

Table 2-1 enlists some of the commonly used control methods for the inverters and their merits and demerits.

Table 2-1: Pros and Cons of some commonly applied Control methods over the VSIs.

Sr. No.	Control method	Pros	Cons
1.	Hysteresis-band controllers [52], [53]	Simple Design	Variable switching frequency, high current ripple
2.	Proportional integral	Simple Design	Fixed steady state error when tracking a sinusoidal reference, poor disturbance rejection
3.	Proportional resonant [13], [14]	Overcomes cons of PI	Careful designing to avoid impact on bandwidth and phase margin, slow response, sensitivity to parameter variation
4.	Deadbeat predictive controllers [16]– [21]	Fast reference tracking, implementation simplicity and low computational cost	Reference tracking and stability are often compromised by changes in the plant parameters or delays
5.	Robust deadbeat predictive controller [54], [55]	Improves robustness of DPC against delays by using Luenberger observer	Does not take into account the fractional part of the total delay. Fractional delay degrades deadbeat performance
6.	Repetitive control [47]	Good tracking performance	Slow response, unsystematic method to stabilize error dynamics

2.3 Robust control for voltage Source Inverters

The VSIs are often found to perform poorly for systems having parameter variations. This is because most control methods do not take into account system uncertainty in their design. During grid operation, changes in line impedance and grid faults are often occurring leading to parameter variations. This sometimes could easily direct the system towards instability [56]. Following is a discussion of some recent works in the direction of robust control design of VSIs.

Deadbeat Control:

One of the popular control method for the inverters is the deadbeat control [57], [58] which provides very good transient performance but its sensitivity to parameter variation causes the system to perform poorly or even lead to instability. To solve this problem disturbance observers have been used. However the overall control scheme becomes complex [57].

H_∞ Control:

The H_∞ robust control method has been used for many years and is well-established. It has also been successfully applied for control of inverters [48], [59]. The disadvantage however is higher order of the controllers. In order to realize the controller, a reduced order approximation is derived, the performance of which is not as good as the original higher order controller. Also the choice of weighting functions is a complicated procedure. Also in [48], the control input signal level has limitations and saturation of the controller is not allowed. Other control schemes such as MPC [60] are simple to implement and are not

computationally exhaustive, but requires high sampling rate and does not provide an analysis of robustness and stability.

Adaptive Sliding Mode Control:

A recent work in the direction of robust control of inverter has been done in [61]. The controller designed using an adaptive sliding mode control scheme shows good performance with filter uncertainties and disturbances. However, on top of the nonlinear sliding mode control law, separate adaptive algorithms are implemented for observing uncertain parameters and to reduce chattering in the control signal. This makes the control design complex and increases the computational hardware requirements.

Multi Resonant Control (MRC):

Multi resonant controllers have also been proposed in literature that try to improve system performance and robustness by reducing the harmonic distortions caused due to uncertainties and unbalanced and nonlinear loads. The major issue in the design of these controllers is the determination of a large number of controller parameters, which is quite burdensome. In a recent related paper[62], an approach for tuning the controller parameters based on phase margin is given and the only three modes of resonant considered.

LQR Based MRC:

In[63], a tuning method based on the linear quadratic regulation (LQR) design is presented. The advantage is that it is applicable for any number of resonant controllers. The drawback however is still a trial and error based tuning of the weighting matrix Q which affects the performance of the controllers. A more recent paper [64] tries to address some of these shortcomings by developing a systematic way of finding the resonant controller gains. A

convex optimization linear matrix inequality (LMI) problem is developed to determine the controller gains, which is applicable to any order of the controller as designed by the user. Good performance with respect to reduced total harmonic distortion is obtained, however the transient durations are slightly large. Also, the method is developed for single phase systems and extension to three phase may not be straightforward. The order of the multi-resonant controllers increases with the number of harmonics to be rejected. Also state-feedback is required which increases the hardware requirements. Therefore the overall cost becomes high to obtain good performance.

A summary of the papers discussed, and some more state-of-the-art work, is presented in Table 2-2.

Table 2-2: Some state-of-the-art robust control methods.

Sr. No.	Control method	Remarks	Published Online
1.	Adaptive sliding mode control [61]	Good robustness and disturbance rejection performance. High computational requirement.	Mar, 2015
2.	Lyapunov function based method [28]	Provides method to design controller with a tradeoff between stability and performance	Aug, 2014
2.	Multi-Resonant Controllers	Good harmonic rejection and THD performance. Cost increases with performance requirements.	Mar, 2014
3.	Adaptive voltage control [9]	Robust to uncertainties, load disturbances, easy to implement, uncertainties considered in filter parameters	Mar, 2014
4.	Robust state feedback control [65]	Robust stability to parametric uncertainty, suitable transient response, designed for single phase inverter	Sep, 2013
5.	Full State Observer Predictive Current Control (FSOPCC) [7]	System robustness to parameter uncertainty improves at the cost of reduction in control bandwidth	Aug, 2013
6.	Sliding mode control [66]	Overshoot-free, fast tracking, robust to parametric uncertainty, only simulations conducted	Jul, 2013
7.	μ -synthesis based robust control [67], [5]	Robust stabilization and tracking, fast response, high control bandwidth, transient response could be improved for disturbances	Apr, 2013

2.4 Proposed work in comparison to the literature

Recent research in the direction of robust control design for VSIs has been focused on improving the tradeoff between robust stability and performance. Some of these works can be found in [30], [48] and [28]. In [28] a discrete time controller is designed, based on stability analysis of the system using Lyapunov function. The proposed method is good in providing a systematic way to design a controller for a required tradeoff between performance and robustness. However it is considering a different problem in the sense that the uncertainty bounds considered are for the *LC* filter parameters. Although the system remains stable for any load variations which is an essential requirement, the performance tuning parameter has no effect on the load uncertainty. Hence it is not possible to improve performance based on bounds on load uncertainty.

In [48] a discrete time H_∞ controller is designed for the same system and uncertainties are considered in the load. The load is modeled as an admittance with known limits of variations. Based on the Lyapunov stability of the system, LMI conditions are developed to design the controller which guarantees asymptotic stability with a certain convergence rate for the allowable uncertainties. Also the effect of disturbance signal is minimized on the output signal. The performance of the proposed control method is compared with that of a commercial UPS inverter and is shown to give better results. The convergence time however appears to be larger because of the root-mean-square (rms) value tracking method which takes relatively large time in the calculation process.

In [30], the grid connected VSI is considered with uncertainties in the line impedance of the grid. The proposed controller is based on H_∞ theory. The controller is designed by

following a standard procedure in which weighting function are selected for robust stability and tracking performance of the uncertain system. The designed controller is of high order, thus a reduced order approximation is obtained for implementation. The results of the proposed method are very good as the controller demonstrates good robustness against uncertain parametric variations. The performance of the controller is compared with PI controller and improvement is shown in terms of THD values for different reference levels of the output current.

In this context, the problem considered in this work is to design a new control methodology for the control of VSIs for standalone and grid-connected modes in presence of system uncertainties. The key point in the robust control design problem is to also provide enhanced performance of the system. The solution developed for the problem is a framework which enables direct and efficient application of robust control theory for VSI, leading to improved performance.

A lot of methods for robust control design exist in control theory for a variety of systems [68]. Now, VSIs can be conveniently modeled in the linear state-space form. Also any parametric uncertainties in the system parameters can be manipulated and split as an additive uncertain term in the plant model. Due to this characteristic of the VSI system, the class of linear systems with time varying norm-bounded uncertainties was chosen and the methods for their control were explored.

Various sophisticated methods in robust control design theory for norm bounded uncertainties such as in [69], [70] exist in literature. Some other similar methods are given in [71]–[73]. Recently in [71] a new set of LMI conditions were presented for observer

based robust state feedback controller design, which were shown to give better results as compared to the old LMIs given by [69], [70]. This paper [71] was initially considered for control design in the proposed work as well, however a mistake was found in it [74] which deprived it of its superiority over the existing work done by [69], [70].

In general the main attribute of the proposed work is to develop a framework and a set of conditions that enables seamless application of the aforementioned [69]–[73] and similar theories for control of inverters which to the best knowledge of the author has not been done. In this work, the robust control theory of [69] is applied for robust control design of VSIs. Novel controller design algorithms are devised using intelligent techniques to tune the robust controller to provide enhanced performance and robustness bargain. Further, the procedure for control design is simple and systematic which will be described in section 5.2 and 5.3. The controller designed is also cost effective as it is observer based and requires only the measurements of the output. The results of the proposed method are compared with that of some relevant works in the literature. For the standalone mode, reference [48] and for grid-connected mode, reference [30] is considered as the most recent and most relevant work. These two papers are used as the benchmarks for comparison. The comparison results show that the performance of the system is improved in both the standalone and grid-connected modes, in terms of less distortions in the signals and smaller time duration to settle back to steady-state. For future work this will pave the way for the application of several methods to design the controller, to compare and analyze, and to select the most appropriate one.

CHAPTER 3

STANDALONE VSI: MODELING AND CONTROL

DESIGN

Robust controller is to be designed for the VSI and *LC* filter system. The control objective is to drive the VSI in standalone mode of operation. Thus the output voltage and frequency will be regulated. The control design method is model based. The first step is to develop a mathematical model to represent the system dynamics.

3.1 Preliminaries

To write the equations of the systems in the *dq* reference frame, space phasors will be used. Consider the following [75].

$$x_a(t) = x_p \cos(\theta(t)) \quad (3-1)$$

$$x_b(t) = x_p \cos\left(\theta(t) - \frac{2\pi}{3}\right) \quad (3-2)$$

$$x_c(t) = x_p \cos\left(\theta(t) + \frac{2\pi}{3}\right) \quad (3-3)$$

with
$$\theta(t) = \theta_0 + \int_0^t \omega'(\tau) d\tau \quad (3-4)$$

where $\mathbf{x}_{abc} = [x_a(t) \ x_b(t) \ x_c(t)]$ represent a balanced three phase function, with x_p , $\omega'(t)$ and θ_0 represent its amplitude, frequency in radians/s and phase angle in radians. The space phasor for \mathbf{x}_{abc} is defined as

$$\vec{x}(t) = \frac{2}{3} \left[x_a(t) + e^{\frac{j2\pi}{3}} x_b(t) + e^{\frac{j4\pi}{3}} x_c(t) \right] \quad (3-5)$$

or
$$\vec{x}(t) = \bar{x} e^{j\theta(t)} \quad (3-6)$$

For the case of constant angular frequency, say ω

$$\vec{x}(t) = x_p e^{j\theta_0} e^{j\omega t} = \bar{x} e^{j\omega t} \quad (3-7)$$

Now define a function $\rho(t)$ as

or
$$\rho(t) = \rho_0 + \int_0^t \omega'(\tau) d\tau \quad (3-8)$$

Shifting the space phasor $\vec{x}(t)$ by the angle $-\rho(t)$ yields

$$\vec{x}(t) e^{-j\rho(t)} = x_p e^{j(\theta_0 - \rho_0)} = x_d(t) + jx_q(t) \quad (3-9)$$

or
$$\vec{x}(t) = \left(x_d(t) + jx_q(t) \right) e^{j\rho(t)} = x_{dq}(t) e^{j\rho(t)} \quad (3-10)$$

where $x_d(t)$ and $x_q(t)$ are the components of \mathbf{x}_{abc} in the dq -frame. While $\theta(t)$ and $\rho(t)$ are necessarily not equal, their first time derivatives must be maintained the same. For brevity the suffix ' (t) ' will be omitted in the dq variables hereon.

3.2 Derivation of mathematical model of the standalone system

Considering the VSI with LC filter as in Figure 3.1. The dynamics of this system can be represented by the following set of space phasor equations

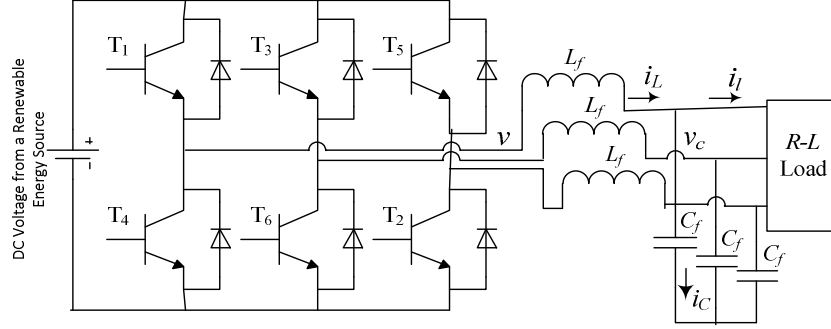


Figure 3.1 Three phase voltage source inverter with output LC filter for standalone operation.

$$\vec{v}(t) - L_f \frac{d\vec{i}(t)}{dt} - \vec{v}_c(t) = 0 \quad (3-11)$$

$$\vec{i}(t) = \vec{i}_c(t) + \vec{i}_l(t) \quad (3-12)$$

$$-\vec{v}_c(t) + R\vec{i}_l(t) + L \frac{d\vec{i}_l(t)}{dt} = 0 \quad (3-13)$$

Now substituting $\vec{v}(t) = v_{dq} e^{j\rho(t)}$, $\vec{i}(t) = i_{dq} e^{j\rho(t)}$, $\vec{v}_c(t) = v_{cdq} e^{j\rho(t)}$ and $\vec{i}_l(t) = i_{ldq} e^{j\rho(t)}$,

Eq. (3-11) \Rightarrow

$$v_{dq} e^{j\rho(t)} - L_f \frac{di_{dq} e^{j\rho(t)}}{dt} - v_{cdq} e^{j\rho(t)} = 0$$

$$(v_d + jv_q) e^{j\rho(t)} - L_f \left(\left(\frac{di_d}{dt} + j \frac{di_q}{dt} \right) e^{j\rho(t)} + j\omega (i_d + j i_q) e^{j\rho(t)} \right) - (v_{cd} + jv_{cq}) e^{j\rho(t)} = 0$$

In a similar manner working on eq. (3-12)-(3-13) and solving for the derivatives, yields eq. (3-14)-(3-19).

$$\frac{di_d}{dt} = \frac{1}{L_f} v_d + \omega i_q - \frac{1}{L_f} v_{cd} \quad (3-14)$$

$$\frac{di_q}{dt} = \frac{1}{L_f} v_q - \omega i_d - \frac{1}{L_f} v_{cq} \quad (3-15)$$

$$\frac{dv_{cd}}{dt} = \frac{1}{C_f} i_d + \omega v_{cq} - \frac{1}{C_f} i_{ld} \quad (3-16)$$

$$\frac{dv_{cq}}{dt} = \frac{1}{C_f} i_q - \omega v_{cd} - \frac{1}{C_f} i_{lq} \quad (3-17)$$

$$\frac{di_{ld}}{dt} = \frac{1}{L} v_{cd} - \frac{R}{L} i_{ld} + \omega i_{lq} \quad (3-18)$$

$$\frac{di_{lq}}{dt} = \frac{1}{L} v_{cq} - \frac{R}{L} i_{lq} - \omega i_{ld} \quad (3-19)$$

Eq. (3-14) – (3-19) represent the mathematical model of the system, where $i_d, i_q, v_d, v_q, v_{cd}, v_{cq}, i_{ld}$ and i_{lq} are dq components of inverter output current, inverter output voltage, filter capacitor voltage and load current respectively and L_f, C_f, R, L represents the filter inductance and capacitance and load resistance and inductance respectively.

3.3 Controller Design for the standalone system

Consider a general linear time invariant (LTI) plant model in the state-space form, with uncertain only in the \mathbf{A} matrix.

$$\dot{\mathbf{x}}(t) = (\mathbf{A} + \Delta\mathbf{A})\mathbf{x}(t) + \mathbf{B}\mathbf{u}(t) \quad (3-20)$$

$$\mathbf{y}(t) = \mathbf{C}\mathbf{x}(t) \quad (3-21)$$

where $\mathbf{x}(t) \in \mathbb{R}^n, \mathbf{y}(t) \in \mathbb{R}^p$ & $\mathbf{u}(t) \in \mathbb{R}^m$ represents the states, output and input vectors

of the system respectively. $\mathbf{A}, \mathbf{B}, \mathbf{C}$ are constant matrices of appropriate dimensions such that (\mathbf{A}, \mathbf{B}) is stabilizable and (\mathbf{A}, \mathbf{C}) is detectable. Bounded uncertainties are considered in the load and are modelled in $\Delta\mathbf{A} = \mathbf{M}\mathbf{\Lambda}\mathbf{N}$ where the uncertainty radius of the system is bounded as $\mathbf{\Lambda}^T\mathbf{\Lambda} \leq \mathbf{I}$. The VSI plant model in eq. (3-14) – (3-19) can easily be translated in the form of eq. (3-20) – (3-21). The states of the system $i_d, i_q, v_{cd}, v_{cq}, i_{ld}$ and i_{lq} , the inputs v_d and v_q and the outputs will be v_{cd} and v_{cq} . The constant system matrices are given in eq. (3-22).

$$\mathbf{A} = \begin{bmatrix} 0 & \omega & -\frac{1}{L_f} & 0 & 0 & 0 \\ -\omega & 0 & 0 & -\frac{1}{L_f} & 0 & 0 \\ \frac{1}{C_f} & 0 & 0 & \omega & -\frac{1}{C_f} & 0 \\ 0 & \frac{1}{C_f} & -\omega & 0 & 0 & -\frac{1}{C_f} \\ 0 & 0 & \frac{1}{L} & 0 & -\frac{R}{L} & \omega \\ 0 & 0 & 0 & \frac{1}{L} & -\omega & -\frac{R}{L} \end{bmatrix}, \mathbf{B} = \begin{bmatrix} \frac{1}{L_f} & 0 \\ 0 & \frac{1}{L_f} \\ 0 & 0 \\ 0 & 0 \\ 0 & 0 \\ 0 & 0 \end{bmatrix},$$

$$\mathbf{C} = \begin{bmatrix} 0 & 0 & 1 & 0 & 0 & 0 \\ 0 & 0 & 0 & 1 & 0 & 0 \end{bmatrix} \quad (3-22)$$

The controller is to be designed such that the system is robustly stable and the output $y(t)$, tracks the reference input $\mathbf{r}(t) \in \mathbb{R}^p$. The uncertainties considered in the load have the following constraints:

$$R = R_0 + \Delta R, \quad L = L_0 + \Delta L \quad (3-23)$$

with
$$-\lambda_R \leq \Delta R \leq \lambda_R \quad -\lambda_L \leq \Delta L \leq \lambda_L \quad (3-24)$$

where R and L are the total resistance and inductance of the load respectively. With these given parameter variations $\Delta\mathbf{A}$ can be determined. But, as described in the later section, it is also very important to determine the arbitrary constant matrices \mathbf{M} and \mathbf{N} , as they are

required to solve for the controller gains. With the availability of fast computation technology, it can be easily observed using any heuristic optimization algorithm that the choice of these arbitrary matrices influence the performance of the designed controller. Customarily these matrices are chosen randomly by trial and error method. Although, this approach can be cumbersome depending on the order of the system which affects the size of these matrices and hence the difficulty in their choice. Additionally it is highly likely, that this choice may not be the best as the user does not try all possible combination of choices. Using heuristic methods to find the optimum choice is a possible but an inefficient approach, since the number of parameters to be optimized are huge and there is no knowledge of their search space. Hence the optimization process can be very time consuming and is prone to be trapped by local optima. Thus by developing methodical means of choice of these matrices, not only the control design process is simplified but also there emerges an efficient way to determine the controller gains of optimum performance. This is accomplished by the proposed method. The details to follow in the next subsection.

3.3.1 Controller for robust stabilization

First the robust stabilization control theory is presented from [70]. A general state space uncertain plant model of the form in eq. (3-20) – (3-21) can be robustly asymptotically stabilized by the following control law with the state estimator in eq. (3-25) – (3-26).

$$\hat{\mathbf{x}}(t) = \mathbf{A}\hat{\mathbf{x}}(t) + \mathbf{B}\mathbf{u}(t) + \mathbf{L}(\mathbf{y}(t) - \mathbf{C}\hat{\mathbf{x}}(t)) \quad (3-25)$$

$$\mathbf{u}(t) = -\mathbf{K}\hat{\mathbf{x}}(t) \quad (3-26)$$

where $\hat{\mathbf{x}}(t) \in \mathbb{R}^n$ represents the estimation of state $\mathbf{x}(t)$. \mathbf{K} and \mathbf{L} are the controller gains, found by solving the LMI given in eq. (3-27) with an equality constraint in eq. (3-28).

$$\begin{bmatrix} \Phi & B\hat{K} & PM \\ * & \Psi & RM \\ * & * & -\sigma_1 I \end{bmatrix} < 0 \quad (3-27)$$

$$PB = B\hat{P} \quad (3-28)$$

where

$$\Phi = A^T P + PA - \hat{K}^T B^T - B\hat{K} + \sigma_1 N^T N + \sigma_2 I,$$

$$\Psi = A^T R + RA - \hat{L}C - C^T \hat{L}^T + \sigma_2 I.$$

The LMI variables, $\mathbf{P} \in \mathbb{R}^{n \times n}$ and $\mathbf{R} \in \mathbb{R}^{n \times n}$ are two positive definite matrices, σ_1, σ_2 are positive scalars and matrices $\hat{\mathbf{P}} \in \mathbb{R}^{m \times m}$, $\hat{\mathbf{K}} \in \mathbb{R}^{n \times m}$ and $\hat{\mathbf{L}} \in \mathbb{R}^{p \times n}$ are such that $\mathbf{K} = \hat{\mathbf{P}}^{-1} \hat{\mathbf{K}}$ and $\mathbf{L} = \mathbf{R}^{-1} \hat{\mathbf{L}}$. The convergence rate h of the system is given in eq. (3-29) where, the function $\lambda_{\max}(\mathbf{W})$, gives the maximum eigenvalue of any matrix \mathbf{W} .

$$h = \sigma_2 / (2 \max(\lambda_{\max}(\mathbf{P}), \lambda_{\max}(\mathbf{R}))) \quad (3-29)$$

The controller designed by the above method guarantees robust stability with convergence rate given in eq. (3-29) if the condition on uncertainty radius of the system $\mathbf{A}^T \mathbf{\Lambda} \leq \mathbf{I}$ is satisfied. Beyond this condition, the system may not be stable, or may have a poorer convergence rate. This condition can be utilized to develop bounds on the uncertain parameters of the system for which the controller is to be designed. Now for robust control design of the VSI, the following theorem is presented. It is reminded that the purpose of the theorem is to provide an efficient way to apply the method of [70] and design an enhanced performance robust controller.

Theorem 3-1: The voltage source inverter system with LC filter and $R - L$ load given by the eq. (3-20) – (3-22), with uncertainty in the load as given by eq. (3-23) – (3-24), can be asymptotically stabilized by the control law in eq. (3-25) – (3-26), with a convergence rate of eq. (3-29). The controller gains are obtained by solving the LMI in eq. (3-27) – (3-28) with the uncertainty matrices given as following:

$$\mathbf{M} = \begin{bmatrix} \mathbf{I}_{4 \times 4} & \mathbf{0}_{4 \times 2} \\ \mathbf{0}_{2 \times 4} & \begin{bmatrix} \frac{1}{\mu} & 0 \\ 0 & \frac{1}{\mu} \end{bmatrix} \end{bmatrix}, \quad \mathbf{N} = \begin{bmatrix} \mathbf{I}_{4 \times 4} & \mathbf{0}_{4 \times 2} \\ \mathbf{0}_{2 \times 4} & \begin{bmatrix} \frac{\mu}{v} & 0 \\ 0 & \frac{\mu}{v} \end{bmatrix} \end{bmatrix} \quad (3-30)$$

where μ and v are two constants given as:

$$\mu = \alpha \bar{\mu}, \quad \bar{\mu} = \frac{L_0^2}{\lambda_L} \quad |\alpha| \leq 1 \quad (3-31)$$

and

$$v = \beta \bar{v} \quad \bar{v} = \sqrt{(1 - \alpha^2)} \left(\frac{L_0^2}{L_0 \lambda_R + R_0 \lambda_L} \right) \quad |\beta| \leq 1 \quad (3-32)$$

Proof: The uncertainties in the system given by eq. (3-23) – (3-24) \Rightarrow eq. (3-20) – (3-22),

$\Delta \mathbf{A}$ can be written as:

$$\Delta \mathbf{A} = \begin{bmatrix} 0 & 0 & 0 & 0 & 0 & 0 \\ 0 & 0 & 0 & 0 & 0 & 0 \\ 0 & 0 & 0 & 0 & 0 & 0 \\ 0 & 0 & 0 & 0 & 0 & 0 \\ 0 & 0 & \bar{\delta}_1 & 0 & -\bar{\delta}_2 & 0 \\ 0 & 0 & 0 & \bar{\delta}_1 & 0 & -\bar{\delta}_2 \end{bmatrix} \quad (3-33)$$

where

$$\bar{\delta}_1 = -\frac{\Delta L}{L_0(L_0 + \Delta L)} = -\frac{\Delta L}{L_0 L} \cong -\frac{\Delta L}{L_0^2} \quad (3-34)$$

$$\bar{\delta}_2 = \frac{L_0 \Delta R - R_0 \Delta L}{L_0 L} \cong \frac{L_0 \Delta R - R_0 \Delta L}{L_0^2} \quad (3-35)$$

considering $\Delta R \ll R_0$ and $\Delta L \ll L_0$. Now a careful rearrangement of $\Delta \mathbf{A}$ is required in the

form of \mathbf{MAN} such that $\mathbf{A}^T \mathbf{A} \leq \mathbf{I}$, as following

$$\mathbf{A} \mathbf{A} = \begin{bmatrix} 1 & 0 & 0 & 0 & 0 & 0 \\ 0 & 1 & 0 & 0 & 0 & 0 \\ 0 & 0 & 1 & 0 & 0 & 0 \\ 0 & 0 & 0 & 1 & 0 & 0 \\ 0 & 0 & 0 & 0 & \frac{1}{\mu} & 0 \\ 0 & 0 & 0 & 0 & 0 & \frac{1}{\mu} \end{bmatrix} \begin{bmatrix} 0 & 0 & 0 & 0 & 0 & 0 \\ 0 & 0 & 0 & 0 & 0 & 0 \\ 0 & 0 & 0 & 0 & 0 & 0 \\ 0 & 0 & 0 & 0 & 0 & 0 \\ 0 & 0 & \mu \bar{\delta}_1 & 0 & -v \bar{\delta}_2 & 0 \\ 0 & 0 & 0 & \mu \bar{\delta}_1 & 0 & -v \bar{\delta}_2 \end{bmatrix} \begin{bmatrix} 1 & 0 & 0 & 0 & 0 & 0 \\ 0 & 1 & 0 & 0 & 0 & 0 \\ 0 & 0 & 1 & 0 & 0 & 0 \\ 0 & 0 & 0 & 1 & 0 & 0 \\ 0 & 0 & 0 & 0 & \frac{\mu}{v} & 0 \\ 0 & 0 & 0 & 0 & 0 & \frac{\mu}{v} \end{bmatrix} \quad (3-36)$$

It can be shown with the choice of \mathbf{A} as in eq. (3-36) ensures $\mathbf{A}^T \mathbf{A} \leq \mathbf{I}$. For this consider the following with $\delta_1 = \mu \bar{\delta}_1$ and $\delta_2 = v \bar{\delta}_2$

$$\mathbf{A}^T \mathbf{A} = \begin{bmatrix} 0 & 0 & 0 & 0 & 0 & 0 \\ 0 & 0 & 0 & 0 & 0 & 0 \\ 0 & 0 & 0 & 0 & \delta_1 & 0 \\ 0 & 0 & 0 & 0 & 0 & \delta_1 \\ 0 & 0 & 0 & 0 & -\delta_2 & 0 \\ 0 & 0 & 0 & 0 & 0 & -\delta_2 \end{bmatrix} \begin{bmatrix} 0 & 0 & 0 & 0 & 0 & 0 \\ 0 & 0 & 0 & 0 & 0 & 0 \\ 0 & 0 & 0 & 0 & 0 & 0 \\ 0 & 0 & 0 & 0 & 0 & 0 \\ 0 & 0 & \delta_1 & 0 & -\delta_2 & 0 \\ 0 & 0 & 0 & \delta_1 & 0 & -\delta_2 \end{bmatrix} \leq \mathbf{I} \quad (3-37)$$

$$\mathbf{A}^T \mathbf{A} = \begin{bmatrix} 0 & 0 & 0 & 0 & 0 & 0 \\ 0 & 0 & 0 & 0 & 0 & 0 \\ 0 & 0 & \delta_1^2 & 0 & -\delta_1 \delta_2 & 0 \\ 0 & 0 & 0 & \delta_1^2 & 0 & -\delta_1 \delta_2 \\ 0 & 0 & -\delta_1 \delta_2 & 0 & \delta_2^2 & 0 \\ 0 & 0 & 0 & -\delta_1 \delta_2 & 0 & \delta_2^2 \end{bmatrix} \leq \mathbf{I} \quad (3-38)$$

$$\text{or } \mathbf{\Gamma} = \mathbf{I} - \mathbf{A}^T \mathbf{A} = \begin{bmatrix} 1 & 0 & 0 & 0 & 0 & 0 \\ 0 & 1 & 0 & 0 & 0 & 0 \\ 0 & 0 & 1 - \delta_1^2 & 0 & \delta_1 \delta_2 & 0 \\ 0 & 0 & 0 & 1 - \delta_1^2 & 0 & \delta_1 \delta_2 \\ 0 & 0 & \delta_1 \delta_2 & 0 & 1 - \delta_2^2 & 0 \\ 0 & 0 & 0 & \delta_1 \delta_2 & 0 & 1 - \delta_2^2 \end{bmatrix} \geq 0 \quad (3-39)$$

Now according to Sylvester's criterion a symmetric matrix is positive definite if and only if all of its principal minors are positive. Let the principal minors of the symmetric matrix $\mathbf{\Gamma}$ are given by P_i for $i = 1, 2, 3 \dots 6$. The first, second and fourth principal minors are clearly positive as given below.

$$P_1 = 1 > 0 \quad P_2 = 1 > 0 \quad P_4 = (1 - \delta_1^2)^2 > 0 \quad (3-40)$$

For the other three principal minors consider the following.

$$P_3 = 1 - \delta_1^2 = 1 - \left(-\mu \frac{\Delta L}{L_0^2}\right)^2 \quad (3-41)$$

$$\text{Let } \mu = \alpha \bar{\mu} = \alpha \frac{L_0^2}{\lambda_L} \Rightarrow P_3 = 1 - \left(\alpha \frac{\Delta L}{\lambda_L}\right)^2 = 1 - \alpha^2 \frac{\Delta L^2}{\lambda_L^2} \quad (3-42)$$

$$\text{If } |\alpha| \leq 1 \Rightarrow P_3 \geq 0. \quad (3-43)$$

Now consider the fifth principal minor.

$$P_5 = \begin{vmatrix} 1 & 0 & 0 & 0 & 0 \\ 0 & 1 & 0 & 0 & 0 \\ 0 & 0 & 1 - \delta_1^2 & 0 & \delta_1 \delta_2 \\ 0 & 0 & 0 & 1 - \delta_1^2 & 0 \\ 0 & 0 & \delta_1 \delta_2 & 0 & 1 - \delta_2^2 \end{vmatrix} = \begin{vmatrix} 1 - \delta_1^2 & 0 & \delta_1 \delta_2 \\ 0 & 1 - \delta_1^2 & 0 \\ \delta_1 \delta_2 & 0 & 1 - \delta_2^2 \end{vmatrix} \quad (3-44)$$

$$P_5 = (1 - \delta_1^2)[(1 - \delta_1^2)(1 - \delta_2^2) - \delta_1^2 \delta_2^2] \quad (3-45)$$

$$P_5 = (1 - \delta_1^2)(1 - \delta_1^2 - \delta_2^2) = (1 - \delta_1^2)^2 - \delta_2^2(1 - \delta_1^2) = P_3^2 - \delta_2^2 P_3 \quad (3-46)$$

If $P_3 - \delta_2^2 \geq 0$ or $P_3 \geq \delta_2^2 \Rightarrow P_5 \geq 0$. Consider the following.

$$P_3 \geq \delta_2^2 \Rightarrow v^2 \left(\frac{L_0 \Delta R - R_0 \Delta L}{L_0^2}\right)^2 \leq 1 - \alpha^2 \frac{\Delta L^2}{\lambda_L^2} \quad (3-47)$$

$$v^2 \leq \left(1 - \alpha^2 \frac{\Delta L^2}{\lambda_L^2}\right) \left(\frac{L_0^2}{L_0 \Delta R - R_0 \Delta L}\right)^2 = \left(\frac{\lambda_L^2 - \alpha^2 \Delta L^2}{\lambda_L^2}\right) \left(\frac{L_0^2}{L_0 \Delta R - R_0 \Delta L}\right)^2 = \Pi \quad (3-48)$$

Now to find the upper bound on v^2 , Π should be minimized. This can be achieved by $\Delta L = -\lambda_L$ and $\Delta R = \lambda_R$.

$$v^2 \leq (1 - \alpha^2) \left(\frac{L_0^2}{L_0\lambda_R + R_0\lambda_L} \right)^2 \quad (3-49)$$

or with $|\beta| \leq 1$

$$v^2 = \beta^2 (1 - \alpha^2) \left(\frac{L_0^2}{L_0\lambda_R + R_0\lambda_L} \right)^2 \quad (3-50)$$

$$v = \beta \sqrt{(1 - \alpha^2)} \left(\frac{L_0^2}{L_0\lambda_R + R_0\lambda_L} \right) = \beta \bar{v} \quad (3-51)$$

Similarly it can be shown that with the above conditions $P_6 \geq 0$. This completes the proof.

□

Remark 3-1: With α and β , *theorem 3-1* leaves two degrees of freedom in the control design process. This means availability of two tuning parameter for the user to adjust the response of the closed loop system. This feature can be utilized to enhance the performance of the system. Any heuristic optimization method can be used such that α and β are chosen according to eq. (3-43) and (3-50) and the best possible performance is achieved. This enhancement in the performance could be maximizing the convergence rate, proximity to the required eigenvalues, damping ratio and/or transient specifications.

3.3.2 Robust stability analysis and limits of parameter variations

Theorem 3-1, given in the previous section provided a method to design robust controller for the VSI system under consideration, using the state space model and some bounds on the uncertainty variation. However it should be noted that, it did not provide the bounds of uncertainty for which robustness of the stability of the system is guaranteed with the designed controller. For this, the following theorem is presented.

Theorem 3-2: The voltage source inverter system with LC filter and $R - L$ load given by the eq. (3-20) – (3-22), is guaranteed to be robustly asymptotically stable with the convergence rate of eq. (3-29), by the control law in eq. (3-25) – (3-26) for all the uncertainties given by eq. (3-52). The controller gains can be obtained by solving the LMI in eq. (3-27) – (3-28) with the uncertainty matrices given in eq. (3-30), where ν is a constant given in eq. (3-32) and μ is another constant given in eq. (3-54).

$$-\bar{\lambda}_R \leq \Delta R \leq \bar{\lambda}_R \quad -\bar{\lambda}_L \leq \Delta L \leq \bar{\lambda}_L \quad (3-52)$$

$$\text{where } \bar{\lambda}_L = \left| \frac{\lambda_L}{\alpha} \right| \quad \text{and} \quad \bar{\lambda}_R = \frac{\lambda_R}{|\beta|\sqrt{(1-\alpha^2)}} + \frac{R_0\lambda_L}{L_0} \left(\frac{1}{|\beta|\sqrt{(1-\alpha^2)}} - \frac{1}{|\alpha|} \right) \quad (3-53)$$

$$\mu = \alpha\bar{\mu}, \quad \bar{\mu} = \frac{L_0^2}{\lambda_L} \quad \underline{\alpha} \leq |\alpha| \leq 1 \quad (3-54)$$

$$\text{where} \quad \underline{\alpha} = \frac{\beta^2}{\left(1 - \frac{\lambda_R L_0}{\lambda_L R_0}\right)^2 + \beta^2} \quad (3-56)$$

Proof: The conditions required for the validity of *theorem 3-1* can be used to provide the proof for this theorem. Considering eq. (3-41) – (3-43),

$$P_3 = 1 - \alpha^2 \frac{\Delta L^2}{\lambda_L^2} \geq 0 \quad (3-57)$$

$$\Rightarrow \quad |\Delta L| \leq \left| \frac{\lambda_L}{\alpha} \right| = \bar{\lambda}_L \quad (3-58)$$

This means as long as the magnitude of variation of load inductance is less or equal to $\bar{\lambda}_L$, the conditions in eq. (3-39) and theorem remains valid. In other words if eq. (3-58) holds, the condition on uncertainty radius of the system is satisfied i.e. $\mathbf{A}^T \mathbf{A} \leq \mathbf{I}$. Thus $\bar{\lambda}_L$ is the

upper bound for the uncertainty in load inductance, which will be greater than or equal to λ_L since $\underline{\alpha} \leq |\alpha| \leq 1$. In a similar manner a condition for variation in load resistance can be derived. Considering eq. (3-39), for the matrix to be positive semi-definite, the diagonal elements must be positive semi-definite. Therefore,

$$1 - \delta_2^2 \geq 0 \quad (3-59)$$

$$1 - \nu^2 \left(\frac{L_0 \Delta R - R_0 \Delta L}{L_0^2} \right)^2 \geq 0 \quad (3-60)$$

The condition in eq. (3-60) should hold for all possible ΔR and ΔL . The worst case is when the negative term is maximum. This occurs when the difference $L_0 \Delta R - R_0 \Delta L$ is maximum. For this, eq. (3-58) implies in eq. (3-60),

$$|\nu| \left| L_0 \Delta R + R_0 \frac{\lambda_L}{|\alpha|} \right| \leq L_0^2 \quad (3-61)$$

$$\left| L_0 \Delta R + R_0 \frac{\lambda_L}{|\alpha|} \right| \leq |L_0 \Delta R| + \left| R_0 \frac{\lambda_L}{|\alpha|} \right| \leq \frac{L_0^2}{|\nu|} \quad (3-62)$$

$$|\Delta R| \leq \frac{L_0}{|\nu|} - \frac{R_0 \lambda_L}{L_0 |\alpha|} \quad (3-63)$$

Substituting ν from eq. (3-32),

$$|\Delta R| \leq \frac{L_0 \lambda_R + R_0 \lambda_L}{L_0 |\beta| \sqrt{(1-\alpha^2)}} - \frac{R_0 \lambda_L}{L_0 |\alpha|} \quad (3-64)$$

or

$$|\Delta R| \leq \frac{\lambda_R}{|\beta| \sqrt{(1-\alpha^2)}} + \frac{R_0 \lambda_L}{L_0} \left(\frac{1}{|\beta| \sqrt{(1-\alpha^2)}} - \frac{1}{|\alpha|} \right) = \bar{\lambda}_R \quad (3-65)$$

where $\bar{\lambda}_R$ is the upper bound on the load resistance uncertainty. Since $|\alpha| \leq 1$, $\bar{\lambda}_R$ tends to be negative as α becomes small. Thus a lower bound on α must be enforced for $\bar{\lambda}_R$ to remain nonnegative, which is given in eq. (3-56). This condition allows the variation in the

magnitude of uncertainty of load resistance up to $\bar{\lambda}_R$ for robust stability with guaranteed convergence rate. It is interesting to observe from eq. (3-58) and eq. (3-65) that as α decreases, $\bar{\lambda}_L$ increases, while $\bar{\lambda}_R$ decreases and vice versa. Thus α acts as a tuning parameter for the controller to provide a tradeoff between allowable variations in load resistance or inductance. For β , $\bar{\lambda}_R$ is inversely related to it, thus its smaller values would yield bigger allowable variations in the load resistance. This completes the proof. \square

3.3.3 Analysis of the derived theorems

The derived theorems present a systematic approach for enhanced performance robust control design for VSI. The conditions to find the \mathbf{M} and \mathbf{N} matrices are sufficient conditions. This means that it is also possible to choose the matrices by any other means to find a feasible solution of the LMI and design the controller. However, the performance of this controller may or may not be as good as of the controller designed by the proposed approach. The proposed theorems provide a way to design the controller and of very good performance, as it will be seen in later chapters.

Also the bounds of uncertain parameters derived from the theorems are conservative. This is because of the initial assumption that the deviations in the parameter will be very small as compared to the nominal values. This assumption however, was important for the derivation of the theorem and thus needs abiding by. The controller that will be designed by the proposed method, will actually robustly stabilize the system for uncertainty bounds higher than the ones mentioned in eq. (3-52). This will be observed in the simulation and experimental results in later chapters. With this approach, what will be the actual bounds for which the system will remain stable, is still in open problem. This can be investigated

in a future work. The utility of the theorems can be obtained by trying to obtain higher uncertainty bounds of eq. (3-52) $[\bar{\lambda}_R, \bar{\lambda}_L]$, as much as possible by choosing higher initial uncertainty bounds $[\lambda_R, \lambda_L]$. The resulting controller will robustly stabilize the VSI system for uncertainty range a little higher than eq. (3-52).

3.3.4 Integral control for set-point tracking

A reference tracking controller for the output voltage can be designed by augmenting integral control to the equation given in eq. (3-26). The output filter capacitor voltage v_{cd} & v_{cq} are considered as output $y(t)$ of the system, which is required to track the specified reference input $r(t)$. Now define a new state vector $v(t)$ as the integral of the error as following:

$$\dot{v}(t) = e(t) = r(t) - y(t) = r(t) - \mathbf{C}\mathbf{x}(t) \quad (3-66)$$

with
$$v(t) = \int_0^t e(t) d\tau \quad (3-67)$$

Provided that eq. (3-68) holds, the reference tracking control law is given by eq. (3-69).

$$\text{rank} \begin{pmatrix} \mathbf{A} & \mathbf{C} \\ \mathbf{B} & \mathbf{0} \end{pmatrix} = n + p \quad (3-68)$$

$$\mathbf{u}(t) = -[\mathbf{K} \quad \mathbf{K}_I] \begin{bmatrix} \hat{\mathbf{x}}(t) \\ \mathbf{v}(t) \end{bmatrix} = -\mathbf{K}\hat{\mathbf{x}}(t) - \mathbf{K}_I \int_0^t e(t) d\tau \quad (3-69)$$

where n and p are the number of states and outputs, respectively. With the integral states augmented in the plant the overall state vector is $\mathbf{x}_{cl}^T(t) = [\mathbf{x}^T(t) \quad \mathbf{v}^T(t)]$. The controller gains in eq. (3-69) will be designed to keep the closed loop system stable (see *remark 3-*

2). Therefore $\dot{\mathbf{x}}_{cl}(t)$ goes to zero with time. This implies $\dot{\mathbf{v}}(t) = \mathbf{e}(t)$ goes to zero with time, accomplishing reference tracking.

Remark 3-2: The estimated states feedback stabilizing controller gain \mathbf{K} is designed using one of the theorems presented earlier. The integral control gain \mathbf{K}_I is designed by an intelligent control design method such that the closed loop system is stable with optimum performance. The integral controller is augmented for reference tracking. Therefore the objective function for optimization will be to achieve fast reference tracking response.

Remark 3-3: To ensure the robustness of the augmented controller a numerical approach is adopted. Consider eq. (3-20) and eq. (3-69), the closed loop state vector coefficient matrix is given as

$$\mathbf{A}_{cl} = \begin{bmatrix} \mathbf{A} - \mathbf{BK} & -\mathbf{BK}_I \\ -\mathbf{C} & \mathbf{0} \end{bmatrix} \quad (3-70)$$

where the augmented state vector is $\mathbf{x}_{cl}^T(t) = [\mathbf{x}^T(t) \quad \mathbf{v}^T(t)]$. For the given load uncertainties in eq. (3-52), the maximum and minimum possible values of R and L are

$$\begin{aligned} R_m &= R_0 - \bar{\lambda}_R \leq R \leq R_0 + \bar{\lambda}_R = R_M \\ L_m &= L_0 - \bar{\lambda}_L \leq L \leq L_0 + \bar{\lambda}_L = L_M \end{aligned} \quad (3-71)$$

The matrix \mathbf{A} of eq. (3-20) changes with the load variations. Let's define a set of \mathbf{A} matrices for all combinations of extrema of R and L , as given in Table 3-1.

Table 3-1: A matrices for all uncertainty extrema combinations.

A	A_0	A_1	A_2	A_3	A_4	A_5	A_6	A_7	A_8
Load resistance	R_0	R_m	R_M	R_0	R_m	R_M	R_0	R_m	R_M
Load inductance	L_0	L_0	L_0	L_m	L_m	L_m	L_M	L_M	L_M

The control law in eq. (3-69) is designed for the nominal load i.e. A_{cl} is Hurwitz for $A = A_0$. Now for $R = R_m$ and hence, for $A = A_1$ if A_{cl} is Hurwitz, then it is Hurwitz for all $R \in [R_0 \ R_m]$. Thus if A_{cl} is Hurwitz with $A = A_i$ for all $i = 0,1,2 \dots 8$, then it is Hurwitz for all load variation in eq. (3-71). This test can be performed after the augmented controller design is complete. If the test fails, K_I is designed again. With this test successful, robustness of the augmented controller is guaranteed.

3.4 Conclusion

The work done in this chapter is summarized in the following points:

- 1- The standalone VSI system with LC filter and RL load of Figure 3.1 was considered in this chapter.
- 2- Using space phasors and abc to dq transformation, a sixth order dynamic model of the system was developed in the rotating dq frame. This dynamic model was then transformed into a MIMO linear state-space form.
- 3- Uncertainties with certain range, were considered in the RL load and were modeled as an additive term to the nominal state coefficient matrix.
- 4- Two novel theorems were derived using the condition on the uncertainty radius of the systems and Sylvester's criterion. These theorems mainly provide a way to

choose the uncertainty coefficient matrices \mathbf{M} and \mathbf{N} , such that a robust controller can be optimally designed.

- 5- The first theorem (*theorem 3-1*), can be used to design a robust controller with the best possible convergence rate of the system.
- 6- The second theorem (*theorem 3-2*), can be used to design a robust controller with a guaranteed convergence rate of the system for a certain range of uncertainties.
- 7- To enable reference tracking of the output voltage, integral controllers are augmented in the stabilizing control law. The integral controller gains will be designed for optimum tracking performance using the intelligent technique DE. This subject is discussed in details in chapter 5.
- 8- In the end a test is presented to establish the robustness of the system with the integral controller augmented.

In the next chapter the grid-connected VSI is considered. Following a similar pattern as of this chapter, new theorems are derived for optimized robust controller design.

CHAPTER 4

GRID-CONNECTED VSI: MODELING AND CONTROL DESIGN

In this chapter the second configuration of the VSI and LC filter system is considered where it is connected to the grid. This configuration has applications in the grid-connected mode of the microgrid. In the first section of this chapter, a mathematical model of this system is developed using the space phasors, in a similar manner as for the standalone configuration. After this in the second section the robust controller is designed for the system.

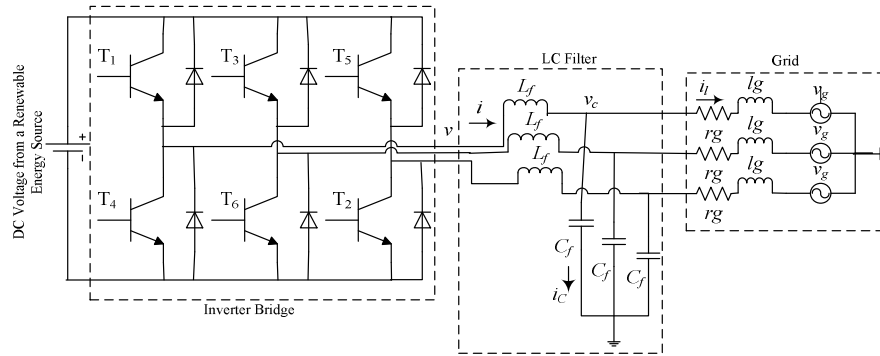


Figure 4.1 The grid connected VSI plus LC filter system.

4.1 Derivation of mathematical model of the grid connected system

The inverter and the LC filter system considered here is shown in Figure 4.1. The following space phasor equations represent the dynamics of the system.

$$\vec{v}(t) - L_f \frac{d\vec{i}(t)}{dt} - \vec{v}_c(t) = 0 \quad (4-1)$$

$$\vec{i}(t) = \vec{i}_c(t) + \vec{i}_l(t) \quad (4-2)$$

$$-\vec{v}_c(t) + r_g \vec{i}_l(t) + l_g \frac{d\vec{i}_l(t)}{dt} + \vec{v}_g(t) = 0 \quad (4-3)$$

Substituting $\vec{v}(t) = v_{dq} e^{j\rho(t)}$, $\vec{i}(t) = i_{dq} e^{j\rho(t)}$, $\vec{v}_c(t) = v_{cdq} e^{j\rho(t)}$, $\vec{i}_l(t) = i_{ldq} e^{j\rho(t)}$ and

$$\vec{v}_g(t) = v_{gdq} e^{j(\omega t + \theta_0)},$$

Eq. (4-1) \Rightarrow

$$v_{dq} e^{j\rho(t)} - L_f \frac{di_{dq} e^{j\rho(t)}}{dt} - v_{cdq} e^{j\rho(t)} = 0$$

$$(v_d + jv_q) e^{j\rho(t)} - L_f \left(\left(\frac{di_d}{dt} + j \frac{di_q}{dt} \right) e^{j\rho(t)} + j\omega (i_d + j i_q) e^{j\rho(t)} \right) - (v_{cd} + jv_{cq}) e^{j\rho(t)} = 0$$

Similarly eq. (4-2) – (4-3) can be worked on and solved for the state derivatives, yielding the dynamic model of the system in eq. (4-4) – (4-9).

$$\frac{di_d}{dt} = \frac{1}{L_f} v_d + \omega i_q - \frac{1}{L_f} v_{cd} \quad (4-4)$$

$$\frac{di_q}{dt} = \frac{1}{L_f} v_q - \omega i_d - \frac{1}{L_f} v_{cq} \quad (4-5)$$

$$\frac{dv_{cd}}{dt} = \frac{1}{C_f} i_d + \omega v_{cq} - \frac{1}{C_f} i_{ld} \quad (4-6)$$

$$\frac{dv_{cq}}{dt} = \frac{1}{C_f} i_q - \omega v_{cd} - \frac{1}{C_f} i_{lq} \quad (4-7)$$

$$\frac{di_{ld}}{dt} = \frac{1}{l_g} v_{cd} - \frac{r_g}{l_g} i_{ld} + \omega i_{lq} - \frac{1}{l_g} v_{gd} \quad (4-8)$$

$$\frac{di_{lq}}{dt} = \frac{1}{l_g} v_{cq} - \frac{r_g}{l_g} i_{lq} - \omega i_{ld} - \frac{1}{l_g} v_{gq} \quad (4-9)$$

where $i_d, i_q, v_d, v_q, v_{cd}, v_{cq}, i_{ld}, i_{lq}, v_{gd}$ and v_{gq} are dq components of the output current and output voltage of the inverter, capacitor voltage in the LC filter, the current injected to the grid and the grid voltage respectively. Filter inductance and capacitance are L_f and C_f and line resistance and inductance are r_g and l_g respectively.

4.2 Controller Design for the grid-connected system

Considering the LTI state-space uncertain plant model as following.

$$\dot{\mathbf{x}}(t) = (\mathbf{A} + \Delta\mathbf{A})\mathbf{x}(t) + \mathbf{B}\mathbf{u}(t) + \mathbf{B}_d\mathbf{d}(t) \quad (4-10)$$

$$\mathbf{y}(t) = \mathbf{C}\mathbf{x}(t) \quad (4-11)$$

where $\mathbf{x}(t) \in \mathbb{R}^n$, $\mathbf{y}(t) \in \mathbb{R}^p$, $\mathbf{u}(t) \in \mathbb{R}^m$ and $\mathbf{d}(t) \in \mathbb{R}^q$ are the state, output, control input and disturbance input vectors of the system respectively. The system constant matrices are $\mathbf{A} \in \mathbb{R}^{n \times n}$, $\mathbf{B} \in \mathbb{R}^{n \times m}$, $\mathbf{B}_d \in \mathbb{R}^{n \times q}$ and $\mathbf{C} \in \mathbb{R}^{p \times n}$, such that the pair (\mathbf{A}, \mathbf{B}) is stabilizable and (\mathbf{A}, \mathbf{C}) is detectable. The uncertainty $\Delta\mathbf{A} = \mathbf{M}\mathbf{\Lambda}\mathbf{N}$ where $\mathbf{\Lambda}^T\mathbf{\Lambda} \leq \mathbf{I}$. The mathematical model of the VSI system developed in eq. (4-4) – (4-9) can be transformed as eq. (4-10) – (4-11). The state variables are $i_d, i_q, v_{cd}, v_{cq}, i_{ld}$ and i_{lq} , while v_d and v_q are the control inputs, v_{gd} and v_{gq} are disturbance inputs and i_{ld} and i_{lq} are the outputs with the following system matrices.

$$\mathbf{A} = \begin{bmatrix} 0 & \omega & -\frac{1}{L_f} & 0 & 0 & 0 \\ -\omega & 0 & 0 & -\frac{1}{L_f} & 0 & 0 \\ \frac{1}{C_f} & 0 & 0 & \omega & -\frac{1}{C_f} & 0 \\ 0 & \frac{1}{C_f} & -\omega & 0 & 0 & -\frac{1}{C_f} \\ 0 & 0 & \frac{1}{l_g} & 0 & -\frac{r_g}{l_g} & \omega \\ 0 & 0 & 0 & \frac{1}{l_g} & -\omega & -\frac{r_g}{l_g} \end{bmatrix}, \mathbf{B} = \begin{bmatrix} \frac{1}{L_f} & 0 \\ 0 & \frac{1}{L_f} \\ 0 & 0 \\ 0 & 0 \\ 0 & 0 \\ 0 & 0 \end{bmatrix}$$

$$\mathbf{B}_d = -\begin{bmatrix} 0 & 0 \\ 0 & 0 \\ 0 & 0 \\ 0 & 0 \\ \frac{1}{l_g} & 0 \\ 0 & \frac{1}{l_g} \end{bmatrix}, \mathbf{C} = \begin{bmatrix} 0 & 0 & 0 & 0 & 1 & 0 \\ 0 & 0 & 0 & 0 & 0 & 1 \end{bmatrix} \quad (4-12)$$

A controller is to be designed to robustly stabilize the system and enable the output $\mathbf{y}(t)$ to track the reference input $\mathbf{r}(t) \in \mathbb{R}^p$. Uncertainties are considered in the line impedance, characterized as following:

$$r_g = r_{g0} + \Delta r_g \quad l_g = l_{g0} + \Delta l_g \quad (4-13)$$

with $-\lambda_R \leq \Delta r_g \leq \lambda_R \quad -\lambda_L \leq \Delta l_g \leq \lambda_L \quad (4-14)$

As discussed in the previous chapter for the standalone case in order to solve for the robust controller gains, the uncertainty coefficient matrices \mathbf{M} and \mathbf{N} are required. These matrices usually are chosen arbitrarily. However it can be easily observed that the choice of these matrices affects the performance of the designed controller. Thus a careful and appropriate choice of these matrices is required to give optimum performance of the controller. Finding \mathbf{M} and \mathbf{N} by trial and error or even by intelligent algorithms method for optimum control

performance, could be computationally highly exhaustive because of the dimensions of these matrices and unknown search space of the elements. The process could take a lot of time and the solution is likely to be just a local optima. Therefore an analytical approach is proposed here to determine these matrices. This approach is derived based on the pattern of uncertainty in the mathematical model of the system. It enables the user to determine the uncertainty coefficient matrices by the selection of just two scalars within a known bounded search space. Thus making the control design process efficient and convenient. The controller is designed systematically and with optimum performance.

4.2.1 Controller for robust stabilization

Now the same robust control theory used for the stabilization control design of standalone system can be applied here [70]. An observer based robust controller can be designed as in eq. (4-15) – (4-16) for a given plant in state space form of eq. (4-10) – (4-11).

$$\dot{\hat{\mathbf{x}}}(t) = \mathbf{A}\hat{\mathbf{x}}(t) + \mathbf{B}\mathbf{u}(t) + \mathbf{L}(\mathbf{y}(t) - \mathbf{C}\hat{\mathbf{x}}(t)) \quad (4-15)$$

$$\mathbf{u}(t) = -\mathbf{K}\hat{\mathbf{x}}(t) \quad (4-16)$$

where $\hat{\mathbf{x}}(t) \in \mathbb{R}^n$ are the states of the observer and the controller and observer gains are \mathbf{K} and \mathbf{L} respectively. The gains are calculated by solving the LMI in eq. (4-17) with the equality constraint in eq. (4-18).

$$\begin{bmatrix} \Phi & \mathbf{B}\hat{\mathbf{K}} & \mathbf{P}\mathbf{M} \\ * & \Psi & \mathbf{R}\mathbf{M} \\ * & * & -\sigma_1\mathbf{I} \end{bmatrix} < \mathbf{0} \quad (4-17)$$

$$\mathbf{P}\mathbf{B} = \mathbf{B}\hat{\mathbf{P}} \quad (4-18)$$

where

$$\Phi = A^T P + PA - \widehat{K}^T B^T - B \widehat{K} + \sigma_1 N^T N + \sigma_2 I,$$

$$\Psi = A^T R + RA - \widehat{L}C - C^T \widehat{L}^T + \sigma_2 I$$

The positive definite matrices $P \in \mathbb{R}^{n \times n}$ and $R \in \mathbb{R}^{n \times n}$, the positive scalars σ_1, σ_2 and matrices $\widehat{P} \in \mathbb{R}^{m \times m}$, $\widehat{K} \in \mathbb{R}^{n \times m}$ and $\widehat{L} \in \mathbb{R}^{p \times n}$ are the LMI variables with $K = \widehat{P}^{-1} \widehat{K}$ and $L = R^{-1} \widehat{L}$. The convergence rate h of the system is given in eq. (4-19) where, the function $\lambda_{max}(M)$, gives the maximum eigenvalue of matrix M .

$$h = \sigma_2 / (2 \max(\lambda_{max}(P), \lambda_{max}(R))) \quad (4-19)$$

Now the following theorem is presented for the application of this method to design an optimum performance robust controller for grid connected VSI.

Theorem 4-1: The grid connected voltage source inverter with an LC filter, given in eq. (4-10) – (4-12), having uncertainty in the line impedance given by eq. (4-13) – (4-14), is stabilized asymptotically with the convergence rate of eq. (4-19), by the controller in eq. (4-15) – (4-16). The controller is designed by solving the LMI in eq. (4-17) with an equality constraint in eq. (4-18) by choosing the uncertainty matrices in eq. (4-20).

$$M = \begin{bmatrix} I_{4 \times 4} & \mathbf{0}_{4 \times 2} \\ \mathbf{0}_{2 \times 4} & \begin{bmatrix} \frac{1}{\mu} & 0 \\ 0 & \frac{1}{\mu} \end{bmatrix} \end{bmatrix}, \quad N = \begin{bmatrix} I_{4 \times 4} & \mathbf{0}_{4 \times 2} \\ \mathbf{0}_{2 \times 4} & \begin{bmatrix} \frac{\mu}{v} & 0 \\ 0 & \frac{\mu}{v} \end{bmatrix} \end{bmatrix} \quad (4-20)$$

where μ and v are two constants given as:

$$\mu = \alpha \bar{\mu}, \quad \bar{\mu} = \frac{l_{g0}^2}{\lambda_L} \quad |\alpha| \leq 1 \quad (4-21)$$

and
$$v = \beta \bar{v} \quad \bar{v} = \sqrt{(1 - \alpha^2)} \left(\frac{l_{g0}^2}{l_{g0}\lambda_R + r_{g0}\lambda_L} \right) \quad |\beta| \leq 1 \quad (4-22)$$

Proof: The uncertainties in the system given by eq. (4-13) – (4-14) \Rightarrow eq. (4-10) – (4-12),

ΔA can be written as:

$$\Delta A = \begin{bmatrix} 0 & 0 & 0 & 0 & 0 & 0 \\ 0 & 0 & 0 & 0 & 0 & 0 \\ 0 & 0 & 0 & 0 & 0 & 0 \\ 0 & 0 & 0 & 0 & 0 & 0 \\ 0 & 0 & \bar{\delta}_1 & 0 & -\bar{\delta}_2 & 0 \\ 0 & 0 & 0 & \bar{\delta}_1 & 0 & -\bar{\delta}_2 \end{bmatrix} \quad (4-23)$$

where
$$\bar{\delta}_1 = -\frac{\Delta l_g}{l_{g0}(l_{g0} + \Delta l_g)} = -\frac{\Delta l_g}{l_{g0}l_g} \cong -\frac{\Delta l_g}{l_{g0}^2} \quad (4-24)$$

$$\bar{\delta}_2 = \frac{l_{g0}\Delta r_g - r_{g0}\Delta l_g}{l_{g0}l_g} \cong \frac{l_{g0}\Delta r_g - r_{g0}\Delta l_g}{l_{g0}^2} \quad (4-25)$$

Now reordering ΔA in the form of \mathbf{MAN} .

$$\Delta A = \begin{bmatrix} 1 & 0 & 0 & 0 & 0 & 0 \\ 0 & 1 & 0 & 0 & 0 & 0 \\ 0 & 0 & 1 & 0 & 0 & 0 \\ 0 & 0 & 0 & 1 & 0 & 0 \\ 0 & 0 & 0 & 0 & \frac{1}{\mu} & 0 \\ 0 & 0 & 0 & 0 & 0 & \frac{1}{\mu} \end{bmatrix} \begin{bmatrix} 0 & 0 & 0 & 0 & 0 & 0 \\ 0 & 0 & 0 & 0 & 0 & 0 \\ 0 & 0 & 0 & 0 & 0 & 0 \\ 0 & 0 & 0 & 0 & 0 & 0 \\ 0 & 0 & \mu\bar{\delta}_1 & 0 & -v\bar{\delta}_2 & 0 \\ 0 & 0 & 0 & \mu\bar{\delta}_1 & 0 & -v\bar{\delta}_2 \end{bmatrix} \begin{bmatrix} 1 & 0 & 0 & 0 & 0 & 0 \\ 0 & 1 & 0 & 0 & 0 & 0 \\ 0 & 0 & 1 & 0 & 0 & 0 \\ 0 & 0 & 0 & 1 & 0 & 0 \\ 0 & 0 & 0 & 0 & \frac{\mu}{v} & 0 \\ 0 & 0 & 0 & 0 & 0 & \frac{\mu}{v} \end{bmatrix} \quad (4-26)$$

For the LMI to be applicable Λ should be such that $\Lambda^T \Lambda \leq I$. With $\delta_1 = \mu\bar{\delta}_1$ and $\delta_2 = v\bar{\delta}_2$,

consider the following.

$$\Lambda^T \Lambda = \begin{bmatrix} 0 & 0 & 0 & 0 & 0 & 0 \\ 0 & 0 & 0 & 0 & 0 & 0 \\ 0 & 0 & 0 & 0 & \delta_1 & 0 \\ 0 & 0 & 0 & 0 & 0 & \delta_1 \\ 0 & 0 & 0 & 0 & -\delta_2 & 0 \\ 0 & 0 & 0 & 0 & 0 & -\delta_2 \end{bmatrix} \begin{bmatrix} 0 & 0 & 0 & 0 & 0 & 0 \\ 0 & 0 & 0 & 0 & 0 & 0 \\ 0 & 0 & 0 & 0 & 0 & 0 \\ 0 & 0 & 0 & 0 & 0 & 0 \\ 0 & 0 & \delta_1 & 0 & -\delta_2 & 0 \\ 0 & 0 & 0 & \delta_1 & 0 & -\delta_2 \end{bmatrix} \leq I \quad (4-27)$$

$$\Lambda^T \Lambda = \begin{bmatrix} 0 & 0 & 0 & 0 & 0 & 0 \\ 0 & 0 & 0 & 0 & 0 & 0 \\ 0 & 0 & \delta_1^2 & 0 & -\delta_1 \delta_2 & 0 \\ 0 & 0 & 0 & \delta_1^2 & 0 & -\delta_1 \delta_2 \\ 0 & 0 & -\delta_1 \delta_2 & 0 & \delta_2^2 & 0 \\ 0 & 0 & 0 & -\delta_1 \delta_2 & 0 & \delta_2^2 \end{bmatrix} \leq \mathbf{I} \quad (4-28)$$

$$\text{or } \Gamma = \mathbf{I} - \Lambda^T \Lambda = \begin{bmatrix} 1 & 0 & 0 & 0 & 0 & 0 \\ 0 & 1 & 0 & 0 & 0 & 0 \\ 0 & 0 & 1 - \delta_1^2 & 0 & \delta_1 \delta_2 & 0 \\ 0 & 0 & 0 & 1 - \delta_1^2 & 0 & \delta_1 \delta_2 \\ 0 & 0 & \delta_1 \delta_2 & 0 & 1 - \delta_2^2 & 0 \\ 0 & 0 & 0 & \delta_1 \delta_2 & 0 & 1 - \delta_2^2 \end{bmatrix} \geq \mathbf{0} \quad (4-29)$$

Using the Sylvester's criterion for positive definiteness, $\Gamma \geq 0$ if and only if all of its principal minors are positive. Say the principal minors of Γ are P_i for $i = 1, 2, 3 \dots 6$. Clearly P_1, P_2 and P_4 are positive as following.

$$P_1 = 1 > 0 \quad P_2 = 1 > 0 \quad P_4 = (1 - \delta_1^2)^2 > 0 \quad (4-30)$$

For the rest consider the following.

$$P_3 = 1 - \delta_1^2 = 1 - \left(-\mu \frac{\Delta l_g}{l_{g0}^2} \right)^2 \quad (4-31)$$

$$\text{Say } \mu = \alpha \bar{\mu} = \alpha \frac{l_{g0}^2}{\lambda_L} \Rightarrow P_3 = 1 - \left(\alpha \frac{\Delta l_g}{\lambda_L} \right)^2 = 1 - \alpha^2 \frac{\Delta l_g^2}{\lambda_L^2} \quad (4-32)$$

$$\text{If } |\alpha| \leq 1 \Rightarrow P_3 \geq 0. \quad (4-33)$$

Similarly consider, the fifth principal minor P_5 .

$$P_5 = \begin{vmatrix} 1 & 0 & 0 & 0 & 0 \\ 0 & 1 & 0 & 0 & 0 \\ 0 & 0 & 1 - \delta_1^2 & 0 & \delta_1 \delta_2 \\ 0 & 0 & 0 & 1 - \delta_1^2 & 0 \\ 0 & 0 & \delta_1 \delta_2 & 0 & 1 - \delta_2^2 \end{vmatrix} = \begin{vmatrix} 1 - \delta_1^2 & 0 & \delta_1 \delta_2 \\ 0 & 1 - \delta_1^2 & 0 \\ \delta_1 \delta_2 & 0 & 1 - \delta_2^2 \end{vmatrix} \quad (4-34)$$

$$P_5 = (1 - \delta_1^2)[(1 - \delta_1^2)(1 - \delta_2^2) - \delta_1^2 \delta_2^2] \quad (4-35)$$

$$P_5 = (1 - \delta_1^2)(1 - \delta_1^2 - \delta_2^2) = (1 - \delta_1^2)^2 - \delta_2^2(1 - \delta_1^2) = P_3^2 - \delta_2^2 P_3 \quad (4-36)$$

If $P_3 - \delta_2^2 \geq 0$ or $P_3 \geq \delta_2^2 \Rightarrow P_5 \geq 0$. Now consider,

$$P_3 \geq \delta_2^2 \Rightarrow v^2 \left(\frac{l_{g0}\Delta r_g - r_{g0}\Delta l_g}{l_{g0}^2} \right)^2 \leq 1 - \alpha^2 \frac{\Delta l_g^2}{\lambda_L^2} \quad (4-37)$$

$$v^2 \leq \left(1 - \alpha^2 \frac{\Delta l_g^2}{\lambda_L^2} \right) \left(\frac{l_{g0}^2}{l_{g0}\Delta r_g - r_{g0}\Delta l_g} \right)^2 = \left(\frac{\lambda_L^2 - \alpha^2 \Delta l_g^2}{\lambda_L^2} \right) \left(\frac{l_{g0}^2}{l_{g0}\Delta r_g - r_{g0}\Delta l_g} \right)^2 = \Pi \quad (4-38)$$

Now by minimizing Π , the upper bound on v^2 can be obtained. For this $\Delta l_g = -\lambda_L$ and $\Delta r_g = \lambda_R$.

$$v^2 \leq (1 - \alpha^2) \left(\frac{l_{g0}^2}{l_{g0}\lambda_R + r_{g0}\lambda_L} \right)^2 \quad (4-39)$$

$$\text{or with } |\beta| \leq 1 \quad v^2 = \beta^2 (1 - \alpha^2) \left(\frac{l_{g0}^2}{l_{g0}\lambda_R + r_{g0}\lambda_L} \right)^2 \quad (4-40)$$

$$v = \beta \sqrt{(1 - \alpha^2)} \left(\frac{l_{g0}}{l_{g0}\lambda_R + r_{g0}\lambda_L} \right) = \beta \bar{v} \quad (4-41)$$

In a similar manner it can be proved that the sixth principal minor $P_6 \geq 0$. This completes the proof. □

Remark 4-1: *Theorem 4-1* introduces two tuning parameters α and β in the control design method. These parameters define the uncertainty coefficient matrices \mathbf{M} and \mathbf{N} and hence the performance of the controller. The performance of the controller can be optimized using any intelligent method by tuning only these two parameters within the search range given by eq. (4-21) and (4-22). Criterion for optimum performance could be maximizing the system convergence rate, closeness to either the target eigenvalues or damping ratios or a combination of both based on specifications of the required transient response.

4.2.2 Robust stability analysis and limits of parameter variations

Similar to the standalone VSI, for the case of grid-connected VSI, *theorem 4-1* provides a method for robust controller design but the uncertainty bounds for which robust stability is guaranteed with certain convergence rate remains unknown. *Theorem 4-2* is presented now to answer this question.

Theorem 4-2: The grid-connected voltage source inverter system with *LC* filter given by the eq. (4-10) – (4-12), is guaranteed to be robustly asymptotically stable with the convergence rate of eq. (4-19), by the control law in eq. (4-15) – (4-16) for all the line impedance uncertainties given by eq. (4-42) – (4-43). The controller gains are obtained by solving the LMI in eq. (4-17) – (4-18) with the uncertainty matrices given in eq. (4-20), where ν is a constant given in eq. (4-22) and μ is another constant given in eq. (4-44) – (4-45).

$$-\bar{\lambda}_R \leq \Delta R \leq \bar{\lambda}_R \quad -\bar{\lambda}_L \leq \Delta L \leq \bar{\lambda}_L \quad (4-42)$$

$$\text{where } \bar{\lambda}_L = \left| \frac{\lambda_L}{\alpha} \right| \quad \text{and} \quad \bar{\lambda}_R = \frac{\lambda_R}{|\beta|\sqrt{(1-\alpha^2)}} + \frac{R_0\lambda_L}{L_0} \left(\frac{1}{|\beta|\sqrt{(1-\alpha^2)}} - \frac{1}{|\alpha|} \right) \quad (4-43)$$

$$\mu = \alpha\bar{\mu}, \quad \bar{\mu} = \frac{L_0^2}{\lambda_L} \quad \underline{\alpha} \leq |\alpha| \leq 1 \quad (4-44)$$

$$\text{where} \quad \underline{\alpha} = \frac{\beta^2}{\left(1 - \frac{\lambda_R L_0}{\lambda_L R_0}\right)^2 + \beta^2} \quad (4-45)$$

Proof: The conditions required for the validity of *theorem 1* can be used to provide the proof for this theorem. Considering eq. (4-31) – (4-33),

$$P_3 = 1 - \alpha^2 \frac{\Delta L_g^2}{\lambda_L^2} \geq 0 \quad (4-46)$$

$$\Rightarrow \quad |\Delta L_g| \leq \left| \frac{\lambda_L}{\alpha} \right| = \bar{\lambda}_L \quad (4-47)$$

This means as long as the magnitude of variation of load inductance is less or equal to $\bar{\lambda}_L$, the conditions in eq. (4-27) and the *theorem 1* remains valid. In other words if eq. (4-47) holds, the condition on uncertainty radius of the system is satisfied i.e. $\mathbf{A}^T \mathbf{A} \leq \mathbf{I}$. Thus $\bar{\lambda}_L$ is the upper bound for the uncertainty in line inductance, which will be greater than or equal to λ_L since $\underline{\alpha} \leq |\alpha| \leq 1$. In a similar manner a condition for variation in line resistance can be derived. Considering eq. (4-29), for the matrix to be positive semi-definite, the diagonal elements must be positive semi-definite. Therefore,

$$1 - \delta_2^2 \geq 0 \quad (4-48)$$

$$1 - v^2 \left(\frac{l_{g0}\Delta r_g - r_{g0}\Delta l_g}{l_{g0}^2} \right)^2 \geq 0 \quad (4-49)$$

The condition in eq. (4-49) should hold for all possible Δr_g and Δl_g . The worst case is when the negative term is maximum. This occurs when the difference $l_{g0}\Delta r_g - r_{g0}\Delta l_g$ is maximum. For this, eq. (4-47) implies in eq. (4-49),

$$|v| \left| l_{g0}\Delta r_g + r_{g0} \frac{\lambda_L}{|\alpha|} \right| \leq L_0^2 \quad (4-50)$$

$$\left| l_{g0}\Delta r_g + r_{g0} \frac{\lambda_L}{|\alpha|} \right| \leq |l_{g0}\Delta r_g| + \left| r_{g0} \frac{\lambda_L}{|\alpha|} \right| \leq \frac{l_{g0}^2}{|v|} \quad (4-51)$$

$$|\Delta r_g| \leq \frac{l_{g0}}{|v|} - \frac{r_{g0}\lambda_L}{l_{g0}|\alpha|} \quad (4-52)$$

Substituting v from eq. (4-22),

$$|\Delta r_g| \leq \frac{l_{g0}\lambda_R + r_{g0}\lambda_L}{l_{g0}|\beta|\sqrt{(1-\alpha^2)}} - \frac{r_{g0}\lambda_L}{l_{g0}|\alpha|} \quad (4-53)$$

or

$$|\Delta r_g| \leq \frac{\lambda_R}{|\beta|\sqrt{(1-\alpha^2)}} + \frac{r_{g0}\lambda_L}{l_{g0}} \left(\frac{1}{|\beta|\sqrt{(1-\alpha^2)}} - \frac{1}{|\alpha|} \right) = \bar{\lambda}_R \quad (4-54)$$

where $\bar{\lambda}_R$ is the upper bound on the line resistance uncertainty. Since $|\alpha| \leq 1$, $\bar{\lambda}_R$ tends to be negative as α becomes small. Thus a lower bound on α must be enforced for $\bar{\lambda}_R$ to remain nonnegative, which is given in eq. (4-45). This condition allows the variation in the magnitude of uncertainty of line resistance up to $\bar{\lambda}_R$ for robust stability with guaranteed convergence rate. An interesting thing to observe from eq. (4-47) and eq. (4-54) is that as α decreases, $\bar{\lambda}_L$ increases, while $\bar{\lambda}_R$ decreases and vice versa. Thus α acts as a tuning parameter for the controller to provide a tradeoff between allowable variations in line resistance or inductance. For β , $\bar{\lambda}_R$ is inversely related to it, thus its smaller values would yield bigger allowable variations in the line resistance. This completes the proof. \square

4.2.3 Integral control for set-point tracking

To control the output power of the inverter, a tracking controller for the output current is designed. The output real and reactive powers in terms of the dq components are given as following.

$$P_0 = \frac{3}{2}(v_{gd}i_{ld} + v_{gq}i_{lq}) \quad (4-55)$$

$$Q_0 = \frac{3}{2}(-v_{gd}i_{lq} + v_{gq}i_{ld}) \quad (4-56)$$

The grid voltage is known and is assumed as $[v_{gd} \ v_{gq}] = [V_{GD} \ 0]$, where V_{GD} is the peak level of the three phase sinusoidal grid voltage. The reference currents can then be calculated as,

$$i_{ldref} = \frac{2}{3V_{GD}}P_{ref} \quad (4-57)$$

$$i_{lqref} = -\frac{2}{3V_{GD}}Q_{ref} \quad (4-58)$$

where P_{ref} and Q_{ref} are the reference real and reactive powers. Similar to the standalone

case, the reference tracking controller for the output current of the inverter can be designed by augmenting the stabilizing control law with integral control. With $\mathbf{y}(t) = [i_{ld} \ i_{lq}]$ and $\mathbf{r}(t) = [i_{ldref} \ i_{lqref}]$, the integrator states are defined as following.

$$\dot{\mathbf{v}}(t) = \mathbf{e}(t) = \mathbf{r}(t) - \mathbf{y}(t) = \mathbf{r}(t) - \mathbf{C}\mathbf{x}(t) \quad (4-59)$$

with
$$\mathbf{v}(t) = \int_0^t \mathbf{e}(\tau) d\tau \quad (4-60)$$

If eq. (4-61) holds the controller for reference tracking is obtained by modifying eq. (4-16) as eq. (4-62).

$$\text{rank} \begin{pmatrix} \mathbf{A} & \mathbf{C} \\ \mathbf{B} & \mathbf{0} \end{pmatrix} = n + p \quad (4-61)$$

$$\mathbf{u}(t) = -[\mathbf{K} \ \mathbf{K}_I] \begin{bmatrix} \hat{\mathbf{x}} \\ \mathbf{v} \end{bmatrix} = -\mathbf{K}\hat{\mathbf{x}} - \mathbf{K}_I \int_0^t \mathbf{e}(\tau) d\tau \quad (4-62)$$

As long as this controller stabilizes the closed loop system, the first derivative of augmented state vector, $\dot{\mathbf{x}}_{cl}^T(t) = [\dot{\mathbf{x}}^T(t) \ \dot{\mathbf{v}}^T(t)]$ goes to zero which implies that $\mathbf{e}(t)$ goes to zero.

Remark 4-2: The theorems presented earlier in this chapter are used to design the stabilizing controller gain \mathbf{K} . The integral controller gain \mathbf{K}_I is designed using an intelligent technique. The objective function to find the optimum controller gains will be based on the performance of reference tracking, which is the main function of the integral controller. Moreover, as integral control is augmented in the control law, any step disturbances will be automatically rejected by the controller.

Remark 4-3: With the augmented control law in eq. (4-62), the robustness of the closed loop system requires revisiting. A numerical approach is undertaken for this analysis, similar to the standalone case. Employing the controller of eq. (4-62) to the system in eq.

(4-10) results in the following closed loop \mathbf{A}_{cl} matrix.

$$\mathbf{A}_{cl} = \begin{bmatrix} \mathbf{A} - \mathbf{BK} & -\mathbf{BK}_I \\ -\mathbf{C} & \mathbf{0} \end{bmatrix} \quad (4-63)$$

The states of the augmented system are $\mathbf{x}_{cl}^T = [\mathbf{x}^T \quad \mathbf{v}^T]$. Now from eq. (4-42) – (4-43) which give the range of variation of the line impedance parameters, following are the extrema of the uncertain parameters.

$$\begin{aligned} r_{gm} &= r_{g0} - \bar{\lambda}_R \leq r_g \leq r_{g0} + \bar{\lambda}_R = r_{gM} \\ l_{gm} &= l_{g0} - \bar{\lambda}_L \leq l_g \leq l_{g0} + \bar{\lambda}_L = l_{gM} \end{aligned} \quad (4-64)$$

The plant matrix \mathbf{A} changes with the parameter variations. Table 4-1 lists all the possible combinations of extrema of r_g and l_g and the corresponding \mathbf{A} matrices.

Table 4-1: A matrices for all uncertainty extrema combinations.

\mathbf{A}	\mathbf{A}_0	\mathbf{A}_1	\mathbf{A}_2	\mathbf{A}_3	\mathbf{A}_4	\mathbf{A}_5	\mathbf{A}_6	\mathbf{A}_7	\mathbf{A}_8
r_g	r_{g0}	r_{gm}	r_{gM}	r_{g0}	r_{gm}	r_{gM}	r_{g0}	r_{gm}	r_{gM}
l_g	l_{g0}	l_{g0}	l_{g0}	l_{gm}	l_{gm}	l_{gm}	l_{gM}	l_{gM}	l_{gM}

The designed controller in eq. (4-62) is for the nominal system, means with $\mathbf{A} = \mathbf{A}_0$, \mathbf{A}_{cl} is Hurwitz. Consider the first combination with $r_g = r_{gm}$ and $l_g = l_{g0}$, gives $\mathbf{A} = \mathbf{A}_1$. If \mathbf{A}_{cl} is Hurwitz for this case then its Hurwitz for all $r_g \in [r_{g0} \quad r_{gm}]$. Similarly for all \mathbf{A}_i with $i \in [0 \quad 8]$, if \mathbf{A}_{cl} is Hurwitz, then it is Hurwitz for all uncertainties in the system as given in eq. (4-64). To ensure the robustness of the system with the augmented controller, the above test can be performed. The integral controller gain \mathbf{K}_I is redesigned until the test is successful.

4.3 Conclusion

The work done in this chapter is summarized in the following points:

- 1- The grid-connected VSI system with LC filter of Figure 4.1 was considered in this chapter.
- 2- Using space phasors and abc to dq transformation, a sixth order dynamic model of the system was developed in the rotating dq frame. This dynamic model was then transformed into a MIMO linear state-space form.
- 3- Uncertainties with certain range, were considered in the line resistance and inductance of the grid connection, and were modeled as an additive term to the nominal state coefficient matrix.
- 4- Two novel theorems were derived using the condition on the uncertainty radius of the systems and Sylvester's criterion. These theorems mainly provide a way to choose the uncertainty coefficient matrices \mathbf{M} and \mathbf{N} , such that a robust controller can be designed with enhanced performance.
- 5- The first theorem (*theorem 4-1*), can be used to design a robust controller with the best possible convergence rate of the system.
- 6- The second theorem (*theorem 4-2*), can be used to design a robust controller with a guaranteed convergence rate of the system for a certain range of uncertainties.
- 7- To enable reference tracking of the output power, integral controllers are augmented in the stabilizing control law. The integral controller gains will be designed for optimum tracking performance using the intelligent technique DE. This subject is discussed in details in chapter 5.

8- In the end a test is presented to establish the robustness of the system with the integral controller augmented.

In the next chapter the controller optimization algorithms are presented for both the standalone and grid-connected systems.

CHAPTER 5

CONTROLLER OPTIMIZATION ALGORITHMS

As described in the previous two chapters, the controllers for the standalone and grid connected VSIs can be designed, using the corresponding control design theorems. However, the arbitrary design parameters α and β require optimization in order to achieve optimum performance of the controller in terms of higher convergence rate and uncertainty bounds. The algorithm is referred to as the intelligent robust stabilizer design (IRSD) and is presented in this chapter for both standalone and grid-connected systems. The optimization algorithms are based on differential evolution (DE). DE is an evolutionary computation method which is well known for its excellent performance [76].

Furthermore, for reference tracking the integral controller is augmented in the stabilization control law. The gains of the integral controller are also intelligently designed to give optimum tracking performance. The details of the optimization algorithm for integral controller gains are also presented in this chapter which are also based on DE. For ease of reference it is called the intelligent robust tracker design (IRTD) algorithm. Before going into the details of the IRSD and IRTD algorithms, a brief overview of the differential evolution technique is presented.

5.1 Differential Evolution

A brief overview of the DE technique is presented here. The DE optimization technique comprises of the following components:

5.1.1 Initialization

This is a preliminary step for the implementation of DE. Foremost, the number of parameters n , to be optimized and their range of variations $[p_{min}^j \ p_{max}^j]$ need to be specified, where p_{min}^j and p_{max}^j are the minimum and maximum limits of the range of the j th parameter p^j . Other parameters that must be specified are the maximum number of generations N_G , the population size per generation N_P . The crossover factor FC and mutation factor FM are also declared in the initialization step. After this an initial population is generated according to eq. (5-1), comprising of N_P solutions, and each solution comprising of n parameters.

$$p_{i,j} = p_{min}^j + r(p_{max}^j - p_{min}^j) \quad \forall \begin{cases} i = 1,2,3 \dots N_P \\ j = 1,2,3 \dots n \end{cases} \quad (5-1)$$

Where r is a random number between 0 and 1.

5.1.2 Cost evaluation and search for best solution

Here the objective function for each solution in the generation is calculated. For a minimization problem, the solution in the current generation having the least value of the objective function is called the local best solution. This n-dimensional vector of the best solution is secured from the current generation and is compared with the best solution obtained out of the previous generations called the global best solution. The better of the two becomes the new global best solution.

5.1.3 Mutation

In DE, the first step forward towards the generation of offspring from the initial population is mutation. Here a mutant vector is generated for every solution in the current generation and stored separately. Thus N_p mutant vectors are obtained, where each mutant vector itself is an n dimensional vector. The following formula was used for generating the mutant vector:

$$\mathcal{M}_i^{g+1} = P_{best}^G + F_M(P_{r1}^g + P_{r2}^g) \quad (5-2)$$

where g represents the current generation, \mathcal{M}_i^{g+1} is the mutant vector for the i th solution of the $(g + 1)^{th}$ generation, P_{best}^G is the global best solution and P_{r1}^g, P_{r2}^g are two randomly selected solutions from the g^{th} generation.

5.1.4 Crossover

The crossover operator in DE enhances diversity in the solutions further. By crossover, a trial solution is generated using each solution in the current generation and its corresponding mutant vector. It is controlled by the crossover factor FC. For each parameter in each solution of the generation, a random number r_{ij} is generated and compared with FC. If r_{ij} is less than or equal to FC then $p_{i,j}$ is copied to the trial solution, otherwise $m_{i,j}$ is copied to the trial solution, where $p_{i,j}$ is the j th parameter of the i th solution in the current generation and $m_{i,j}$ is the j th parameter of i th mutant vector. Thus at the end of crossover operation, N_p trial solutions are obtained.

5.1.5 Selection

This is the last step of the DE optimization algorithm. Here each solution in the current generation is compared with its corresponding trial solution. The trial solutions which show lower cost replaces their corresponding original solutions in the current generation. Thus after completion of the selection process the new generation is obtained.

5.1.6 Termination and its Criterion

The DE algorithm can be terminated if the cost function is minimized to the desired value J_d . Apart from this, other stopping criteria may be set such as the maximum number of generation is reached or the best solution does not change for a specified number of generations etc.

5.2 Control design algorithms for standalone system

In this section, the algorithms for control design of the standalone system are described in details by means of flowcharts. First a flowchart that gives the overview of the control design process is given in Figure 5.1. This flowchart describe the major three phases of the algorithm for standalone case; initialization, IRSD algorithm and IRTD algorithm, which are described further in the subsections to follow.

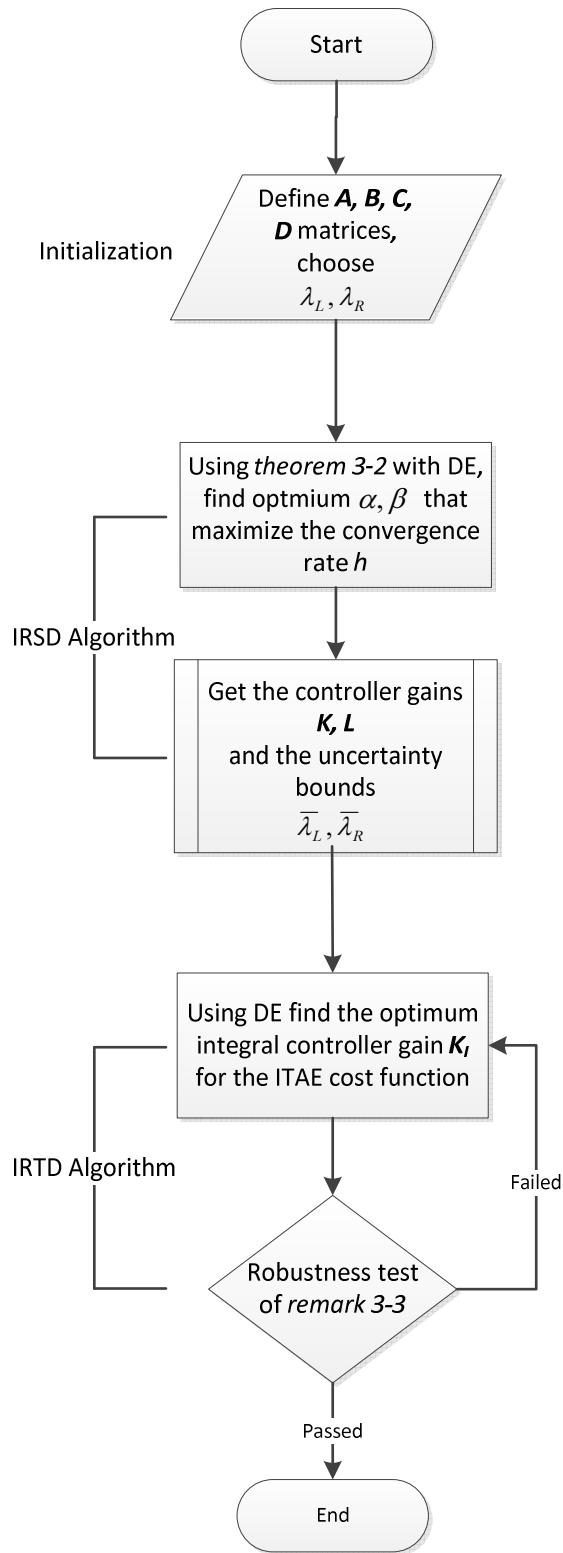


Figure 5.1 Overall control design algorithm for standalone system.

5.2.1 Phase I: Initialization

In this step all the system constant parameters, such as frequency, resistances, inductances, etc. and the system matrices are specified. Also the initial bounds of uncertainty λ_R and λ_L of eq. (3-23) – (3-24) are chosen in this step. The flowchart is shown in Figure 5.2.

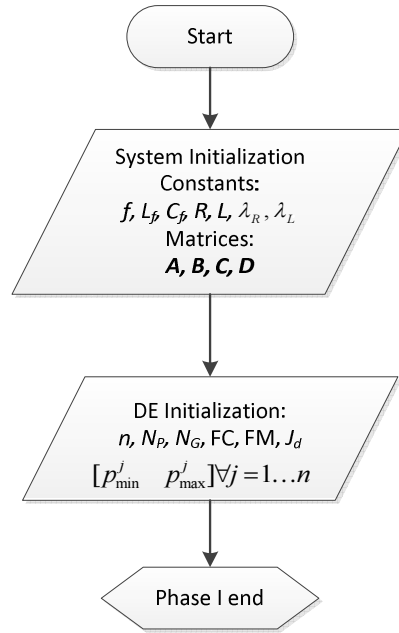


Figure 5.2 Initialization of control design algorithm for standalone case.

5.2.2 Phase II: The IRSD algorithm

In phase two the IRSD algorithm begins where *theorem 3-1* or *theorem 3-2* is used for the robust stabilizing controller design. If it is only required to obtain the best convergence rate, then *theorem 3-1* should be used. However *theorem 3-2* should be used if a guaranteed best convergence rate for some bounds of uncertainties is required. The optimization technique used is DE, however any other technique can also be used. The flowchart is shown in Figure 5.3. *Theorem 3-2* is applied in the illustrated case.

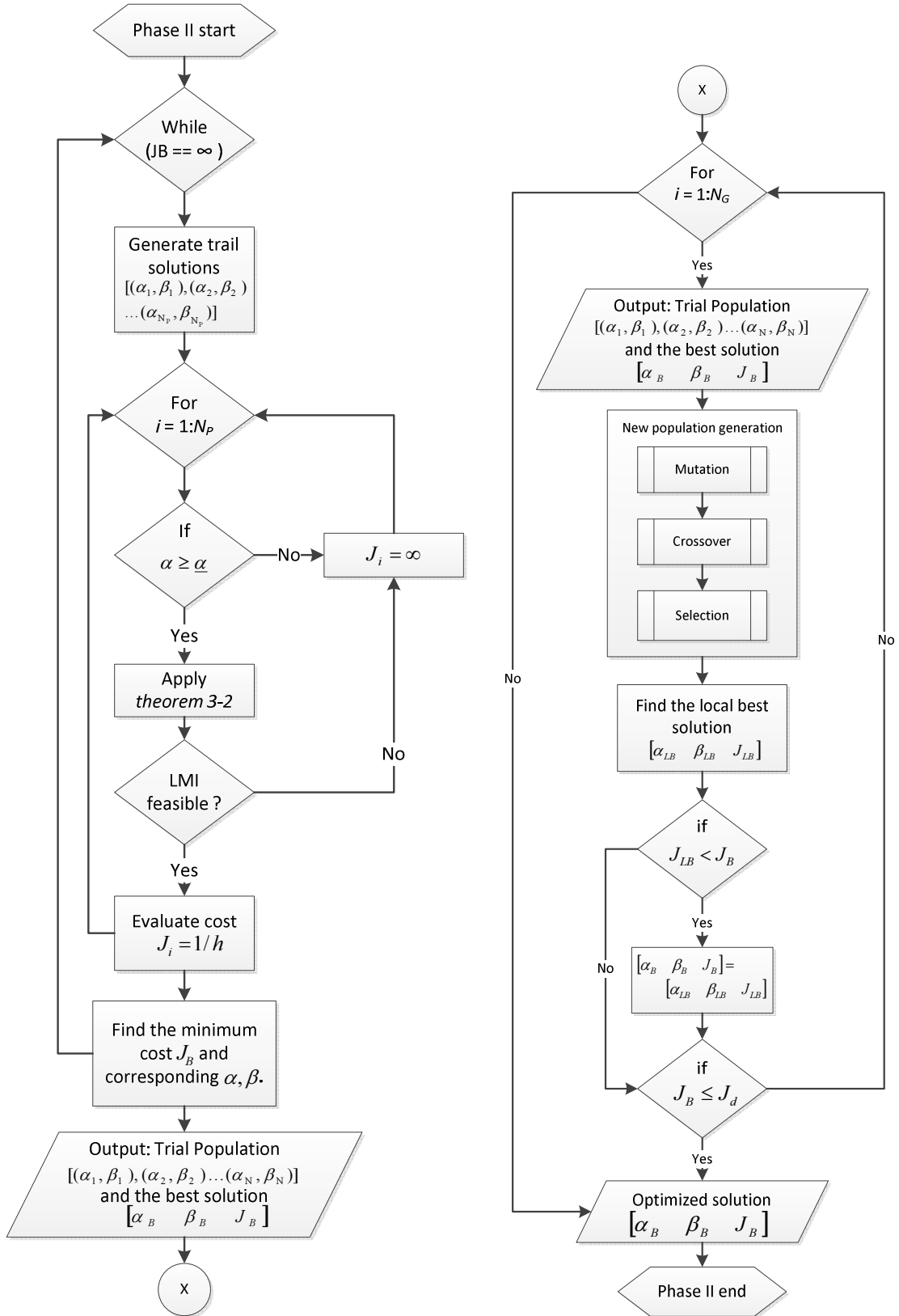


Figure 5.3 IRSD algorithm for standalone case.

The cost function to be minimized is taken as inverse of the convergence rate.

$$J = 1/h \quad (5-3)$$

where the convergence rate h is given in eq. (3-29). The convergence rate is maximized as J is minimized.

5.2.3 Phase III: The IRTD algorithm

The IRTD algorithm begins in the third and last phase. Now the tracking controller K_I is designed based on optimization approach using DE again. For this a simple state-space model based simulation of the closed loop system is implemented in SIMULINK with a cost function of integral time absolute of error (ITAE) of the system, given as following.

$$J = \int t |e(t)| dt \quad (5-4)$$

The tracking controller designed should be tested for stability of the system for given uncertainties as discussed in *remark 3-3*. Until this test is not passed K_I should be designed again. It should be noted that, in case *theorem 3-1* is used $\bar{\lambda}_R$ and $\bar{\lambda}_L$ are chosen by the user to determine the uncertainties extrema. The flowchart is shown in Figure 5.4.

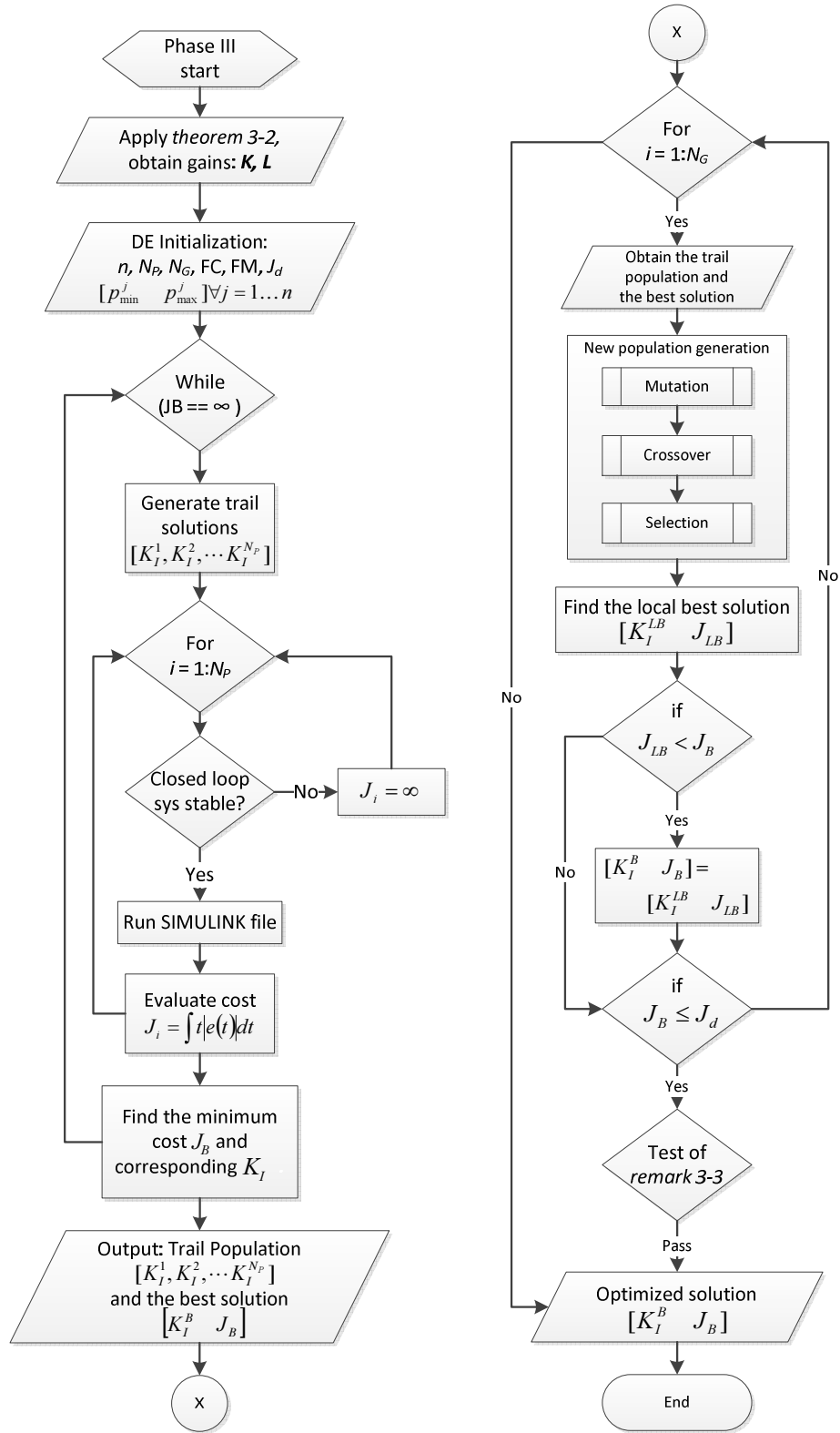


Figure 5.4 IRTD algorithm for standalone case.

5.3 Control design algorithms for grid-connected system

In this section, the algorithms for control design of the grid-connected system are described in details by means of flowcharts. First a flowchart that gives the overview of the control design process is given in Figure 5.5. The Figure 5.5 shows the major three phases of the algorithm for the grid-connected case. These are; initialization, IRSD algorithm and IRTD algorithm. The details of each phase is given in the subsections to follow.

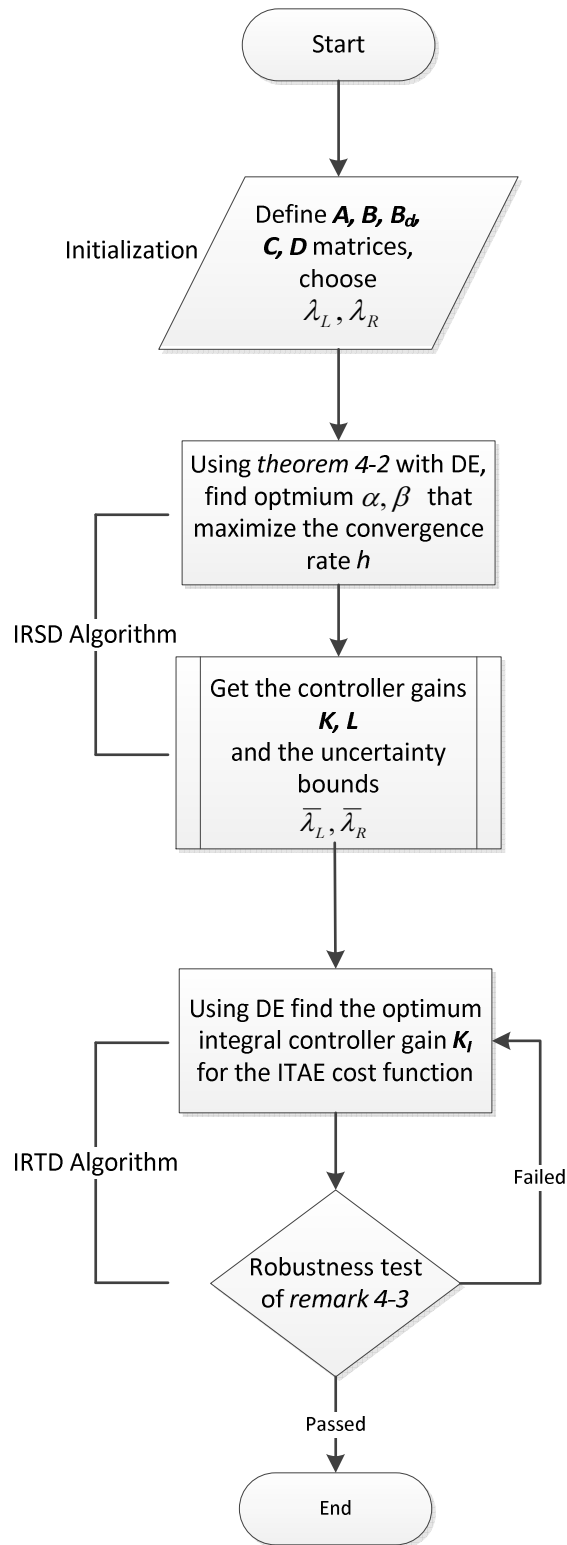


Figure 5.5 Overall control design algorithm for grid-connected system.

5.3.1 Phase I: Initialization

Similar to the standalone case, the constant parameters and matrices of the system are defined in this phase. The initial bounds of uncertainty λ_R and λ_L of eq. (4-13) – (4-14) are also chosen in this step. The flowchart is shown in Figure 5.6.

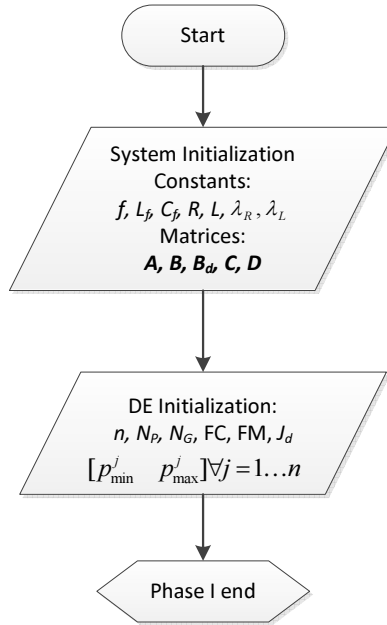


Figure 5.6 Initialization of control design algorithm for grid-connected case.

5.3.2 Phase II: The IRSD algorithm

The IRSD algorithm begins in phase II, where the robust stabilizing controller is design using either *theorem 4-1* or *theorem 4-2*. For the best convergence rate only *theorem 4-1* should be used. *Theorem 4-2* should be used if for some bounds of uncertainties a guaranteed best convergence rate is required. The optimization technique used here is DE again. The flowchart is shown in Figure 5.7. In the illustrated case *theorem 4-2* is applied.

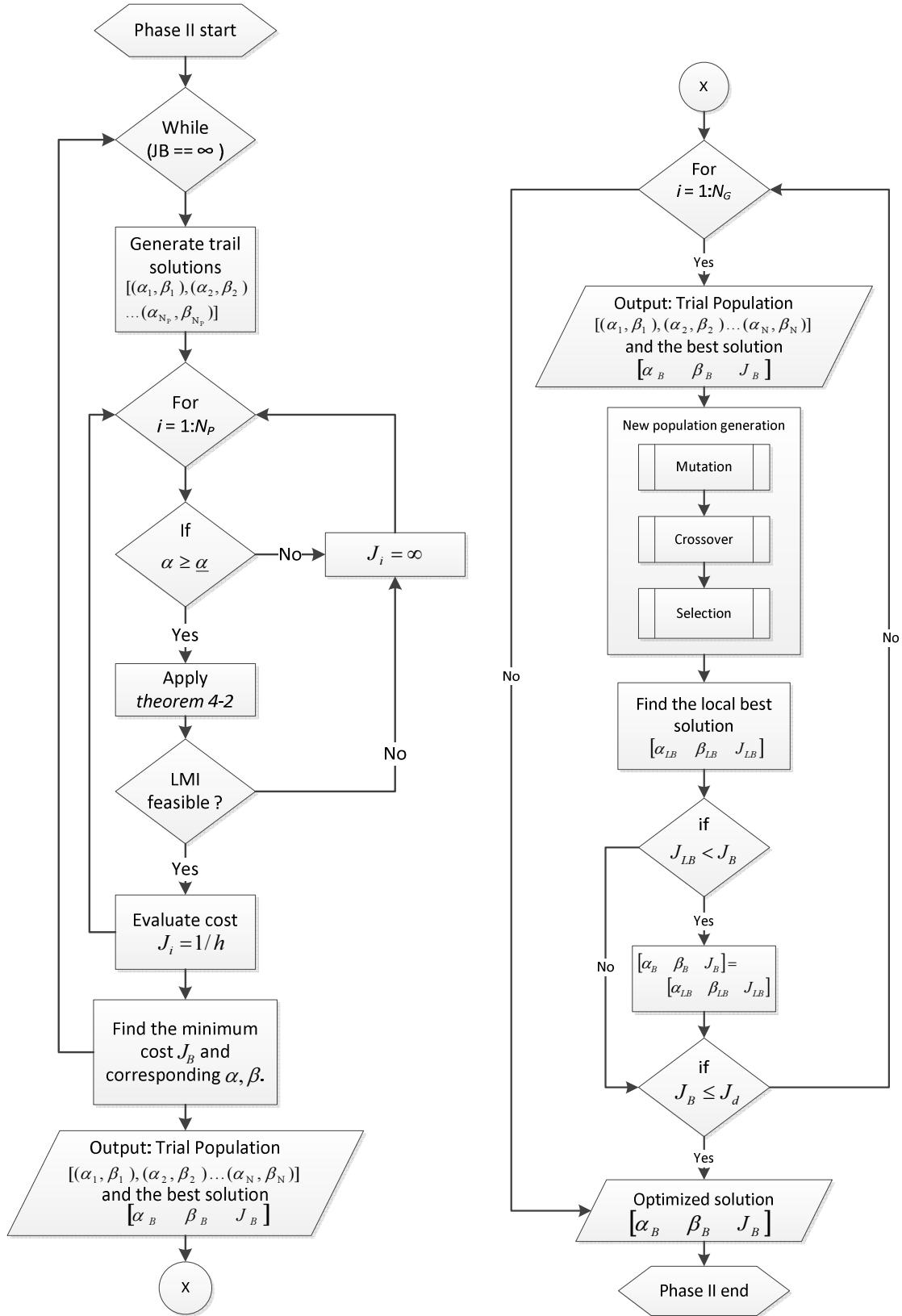


Figure 5.7 IRSD algorithm for grid-connected case.

Similar to the case of standalone system, the cost function to be minimized is taken as inverse of the convergence rate, as following:

$$J = 1/h \quad (5-5)$$

where the convergence rate h is given in eq. (4-29). The convergence rate is maximized as J is minimized. The result of the IRSD algorithm is the optimized α, β values which are used for the optimized robust stabilization controller gains calculation using *theorem 4-2*.

5.3.3 Phase III: The IRTD algorithm

The third and last phase is the IRTD algorithm. The tracking controller K_I is designed now based on the intelligent technique DE. A simple state-space model based simulation of the closed loop system is implemented in SIMULINK for this. The cost function chosen is integral time absolute of error (ITAE) of the system, given as following.

$$J = \int t |e(t)| dt \quad (5-6)$$

The IRTD algorithm obtains the optimized α, β parameters from phase II, to find the robust stabilizing controller gain K and L and then it proceeds to find the last piece in the puzzle, the gain K_I .

The designed tracking controller should also be tested for stability of the system for given uncertainties as discussed in *remark 4-3*. Until this test is not passed K_I should be designed again. Another point to note is that $\bar{\lambda}_R$ and $\bar{\lambda}_L$ result from IRSD if *theorem 4-2* is used. If *theorem 4-1* is used in IRSD, $\bar{\lambda}_R$ and $\bar{\lambda}_L$ are left for the user to choose, to determine the uncertainties extrema. The flowchart is shown in Figure 5.8.

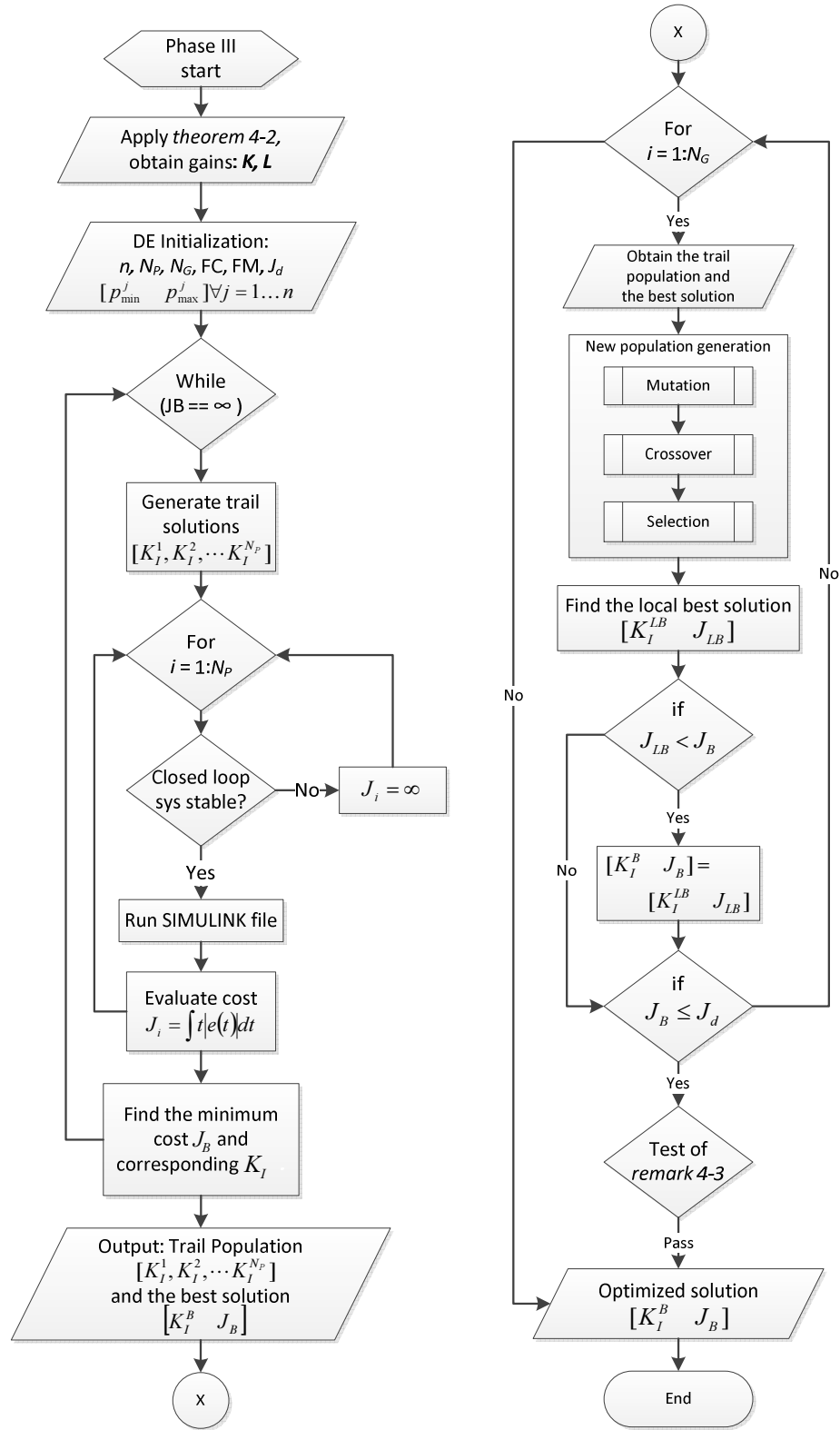


Figure 5.8 IRTD algorithm for grid-connected case.

5.4 Conclusion

This chapter presented a detailed discussion of controller optimization algorithms.

Following points summarize the major components of this chapter.

- 1- A brief overview of the evolutionary algorithm differential evolution.
- 2- Algorithm to design optimum robust stabilization controller for standalone VSI (IRSD for standalone VSI).
- 3- Algorithm to design optimum robust tracking controller for standalone VSI (IRTD for standalone VSI).
- 4- Algorithm to design optimum robust stabilization controller for grid-connected VSI (IRSD for grid-connected VSI).
- 5- Algorithm to design optimum robust tracking controller for grid-connected VSI (IRTD for grid-connected VSI).

The next chapter presents the details of implementation of the proposed controllers, for simulations and experimental work.

CHAPTER 6

PROPOSED CONTROLLER IMPLEMENTATION

In this chapter the details regarding the implementation of the controller are discussed. One of the platforms used for this is MATLAB/SIMULINK, which is used for implementing the optimization algorithms IRSD and IRTD, and to simulate the systems with the proposed controllers. The other platform is the RTDS plus dSPACE DS1103 controller setup. This setup is used to evaluate the performance of the system by RTHIL experimental work.

6.1 MATLAB Implementations

MATLAB is used to accomplish two very important tasks in this work. One is the implementation of the optimization algorithms for both the standalone and grid-connected cases. Second is simulations of the two systems with the proposed controllers to obtain the simulation results under different test cases. The details of each will follow.

6.1.1 Implementation of algorithms

MATLAB programming is used for implementation of all the optimization algorithms. In addition to the standard package some third-party toolboxes were also used/required for the implementation of the algorithms.

For solving the LMIs generally the MATLAB LMI Toolbox is enough. However, the LMI

solved for the proposed controller design method had an equality constraint. To solve the LMI with equality constraint *YALMIP* [77] was used. Another tool known as the *SCILAB* could also be used for this purpose. *SCILAB* is another software used for numerical computation for engineering and scientific applications. The reason of choosing *YALMIP* was that it is a toolbox which is easily integrated with MATLAB. Thus one can use all the functionality of this toolbox from within MATLAB, and avoid the inconvenience of working on another software. To solve the LMI problems more efficiently, some advanced semi-definite programming (SP) solvers were also used. These included *SEDUMI*, *SDPT3* and *MOSEK*. Among these and the built-in MATLAB LMI solver, *MOSEK* [78] was found the most efficient.

For simulation of the system in the standalone and grid-connected modes with their respective proposed controllers, the *SimPowerSys* toolbox was used in the MATLAB/SIMULINK environment. The details will follow in the next subsections.

6.1.2 Implementation of the standalone system

The schematic in Figure 6.1 describes the implementation approach of the proposed controller. The main idea is that the control signals as calculated by eq. (3-69) are used as the modulating signals for the PWM generator which controls the switching of the inverter and all the signals measurements are taken in per unit. This per unit measurement approach with voltage base value equal to $V_{DC}/2$ is equivalent to calculating the modulation signal based an ideal average model of the PMW inverter [75], where V_{DC} is the dc source voltage.

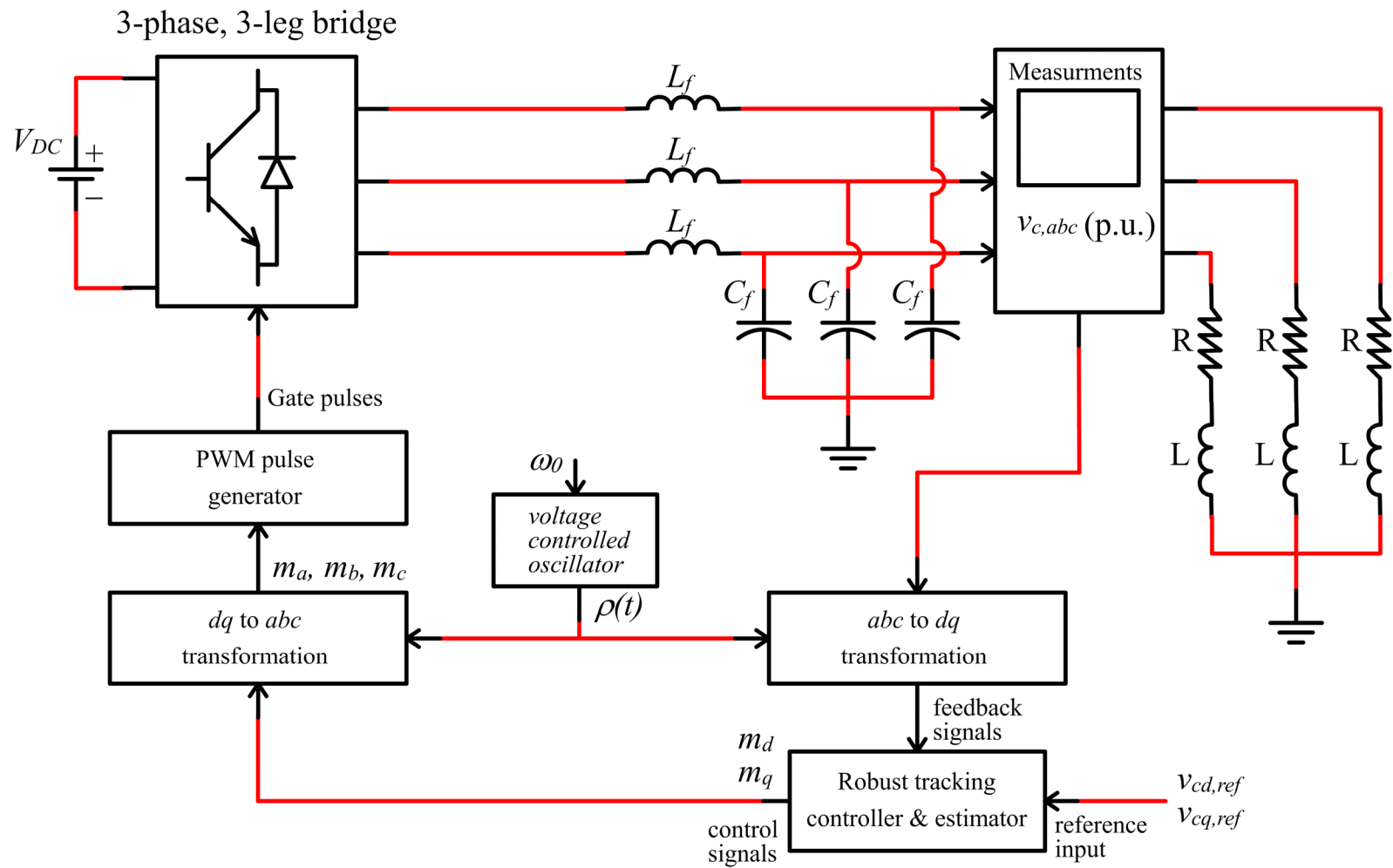


Figure 6.1 Schematic of the standalone VSI system with proposed controller.

$$m_d(t) = \frac{V_{DC}}{2} v_d(t) \quad (6-1)$$

$$m_q(t) = \frac{V_{DC}}{2} v_q(t) \quad (6-2)$$

where m_d and m_q are the dq components of the three phase modulation signals. The three phase sinusoidal modulation signal m_a, m_b and m_c are obtained by transformation from dq to abc frame. The angle $\rho(t)$ required for the transformations is generated with a constant frequency input ω_0 to a simple voltage controller oscillator which is an integrator that resets its state when its output reaches 2π . The gate pulses are generated by the conventional PWM generation method in which pulses are generated by the comparison of the sinusoidal modulation signal with a high frequency triangular wave.

In the figures to follow, the MATLAB schematics for the standalone case are shown. Various MATLAB versions have been used over the years during this work. The schematics presented now are in the latest MATLAB version 2015a.

The standalone VSI system implementation in MATLAB is shown in Figure 6.2. For Implementation of the VSI system plant, the *SimPowerSys* blocks are used. Other blocks are from the general SIMULINK library. Some step function blocks in Figure 6.2 are shown faded. This indicates that these blocks are inactive in the schematic as they are ‘commented out.’ The purpose of keeping these blocks is to generate various reference inputs when the reference tracking test is performed. Similarly a resistance block is connected in parallel to the load resistance and an inductance block is connected in parallel to the load inductance, each through a circuit breaker. These blocks are used to create variations in RL load in the robustness and disturbance tests.

Further, there are some subsystems shown in this schematic. The ‘All Measurement’ block is to collect all the signals in the system and generate the feedback signal for the ‘Robust Controller’ block which has the proposed controller. The schematics of these subsystems are shown in Figure 6.3 and Figure 6.4.

In Figure 6.5 the schematic shown is used for the cost function minimization in the IRTD algorithm for the standalone VSI case. This implementation is based only on control blocks which makes it faster in execution. Thus the optimization process is very fast using this file.

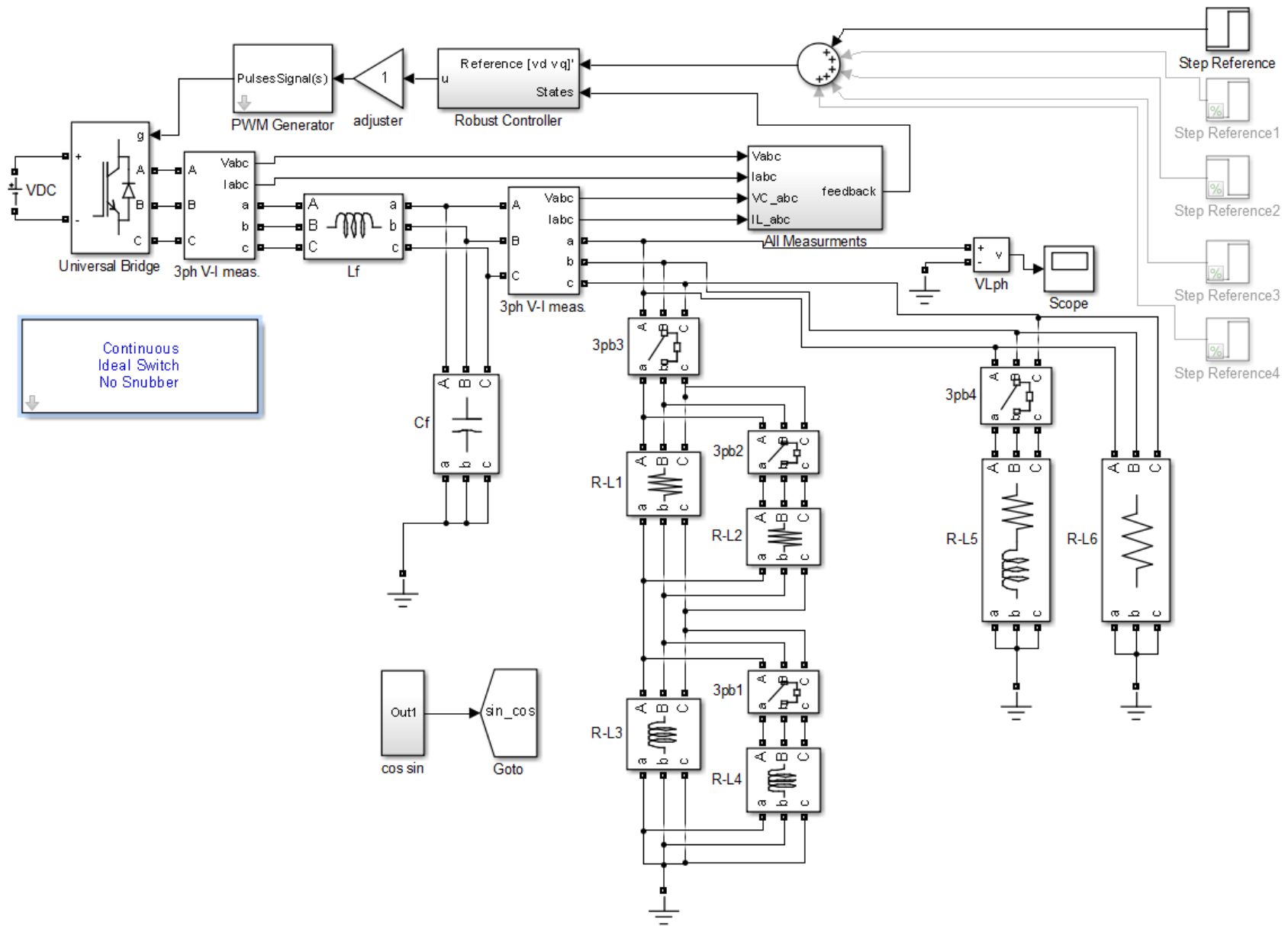


Figure 6.2 MATLAB implementation of standalone VSI system.

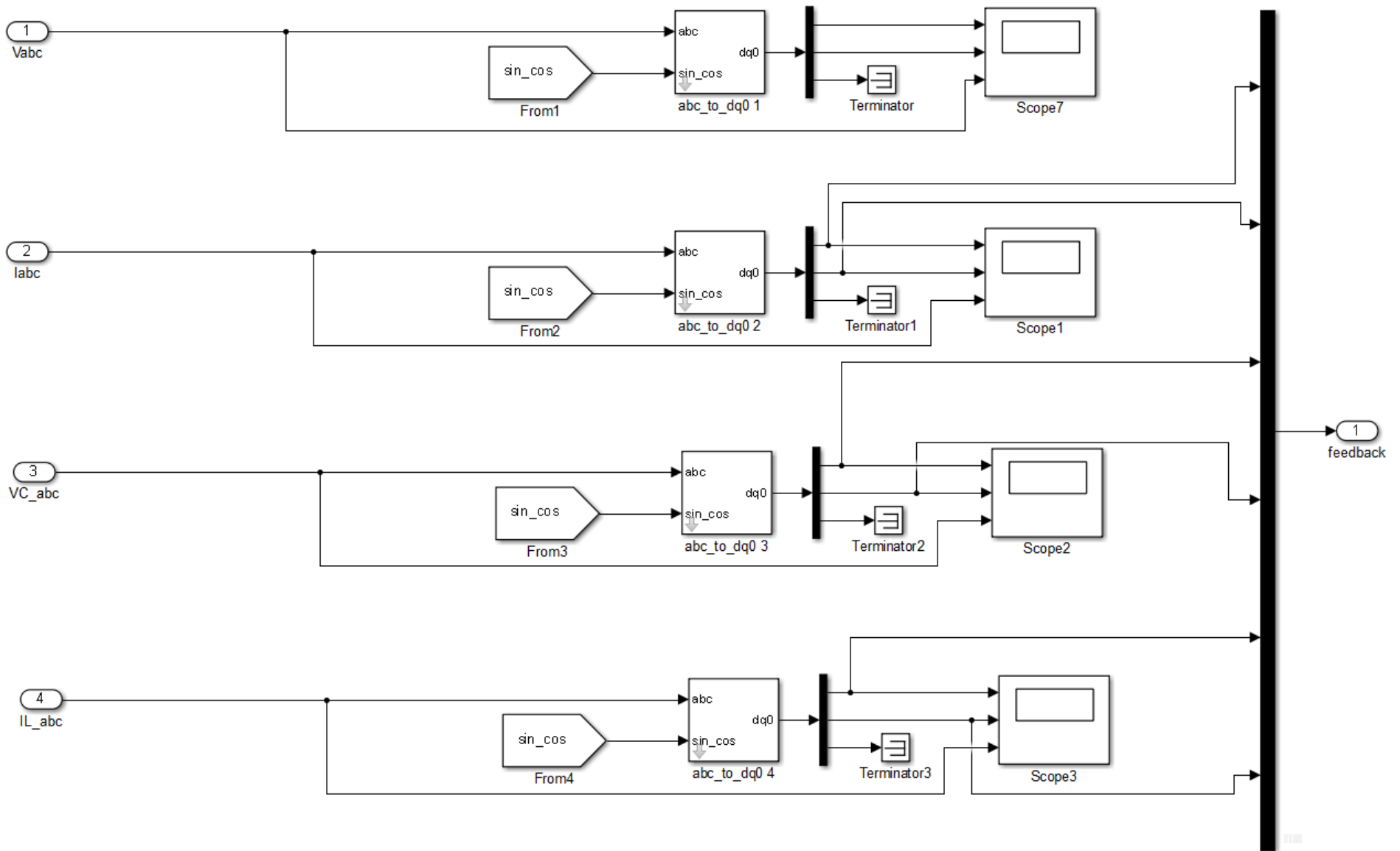


Figure 6.3 Standalone VSI: Schematic of subsystem 'All Measurements.'

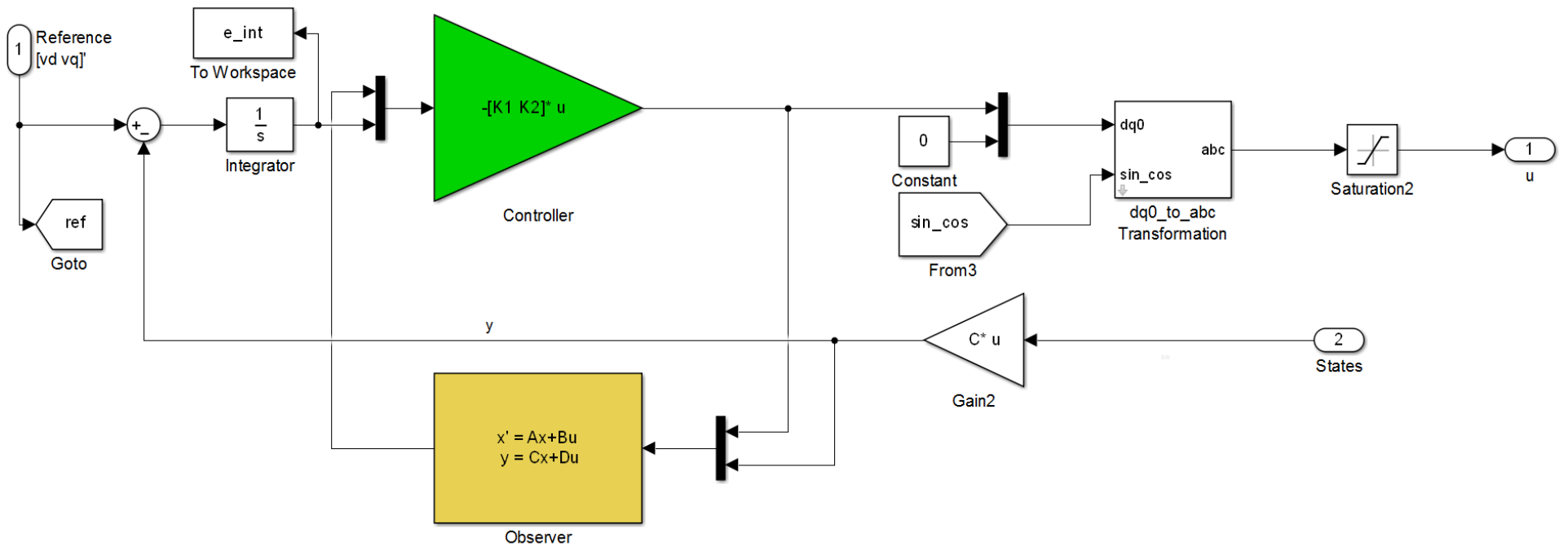


Figure 6.4 Standalone VSI: Schematic of subsystem 'Robust Controller.'

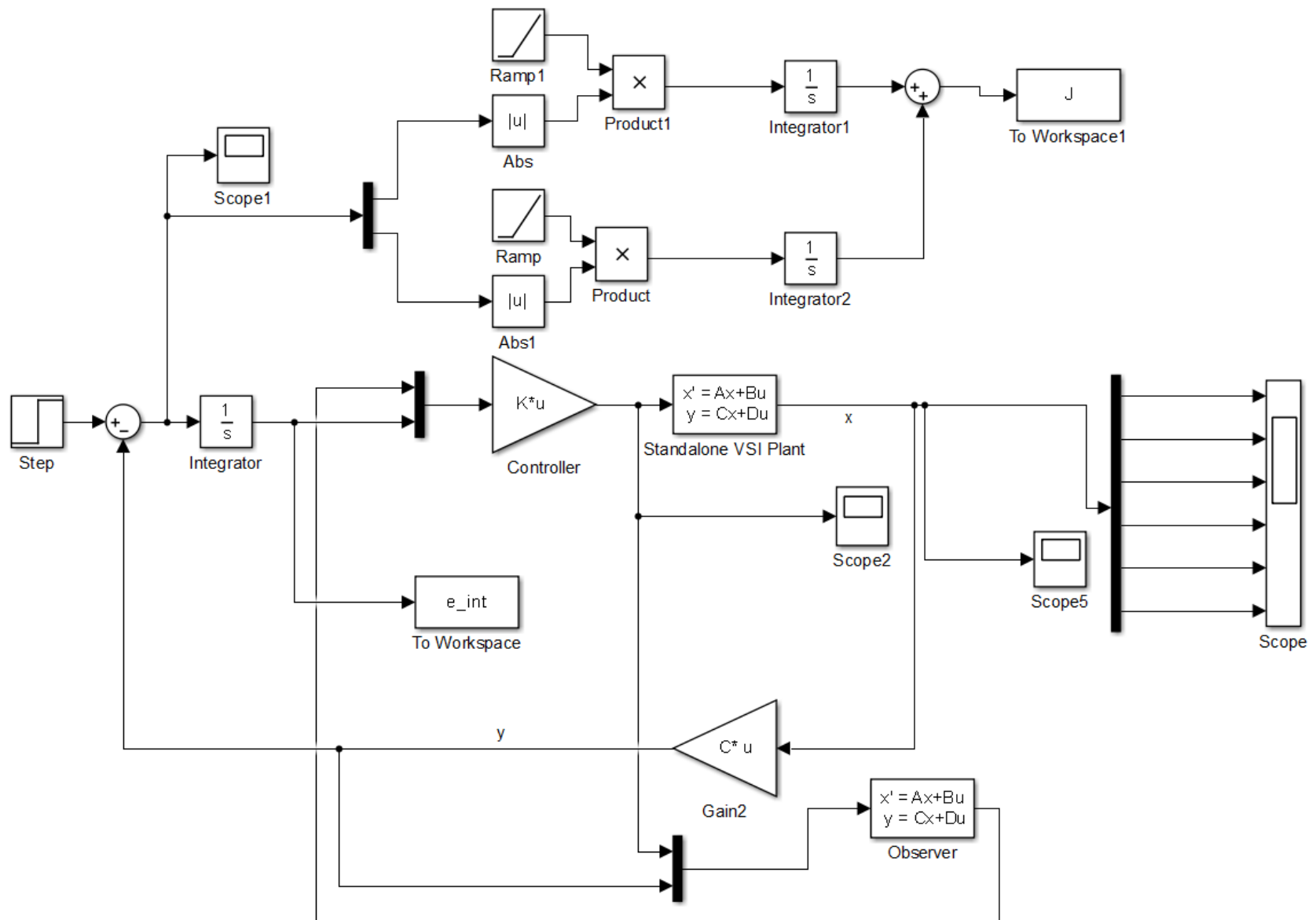


Figure 6.5 Standalone VSI: Schematic of Simulink file for IRTD algorithm.

6.1.3 Implementation of the grid-connected system

The implementation scheme of the proposed controller is presented in Figure 6.6. The power system components are connected as described in Figure 4.1. The measurements are required only for two quantities, one of which is the load current for the controller and other one is the grid voltage which is used by the PLL (phase-locked-loop) to provide the angle $\rho(t)$ for dq transformation.

Similar to the standalone case, with all the measurements taken in per unit and $V_{base} = V_{DC}/2$, the control signals obtained from eq. (4-34) act as the dq components of the three phase modulation signals [75]. The equations of the modulating signals eq. (6-1), (6-2), are same as described for the standalone system, where V_{DC} is the voltage of the dc source. These signals are transformed to abc signals and given to the PWM generator, where they are compared with the triangular waves to generate pulses for the control of the inverter bridge.

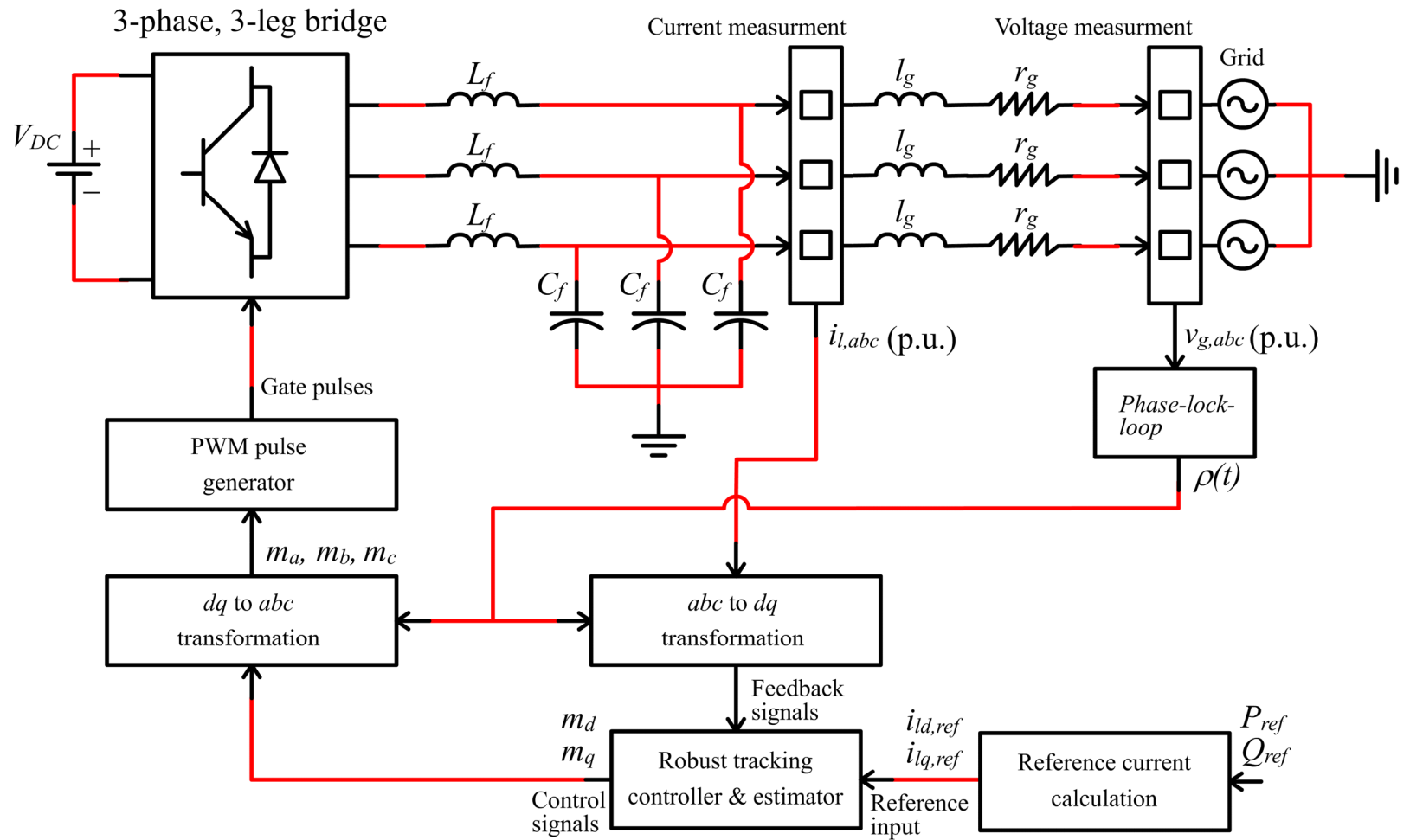


Figure 6.6 Controller implementation for grid connected VSI.

The grid-connected VSI system implementation in MATLAB is shown in Figure 6.8. Again the *SimPowerSys* blocks are used for implementation of the VSI system plant model. Other blocks are form the general SIMULINK library. This schematic gives the overall structure of the system and has few subsystems inside. The ‘P to I’ is to convert power reference to current reference as shown in Figure 6.7. The ‘All Measurement’ block here also is to collect all the signals in the system and generate the feedback signal for the ‘Robust Controller’ in which the controller is implemented. The schematics for these two subsystems are shown in Figure 6.9 and Figure 6.10.

In Figure 6.11 the schematic shown is used for the cost function minimization in the IRTD algorithm for the grid-connected VSI case. The reason for using this implementation for optimization is smaller execution time which makes the optimization process very fast.

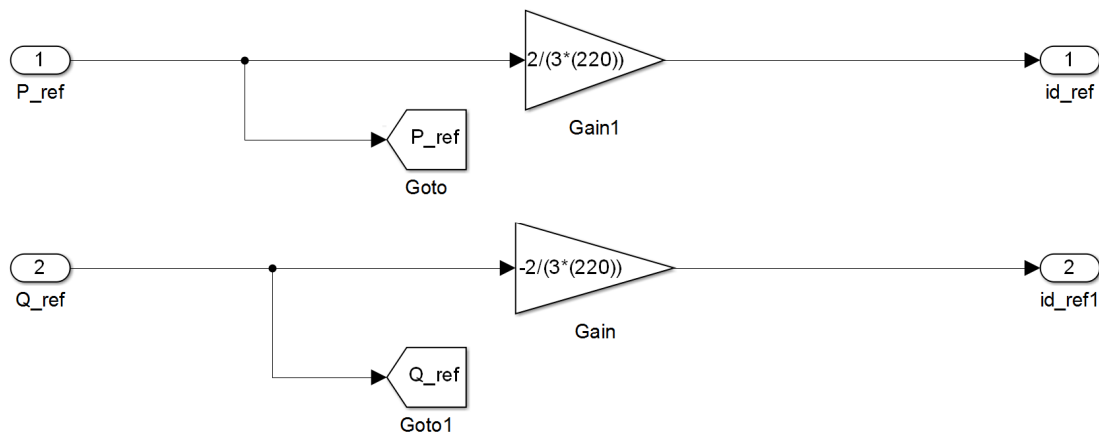


Figure 6.7 Grid-connected VSI: The ‘P to I’ subsystem

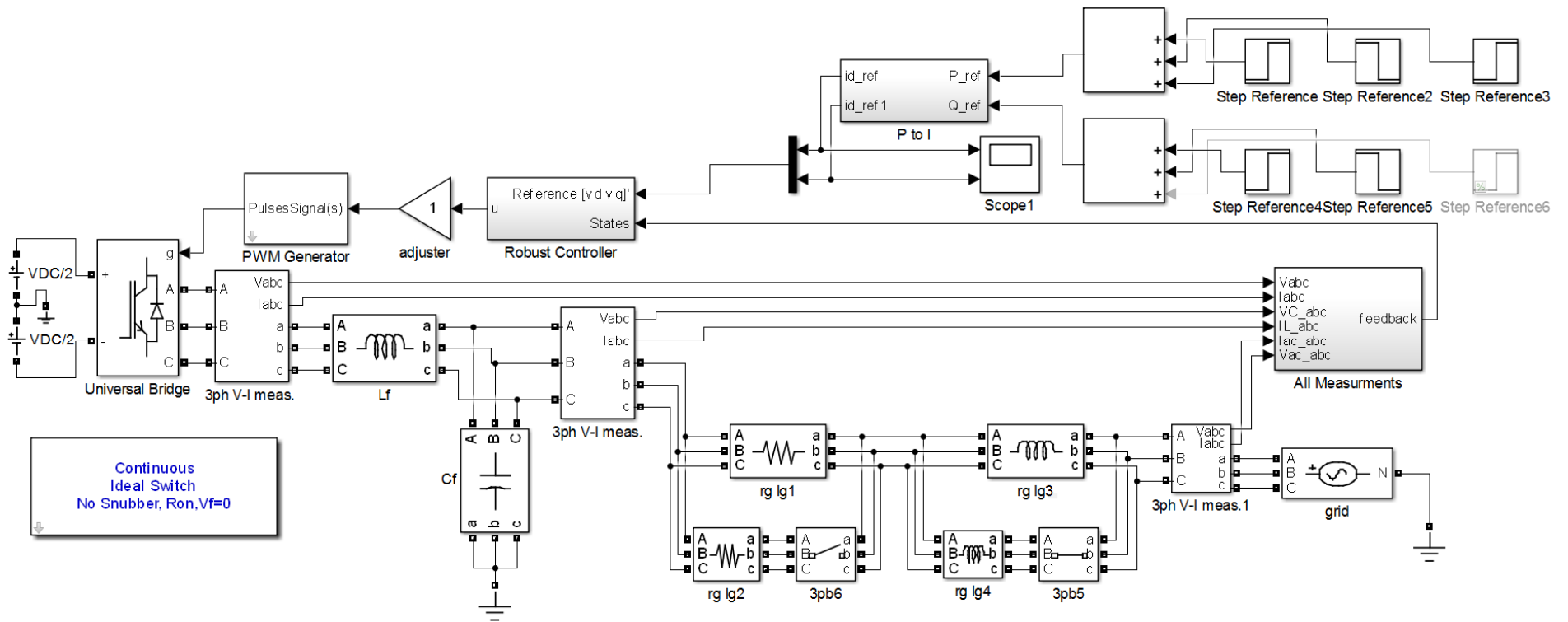


Figure 6.8 MATLAB implementation of grid-connected VSI system.

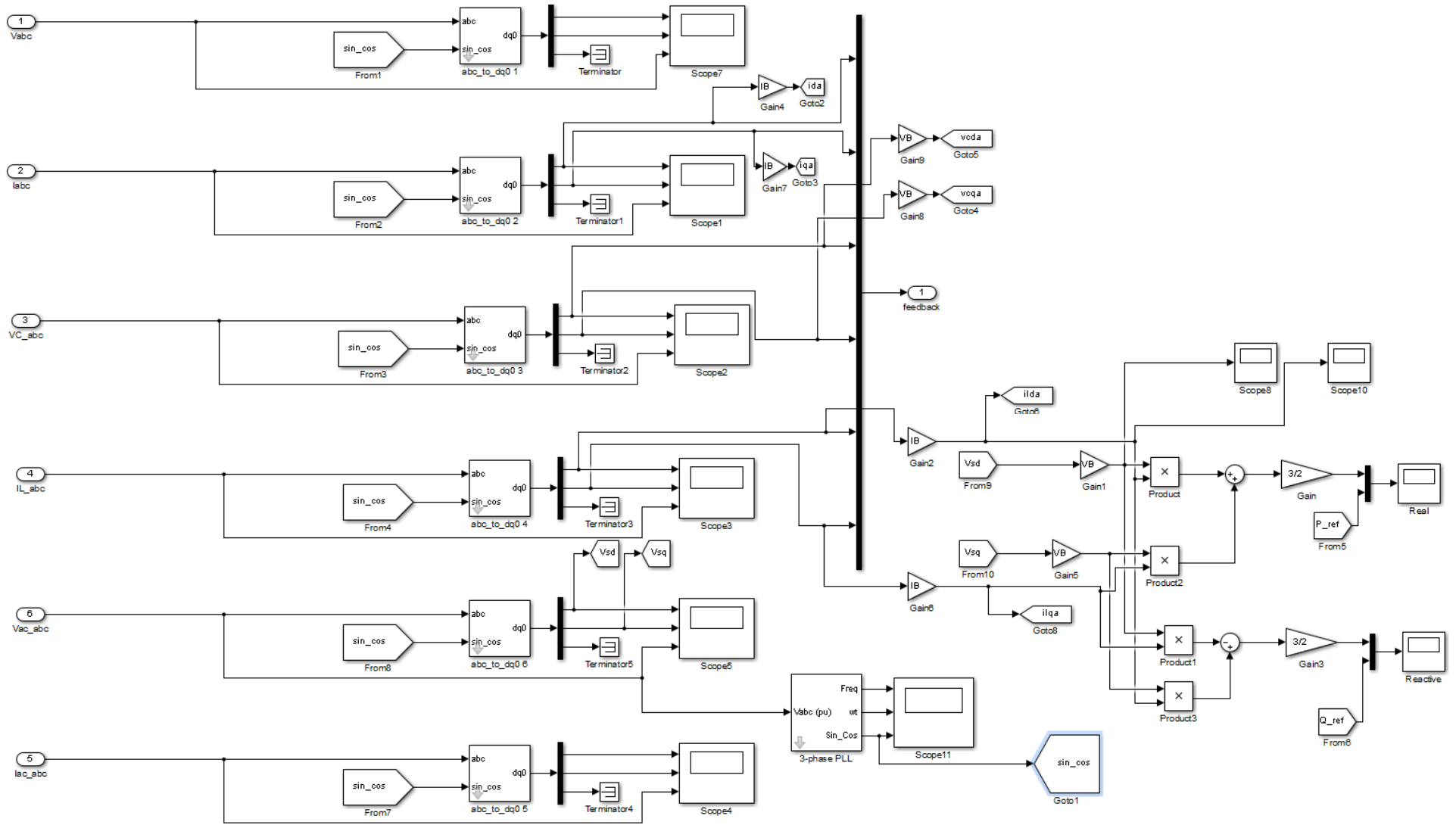


Figure 6.9 Grid-connected VSI: Schematic of subsystem 'All Measurements.'

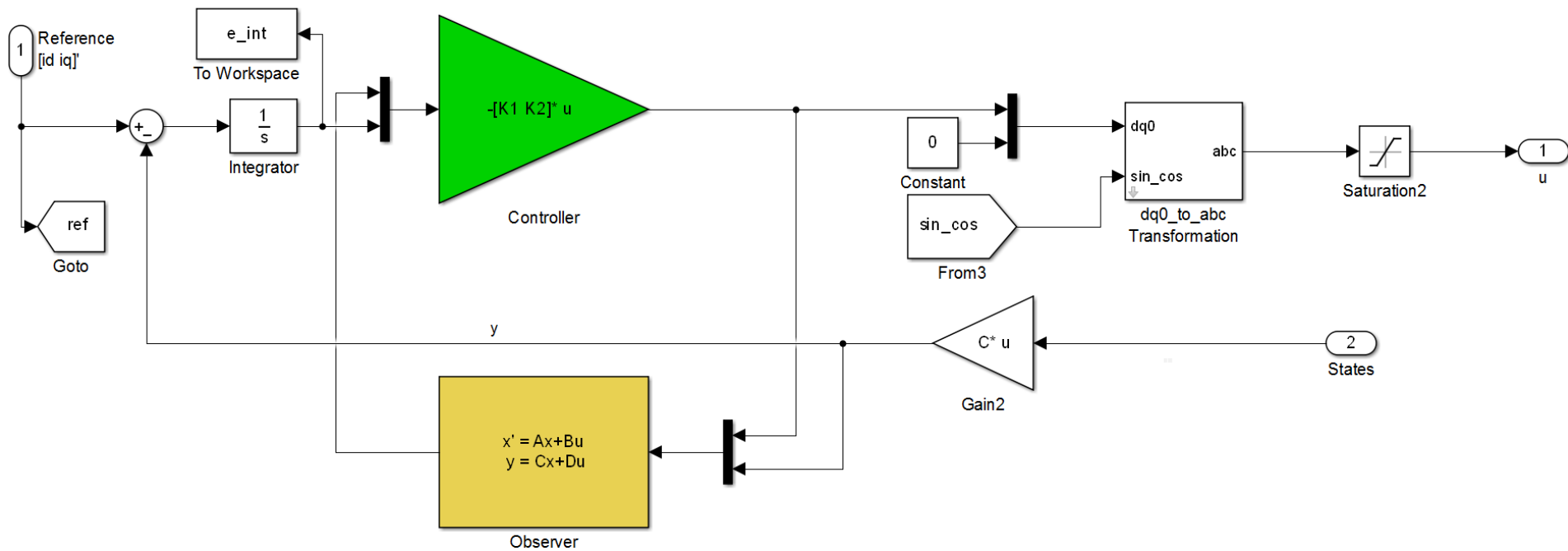


Figure 6.10 Grid-connected VSI: Schematic of subsystem Robust Controller.'

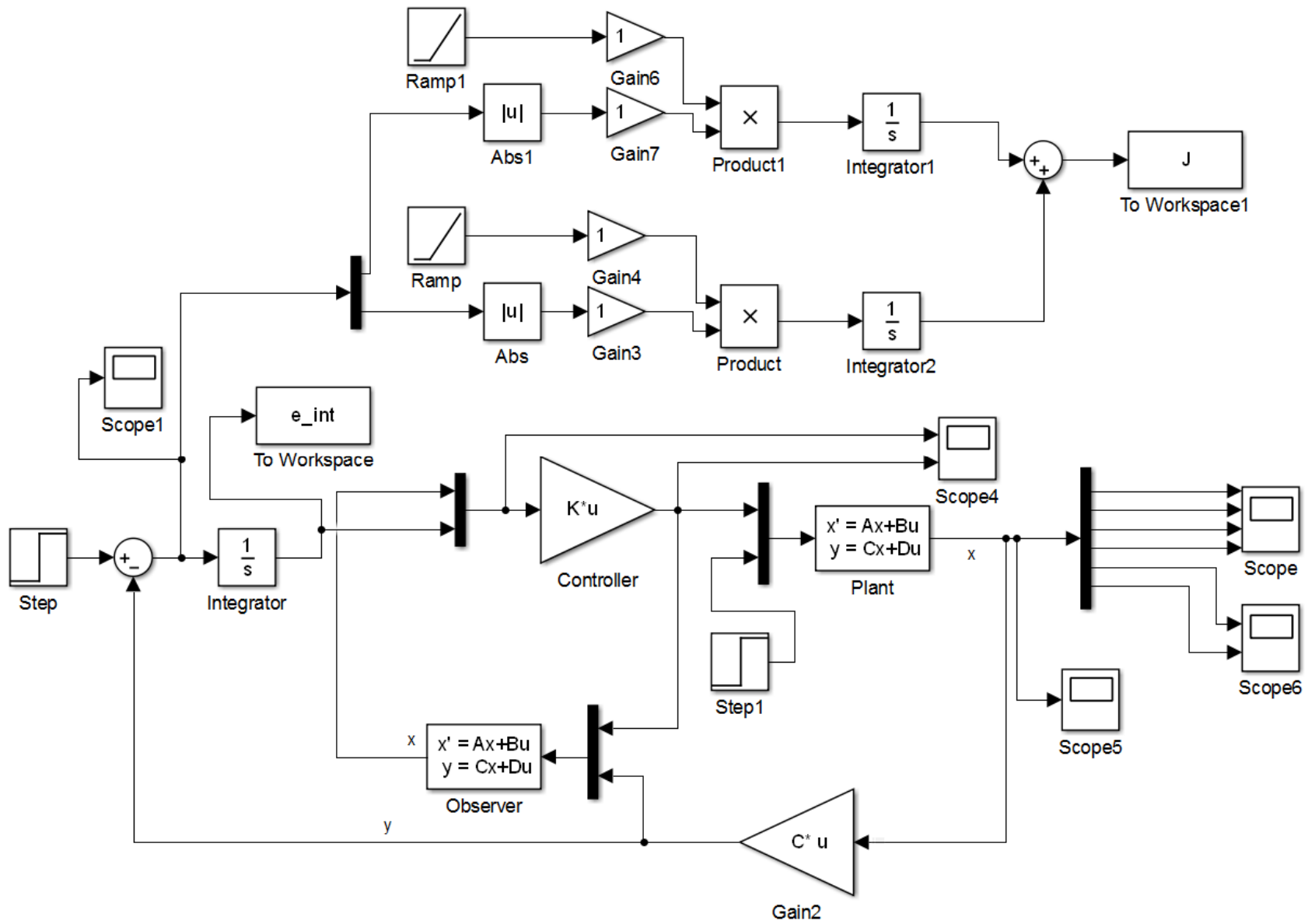


Figure 6.11 Grid-connected VSI: Schematic of Simulink file for IRTD algorithm.

6.2 RTDS plus DS1103 Implementation

To determine the effectiveness of the proposed control method experimental work is done by real time simulations with hardware in the loop (RTHIL setup). Real time digital simulator, RTDS® is used for plant simulation in real time and the controller is developed on dSPACE DS1103 controller board. The experimental hardware arrangement is shown in Figure 6.12. The interconnection of various hardware components is illustrated in Figure 6.13.

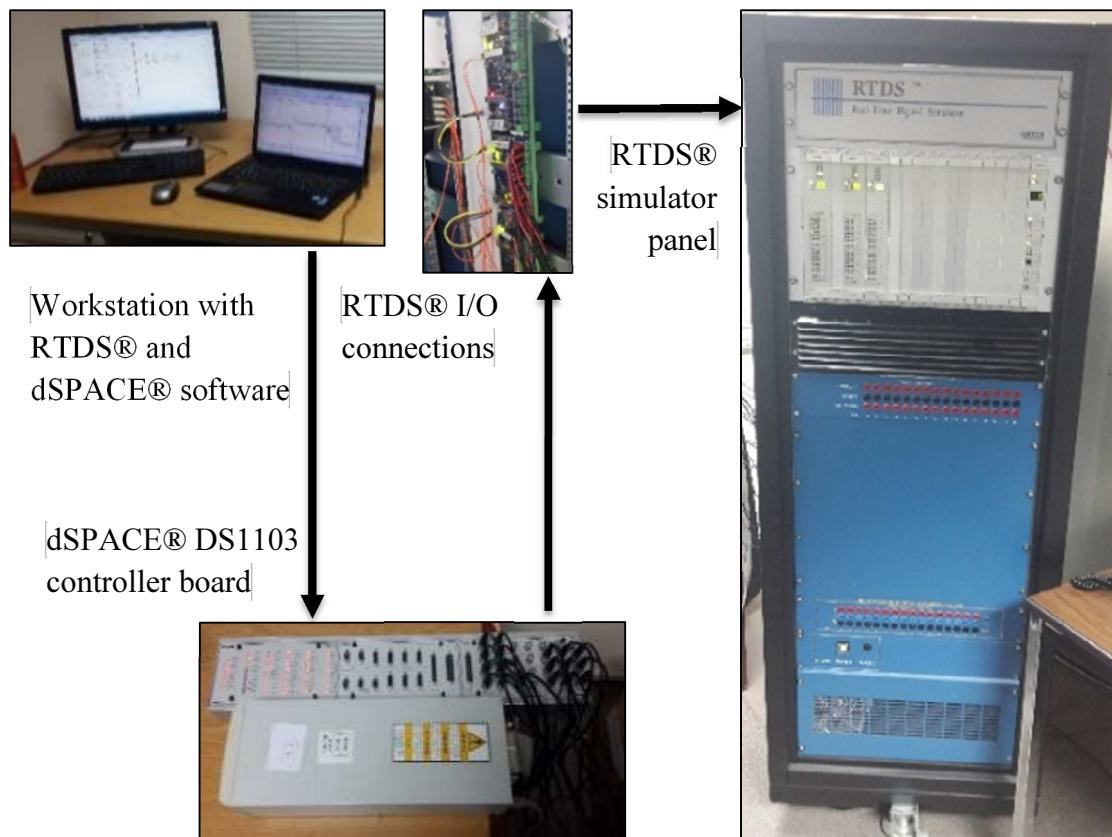


Figure 6.12 Hardware arrangement.

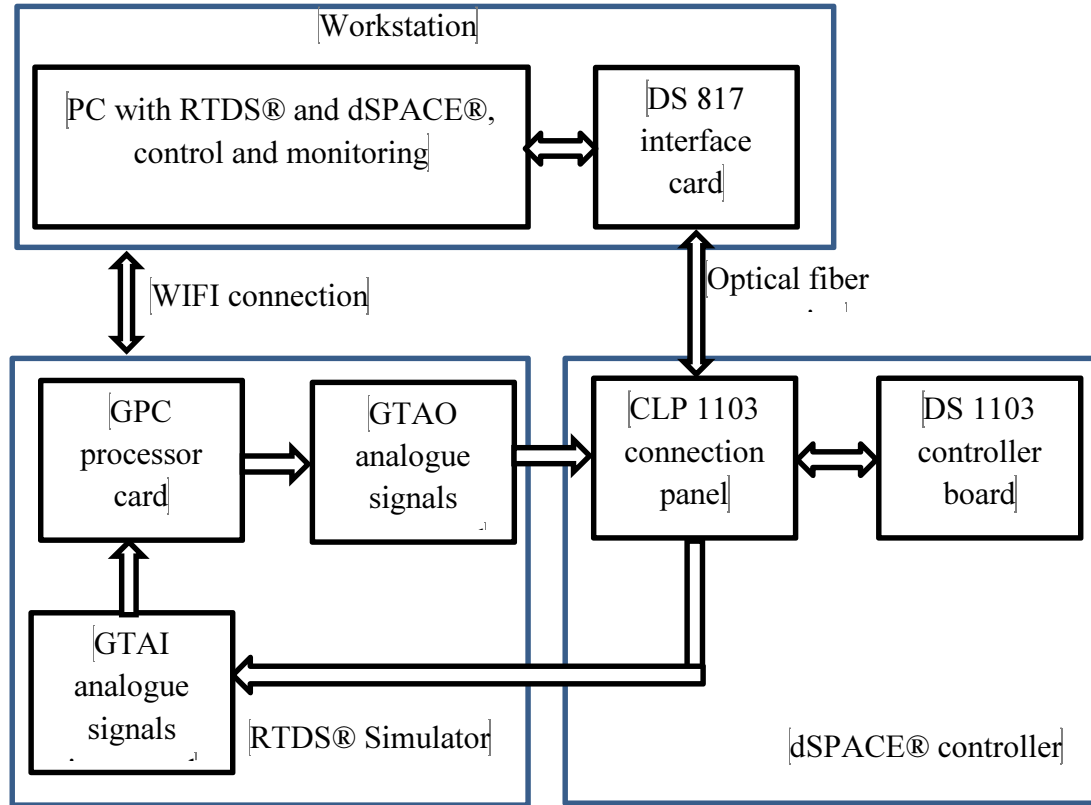
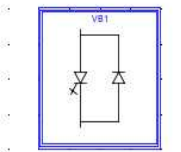
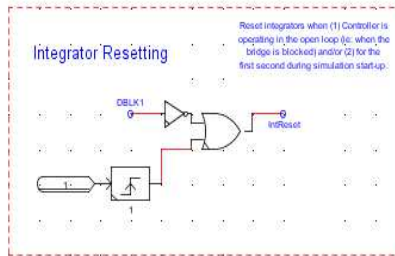
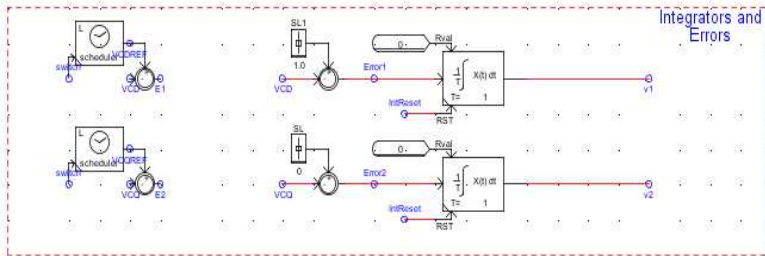


Figure 6.13 Interconnection of hardware components.

In the subsections to follow the schematics for real-time hardware-in-the-loop (RTHIL) experiments are presented. The real-time simulation of the VSI plants are implemented in RSCAD, the software package for RTDS. A very good reference to see the functionality and applications of RTDS is [79]. The latest RSCAD version 4.004.1 has been used for the implementations. The controller is implemented on the dSPACE DS1103 controller board using the integrated dSPACE SIMULINK library toolbox. First the standalone VSI schematics are provided.

6.2.1 Schematics of standalone VSI system in RSCAD

The standalone VSI system implementation in RSCAD comprises of two major parts; large-time-step system and small-time-step system. The large time step system has all the control blocks. The schematic of the large-time-step part is shown in Figure 6.14. The large-time-step part handles all tasks related to control such as handling of feedback signals, reference generation, dealing with input/output signals etc. For Implementation of the VSI system plant, the small-time-step blocks are used. The schematic is shown in Figure 6.15. This part has all the power system block, such as the inverter-bridge, LC filter, load resistance and inductances, PWM generators etc. The large time-step is $50\mu sec$ and the small time-step is approximately $2\mu sec$.



Robust Control of VSI In Standalone Mode

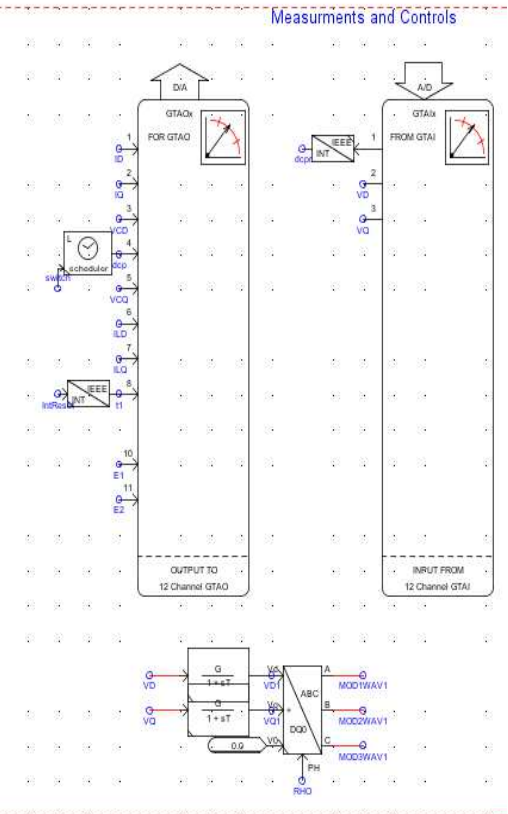
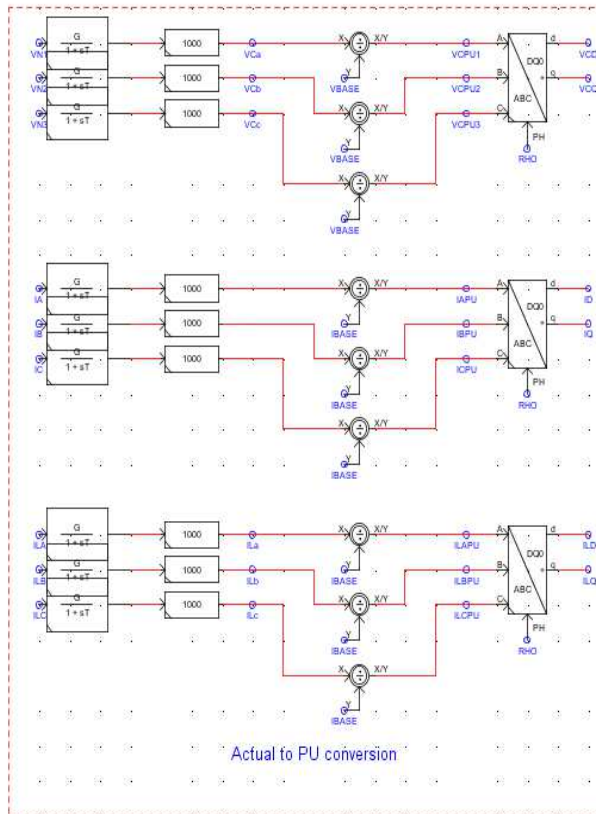
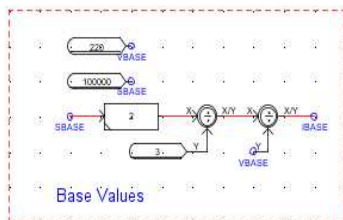
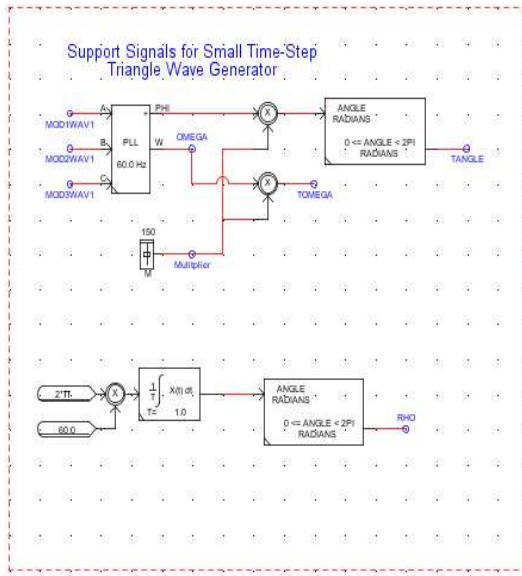
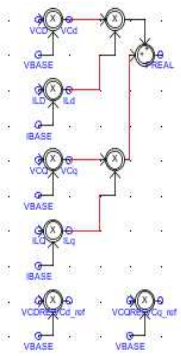


Figure 6.14 Standalone VSI: Large-time-step schematic in RSCAD.

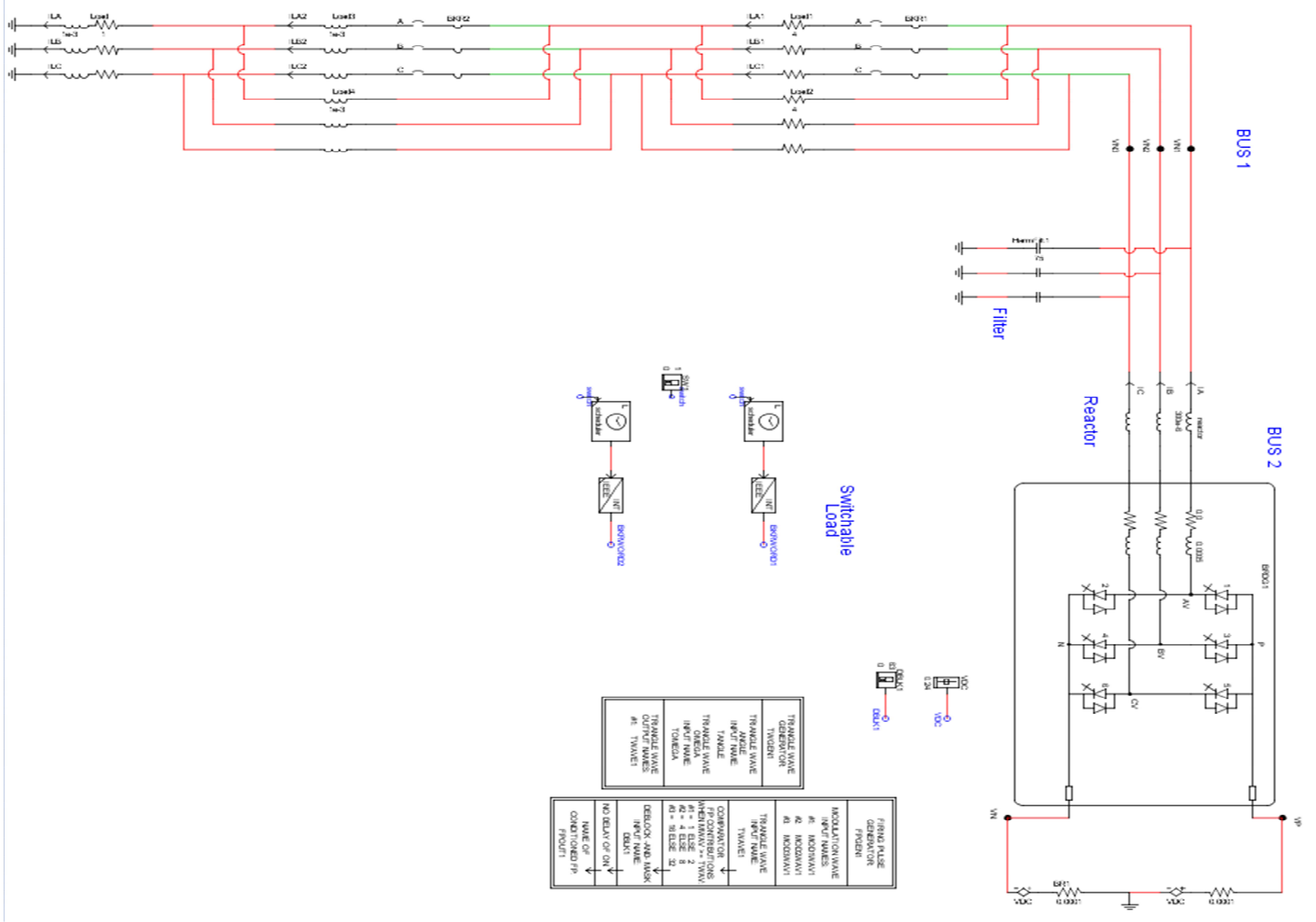


Figure 6.15 Standalone VSI: Small-time-step schematic in RSCAD.

6.2.2 Schematics of grid-connected VSI system in RSCAD

The grid-connected VSI system implementation in RSCAD is shown in the figures to follow. This system also comprises of the two major parts, the large-time-step and the small-time-step systems. The large time step system for the grid-connected VSI case is shown in Figure 6.16. All the blocks related to control of the system are in this part. For Implementation of the grid-connected VSI system plant, the small-time-step blocks are used. The schematic is shown in Figure 6.17.

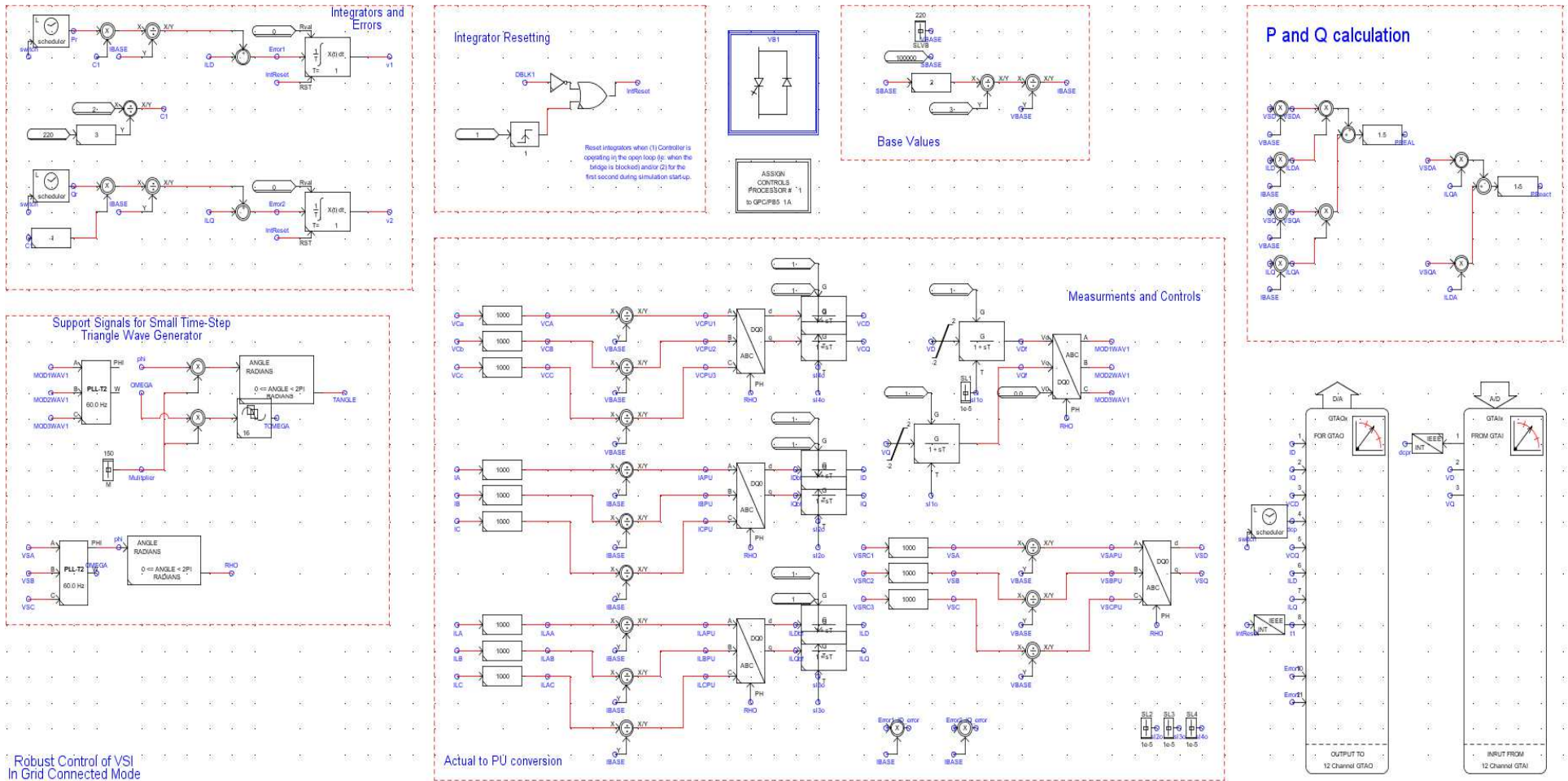


Figure 6.16 Grid-connected VSI: Large-time-step schematic in RSCAD

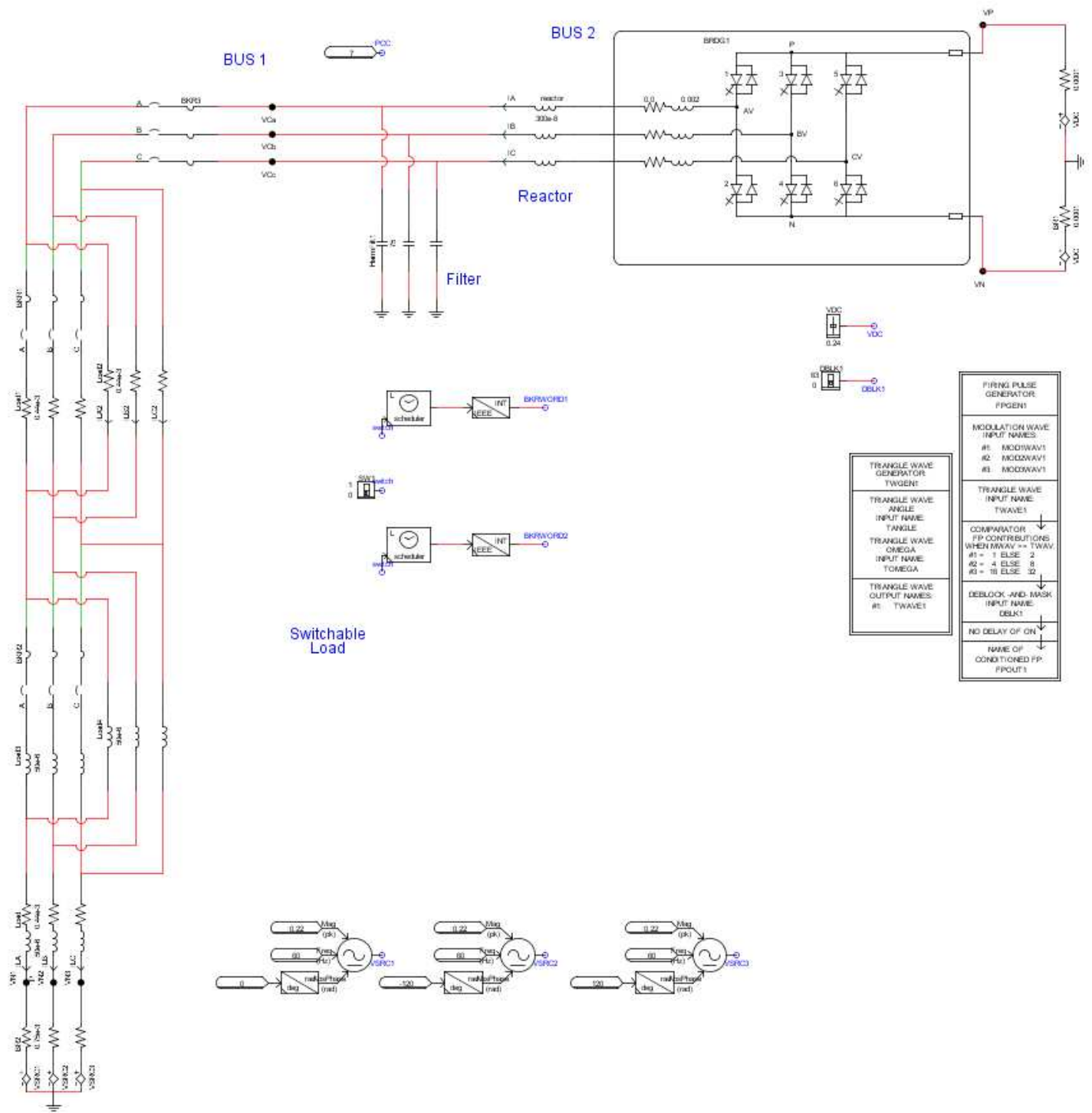


Figure 6.17 Grid-connected VSI: Small-time-step schematic in RSCAD.

6.2.3 Schematics of controller for standalone and grid-connected VSI on DS1103 controller board

The controller implementation on DS1103 DSP board is a fairly simple process. A dSPACE toolbox 'rti1103' is integrated with SIMULINK, which is a library of all the blocks to send and receive signals in the DS1103 board. Thus using the I/O blocks from rti1103 and the default control blocks of SIMULINK the desired controller can be implemented. After the controller is implemented it can be downloaded to the board using 'Build Model' command. The schematics of the implementation of the controller for the two cases, standalone and grid-connected VSI, are shown in Figure 6.18 and Figure 6.19 respectively.

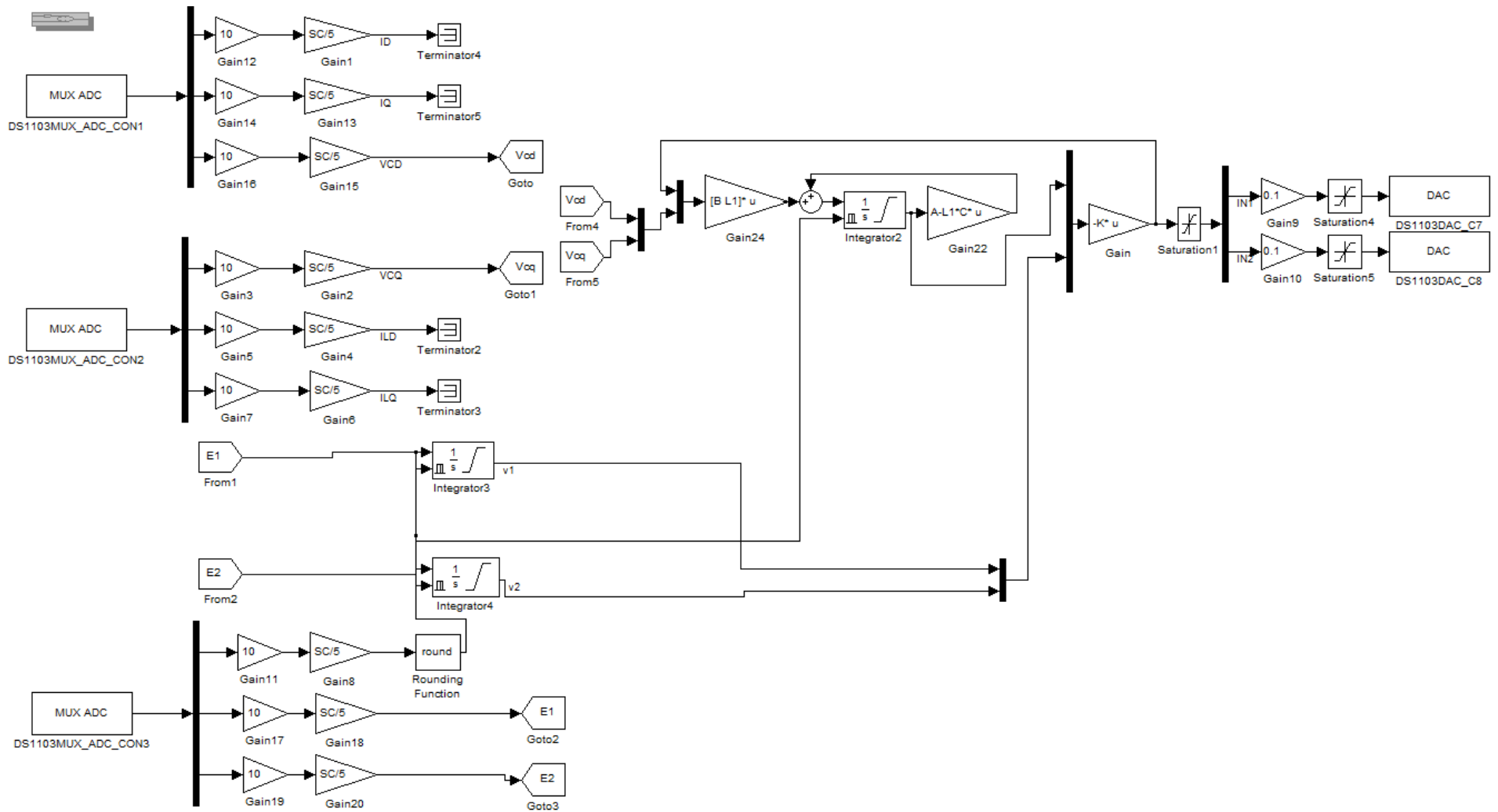


Figure 6.18 Standalone VSI: Controller schematic for DS1103.

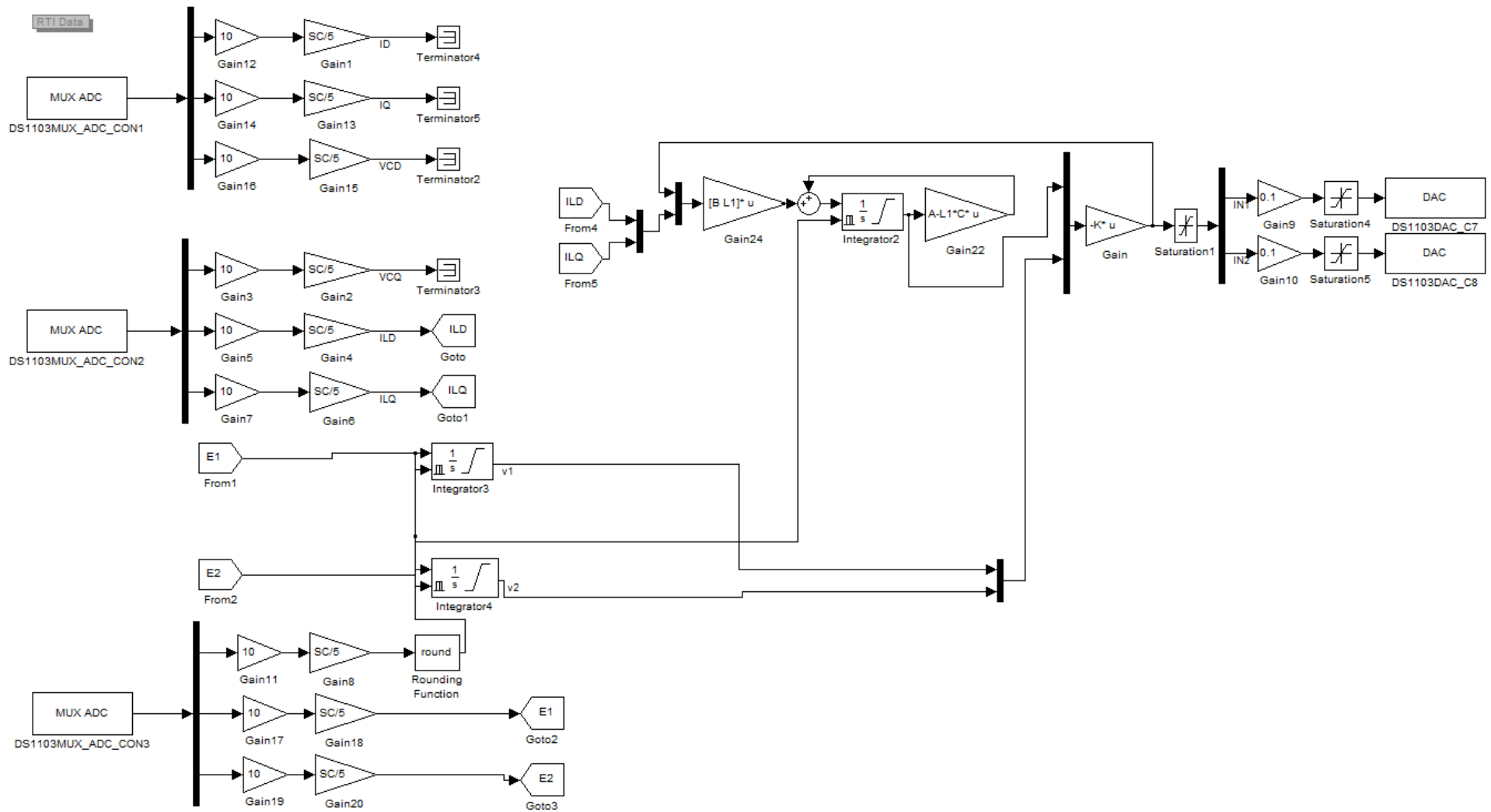


Figure 6.19 Grid-connected VSI: Controller schematic for DS1103.

CHAPTER 7

RESULTS AND ANALYSIS: STANDALONE VSI

In this chapter the results of proposed control design method for standalone VSI are described which include results of the algorithms for controller design, the results of simulations and the results of the RTHIL experimental work.

7.1 Results of the algorithms

The 3-phase, 3-leg inverter with LC filter of Figure 3.1 is considered. The constant parameters of the system are given in Table 7-1. The robust stabilizing controller is designed using the IRSD algorithm mentioned in chapter 5 for the standalone system. The freedom in choice of α and β is utilized to maximize the convergence rate of the system using a very fast, efficient and robust intelligent algorithm, differential evolution (DE) [80]–[82]. For solving the LMIs, generally the MATLAB® LMI Toolbox is enough. However for solving LMIs with equality constraints which is the case here as well, additional tools such as YALMIP [77] are required. The resulting controller parameters and gains are given as following.

7.1.1 IRSD results

The IRSD results are presented now. The system constants were defined according to Table 7-1. Also the initial uncertainty bounds chosen are shown in this table. The parameters used to initialize DE are shown in Table 7-2.

Table 7-1: System constants for standalone VSI.

Parameter	Symbol	Value
Frequency	f	60 Hz
DC voltage	V_{DC}	480 V
Filter capacitance	C_f	75 μ F
Filter inductance	L_f	0.8 mH
Nominal load resistance	R_0	5 Ω
Nominal load inductance	L_0	2 mH
Load resistance uncertainty	λ_R	250m Ω
Load inductance uncertainty	λ_L	20 μ H
Reference output voltage	$[V_{cd,ref} \quad V_{cq,ref}]$	[220 0] V
Base voltage (phase-neutral)	V_B	220 V
Base 3 phase power	S_B	100 kVA
Carrier frequency	f_c	9 kHz

Table 7-2: DE parameters of IRSD algorithm for standalone mode.

Parameter	Symbol	Value
No. of parameters to be optimized	n	2
Population size	N_P	20
No. of generations	N_G	20
Crossover Factor	FC	0.6
Mutation Factor	FM	0.5
Desired cost	J_d	1e-3

The cost function minimization plot is given in Figure 7.1. The optimized parameters and gains are provided in Table 7-3.

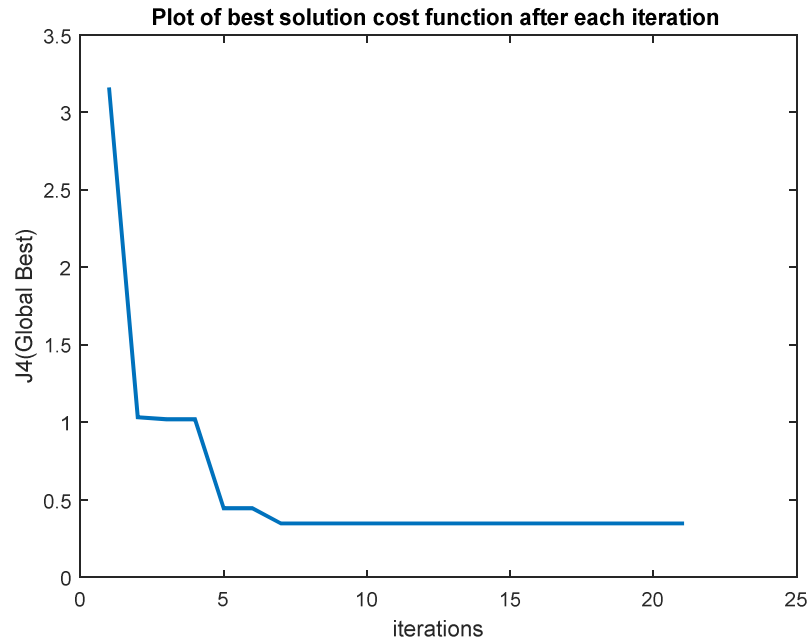


Figure 7.1 Cost minimization in standalone IRSD algorithm.

Table 7-3: Results of IRSD algorithm for standalone case.

Parameter	Symbol	Value
Tuning parameters	$[\alpha \ \beta]$	[0.0624 0.3277]
Lower bound of α	$\underline{\alpha}$	0.0545
Stabilizing controller gain	K	$\begin{bmatrix} 0.98 & 0 & -0.266 & 0 & -1.7 & 0 \\ 0 & 0.98 & 0 & -0.266 & 0 & -1.7 \end{bmatrix}$
Observer gain	L	$\begin{bmatrix} -67.4 & 0 & 10865 & 0 & -160 & 0 \\ 0 & -67.4 & 0 & 10865 & 0 & -160 \end{bmatrix}^T$
Convergence rate	h	2.8745
RL Load uncertainty bounds	$[\bar{\lambda}_R \ \bar{\lambda}_L]$	[0.117 Ω 0.32mH]

The obtained convergence rate is very good. Also the load uncertainty bounds are good. The uncertainty bound for line inductance has increased considerably from the initially chosen value. Though the uncertainty bound for line resistance is decreased from its initial choice. If required this bound can be increased using a multi-objective cost function in the cost function that maximizes the uncertainty bound along with the convergence rate. Now the tracking controller is designed in the next section.

7.1.2 IRTD results

The tracking/integral control gains are calculated for optimum tracking performance using the IRTD algorithm for standalone VSI. The designed tracking controller also successfully passes the robustness test which is performed as mentioned in *remark 3-3*. This establishes guaranteed robustness of controller for the given uncertainty. This completes the design of control algorithm of section 5.2. The results of this algorithm and its initialization parameters are given in Table 7-4.

Table 7-4: DE parameters and results of IRTD algorithm for standalone mode.

Parameter	Symbol	Value
No. of parameters to be optimized	n	4
Population size	N_p	20
No. of generations	N_G	100
Crossover Factor	FC	0.6
Mutation Factor	FM	0.5
Desired cost	J_d	1e-6
Integral controller gain	K_I	$\begin{bmatrix} -1372 & 289.3 \\ -80.9 & -1199 \end{bmatrix}$

The plot of the cost function minimized during the iterations of the algorithm is shown in Figure 7.2.

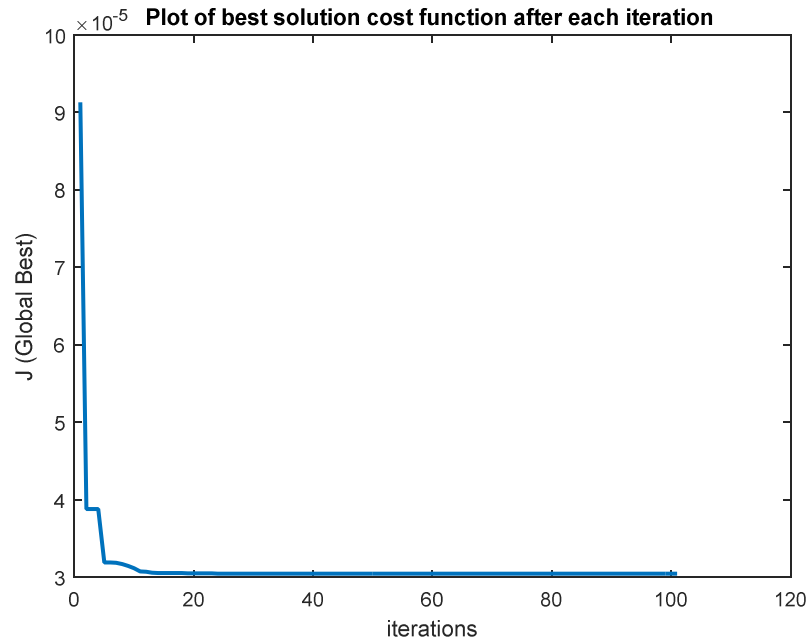


Figure 7.2 Cost function plot of IRTD algorithm for standalone mode.

7.2 Simulation results

The performance of the designed controller is tested in three cases where in each case a different property is analyzed. Following is the list of the three tests, the specifications of which are listed in Table 7-5.

Case I: Robustness test

Case II: Disturbance test

Case III: Tracking performance test

The first case is the robustness test where the performance is observed in the presence of small variations in load resistance and inductance. In the second case the performance of the system is observed for load disturbances, when a relatively large change occurs in the

load. The third case is solely for the tracking performance of the system. The system is run for various reference levels for the load voltage. For all cases the system starts at time $t = 0$ with zero reference input, hence the load voltages and currents are initially zero. At time $t = 10 \text{ msec}$, the reference is changed to $[V_{cd,ref} \ V_{cq,ref}] = [220 \ 0]V$. Rest is different in each case.

Table 7-5: Simulation and experimental tests variations.

Robustness Test						
Time (msec)	0	30	50	70	90	
$R (\Omega)$	5	4.8	4.8	5	5	
$L (mH)$	2	2	1.95	1.95	2	
Disturbance Test						
Time (msec)	0	30	50	70	90	
$R (\Omega)$	5	3	3	5	5	
$L (mH)$	2	2	1.5	1.5	2	
Tracking Performance Test						
Time (msec)	0	10	30	50	70	90
V_{cdref}	0	220	220	200	200	220
V_{cqref}	0	0	20	20	0	0

Case I: Robustness test

This test is intended to see how small uncertainties in load may affect the performance of the system. The variations in the load are as given in Table 7-5. As seen in Figure 7.3, the v_{cd} and v_{cq} signals are very smooth and there are no noticeable spikes for the whole

duration when different variations are acting. Also $v_{c,abc}$ remains a very smooth three phase sinusoidal signal. This show good robustness properties of the controller. The load current changes can be seen in Figure 7.4 which are as expected.

Case II: Disturbance test

In this case large load disturbances are applied to the system as given in Table 7-5. As the results show in Figure 7.6 the variations in load are quite large. At $t = 30msec$, when the load resistance changes from 5Ω to 3Ω , the magnitude of i_{Ld} increases from about 40A to 70A and that of i_{Lq} increases from about 6A to 18A. These big variations in the load current cause some distortions in the load voltage as well, which are noticeable in Figure 7.5. However the magnitudes of the distortions in load voltage are relatively very small and seem to settle within 10 to 15msec. The same behavior follows with the forthcoming load variations at $t = 50, 70$ and $90msec$. Hence the performance of the controller is considered satisfactory for this case too.

Case III: Tracking performance test

The tracking performance is tested for several reference input signals. Figure 7.7 and Figure 7.8 show the results. The initial 20 msec response is skipped because it is same as other cases. The later part shows the tracking performance for different reference inputs as per Table 7-5. First at $t = 30msec$ a reference of 20V is given to v_{cq} which it tracks in around 20msec. Similar behavior is observed for the remaining sequence of the reference inputs. The output tracks the reference very quickly and without any big overshoots or undershoots.

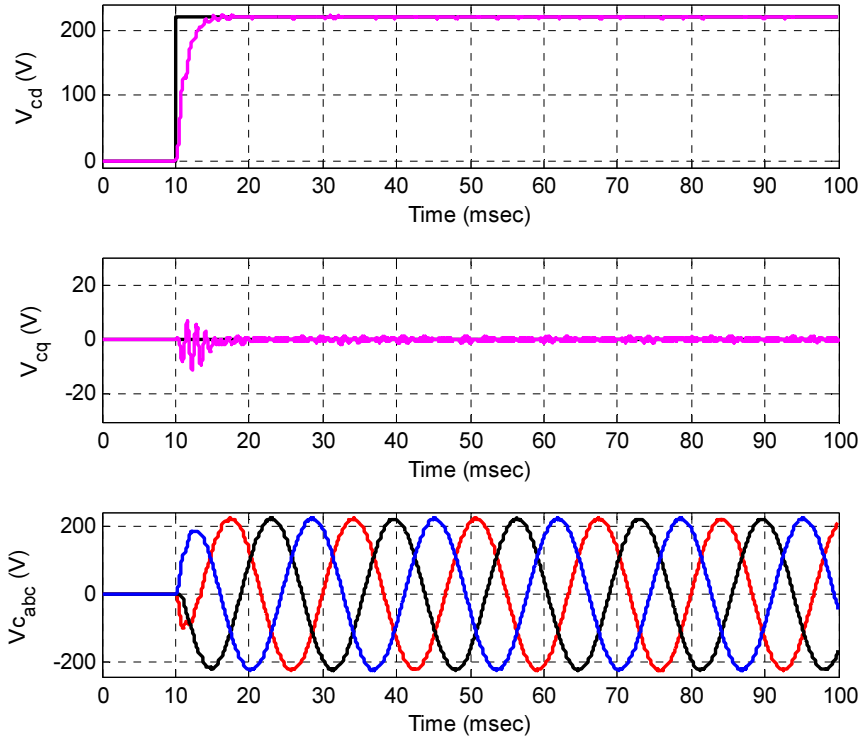


Figure 7.3 Standalone VSI: Output/load voltage in robustness test simulation.

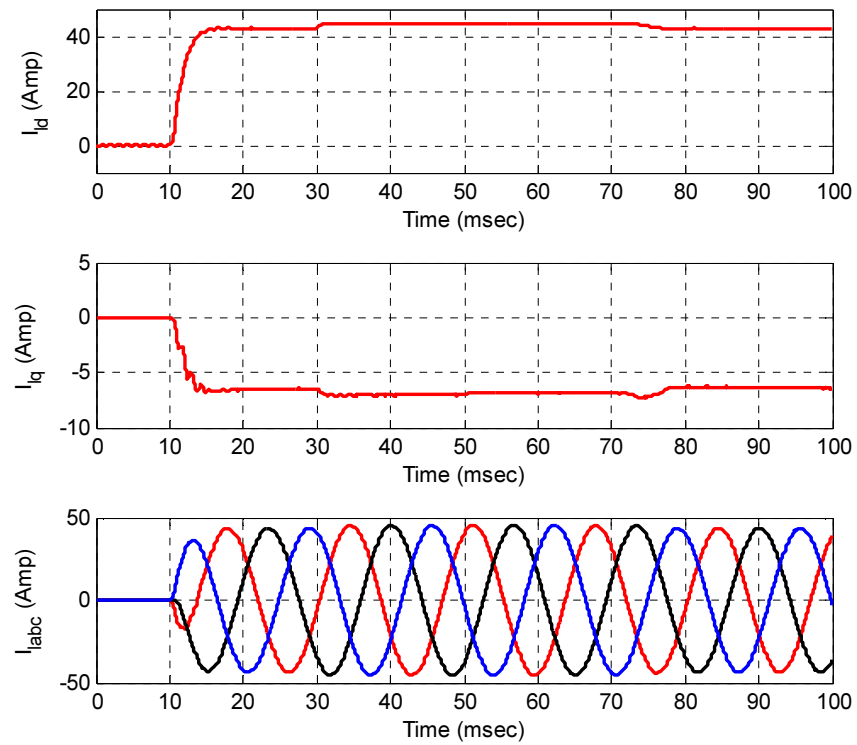


Figure 7.4 Standalone VSI: Output/load current in robustness test simulation.

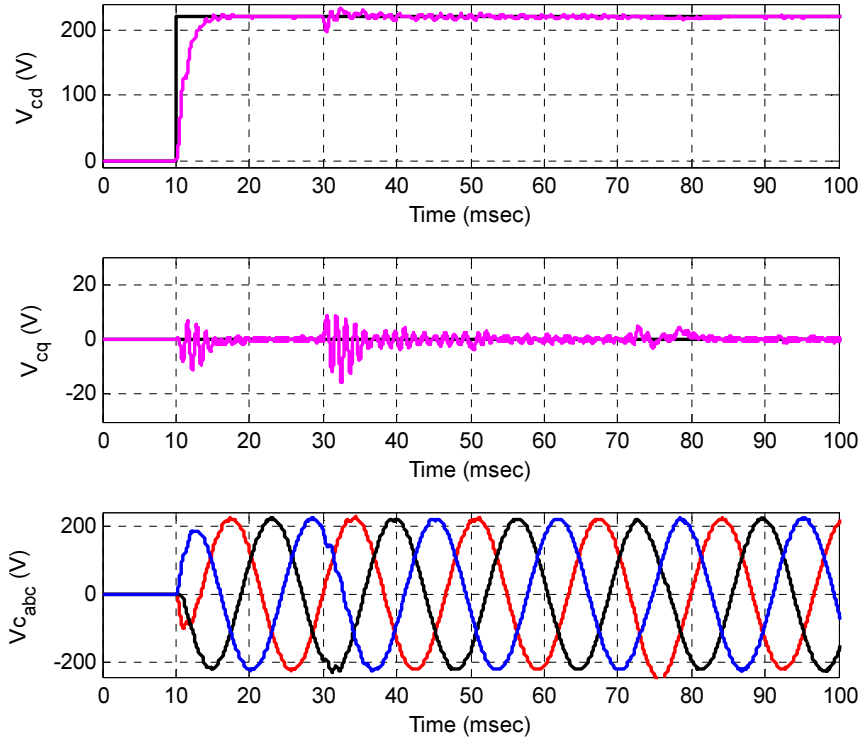


Figure 7.5 Standalone VSI: Output/load voltage in disturbance test simulation.

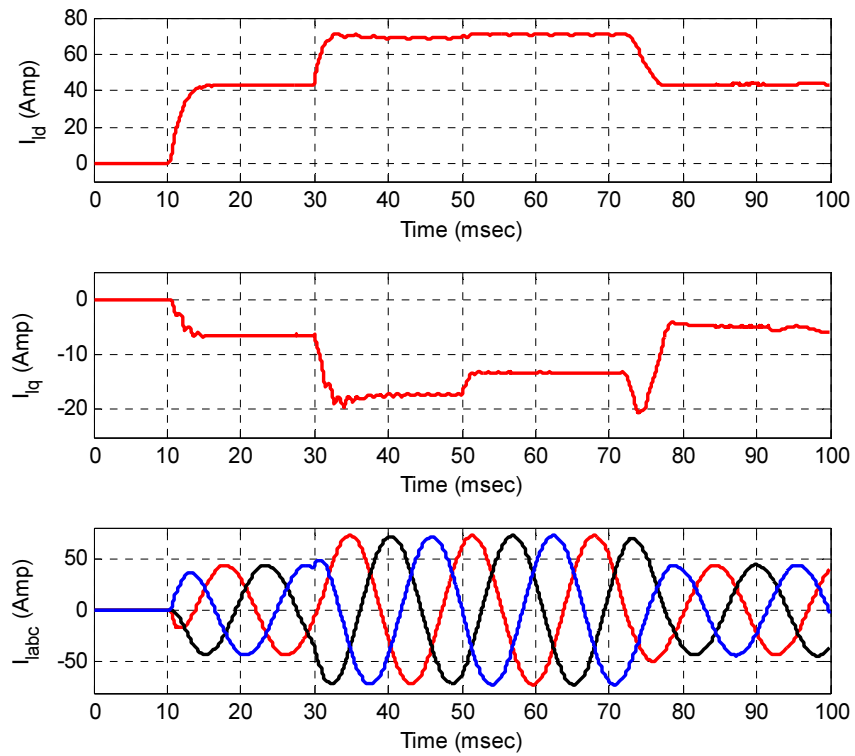


Figure 7.6 Standalone VSI: Output/load current in disturbance test simulation.

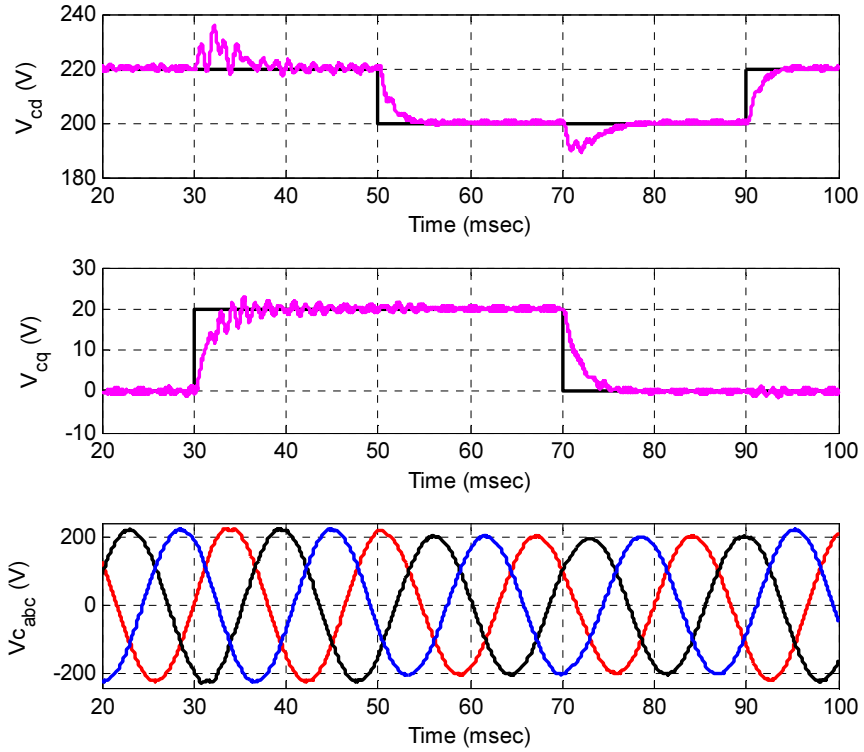


Figure 7.7 Standalone VSI: Output/load voltage in tracking performance test simulation.

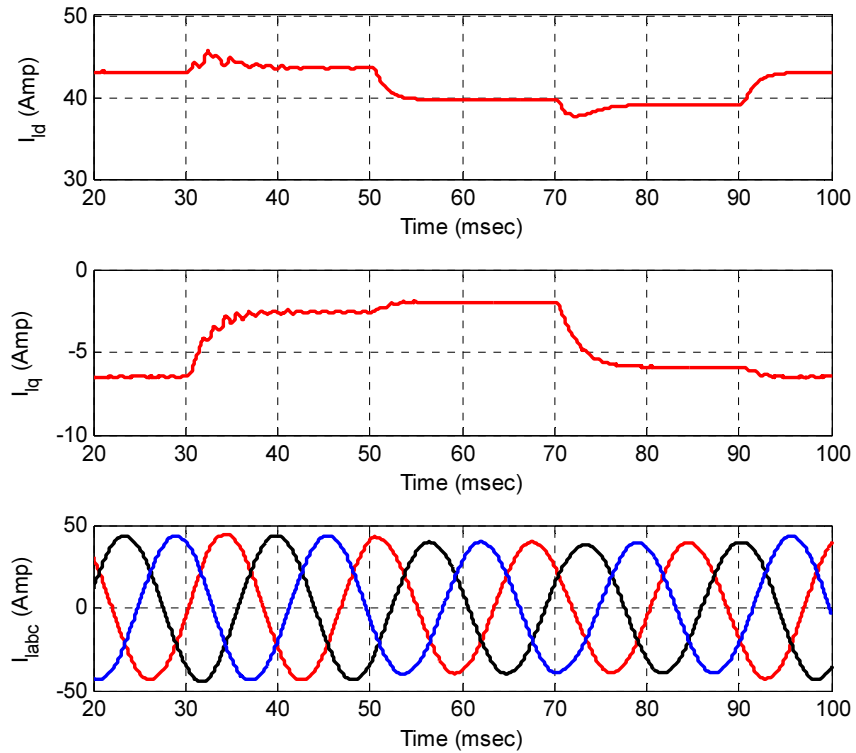


Figure 7.8 Standalone VSI: Output/load current in tracking performance test simulation.

7.3 Experimental results

The experimental results are presented in the figures to follow. Same pattern of tests in followed in the experimental results as simulation results.

Case I: Robustness Test

A robustness test is performed by introducing small uncertainties in the load as given in Table 7-5. The results are presented in Figure 7.9 which shows the dq -components of the output voltage and also three phase voltage waveform. Very smooth profile dq and three phase signals are obtained here as well, which established excellent robustness properties of the controller. The changes occurring in the load current can also be observed in Figure 7.10.

Case II: Disturbance Test

A larger load disturbance is applied to the system in this case as given in Table 7-5. Small variations in the dq -component of the load voltage are observed here, but these distortions vanish very quickly and the system settles back to the reference values as shown in Figure 7.11. This yields a very smooth profile of the three phase ac output voltage, where any variations are hardly noticed. The changes in the load current are expected due to the change in load as shown in Figure 7.12. As soon as the transition period is over, a fairly smooth steady state signals are obtained for the load current as well.

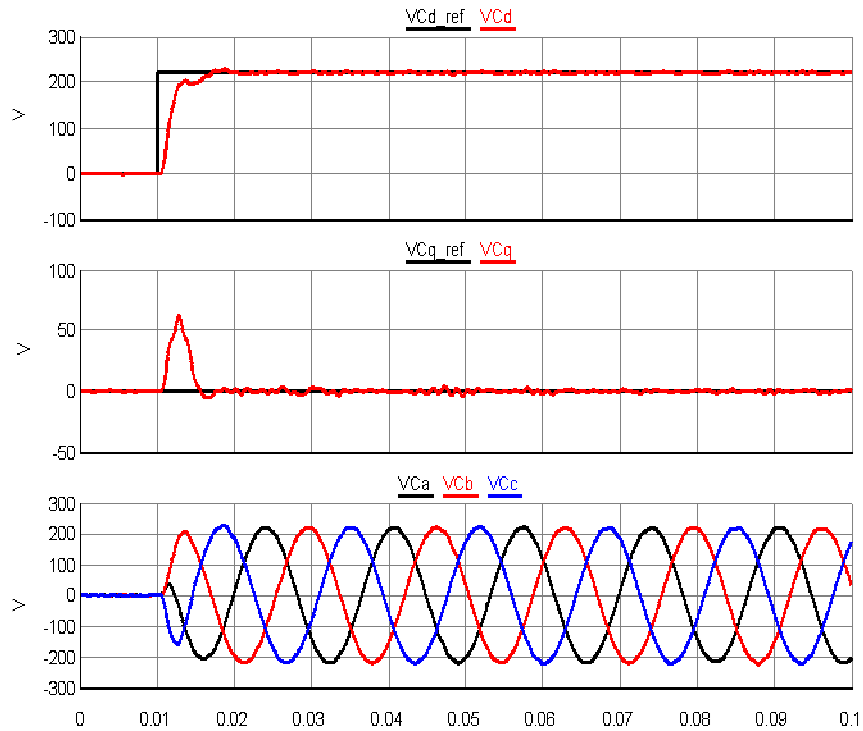


Figure 7.9 Standalone VSI: Output/load voltage in robustness test experiment.

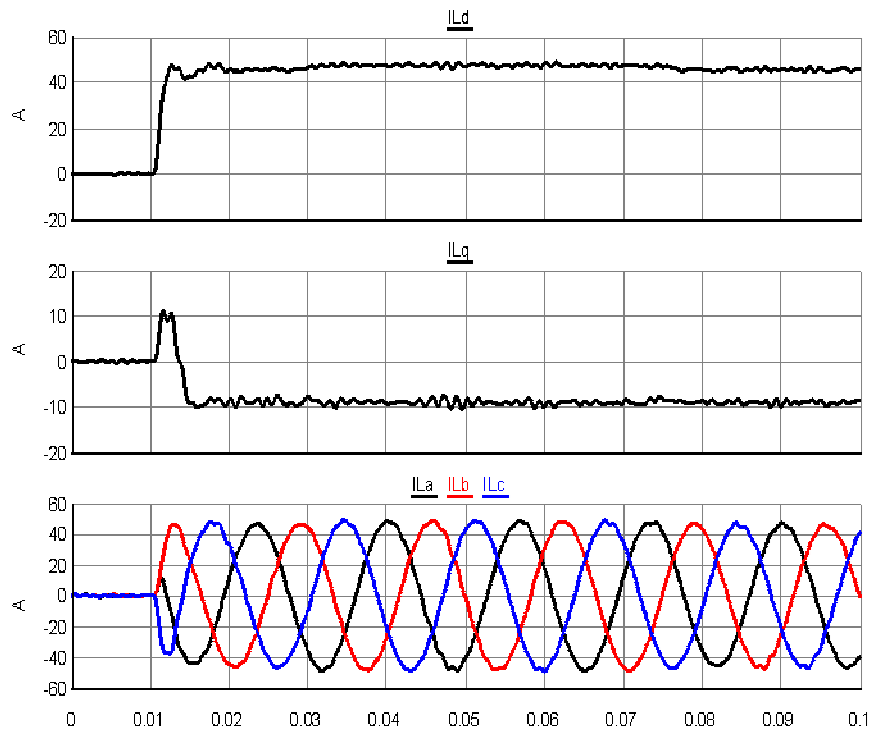


Figure 7.10 Standalone VSI: Output/load current in robustness test experiment.

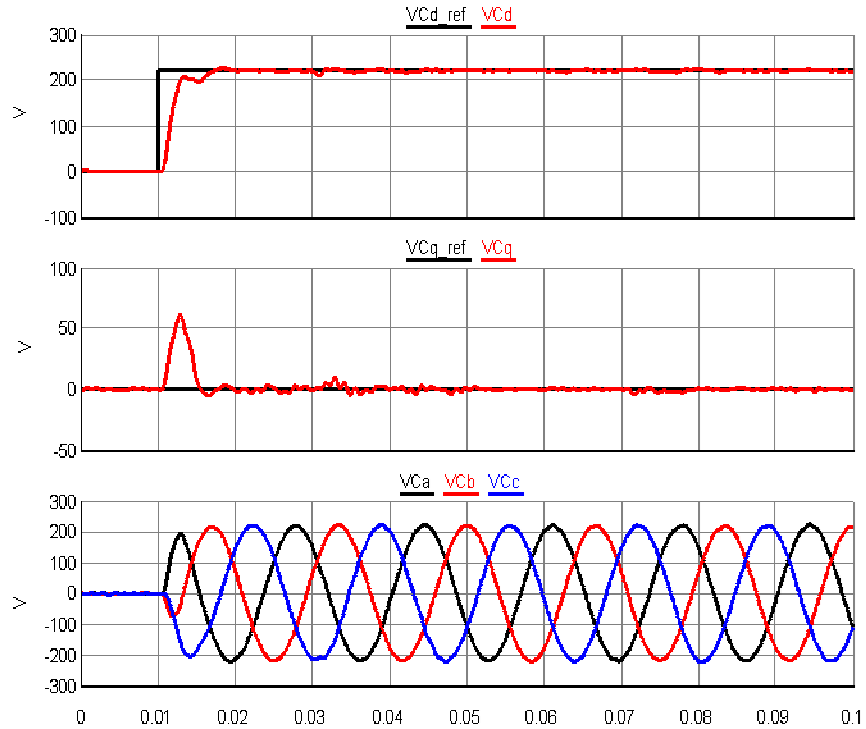


Figure 7.11 Standalone VSI: Output/load voltage in disturbance test experiment.

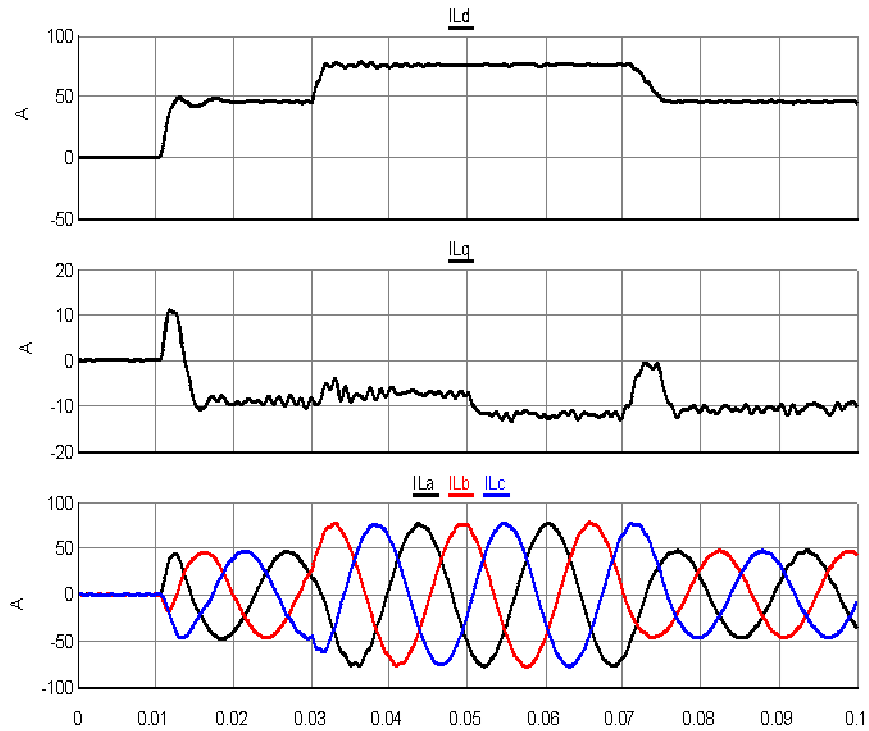


Figure 7.12 Standalone VSI: Output/load current in disturbance test experiment.

Case III: Tracking Performance Test

Now the tracking performance of the controller is evaluated experimentally by giving several reference input signals to the system as given in Table 7-5. As the results show in Figure 7.13, the output voltage dq -components are tracking the provided reference levels efficiently. Both dq -components of the voltage reach to the new reference levels in less than 10 msec without any large shoots which shows good transient behavior and then stay at the reference levels with very small distortions showing good steady state characteristics. The load current magnitudes change accordingly with the changes in the voltage signals as given in Figure 7.14.

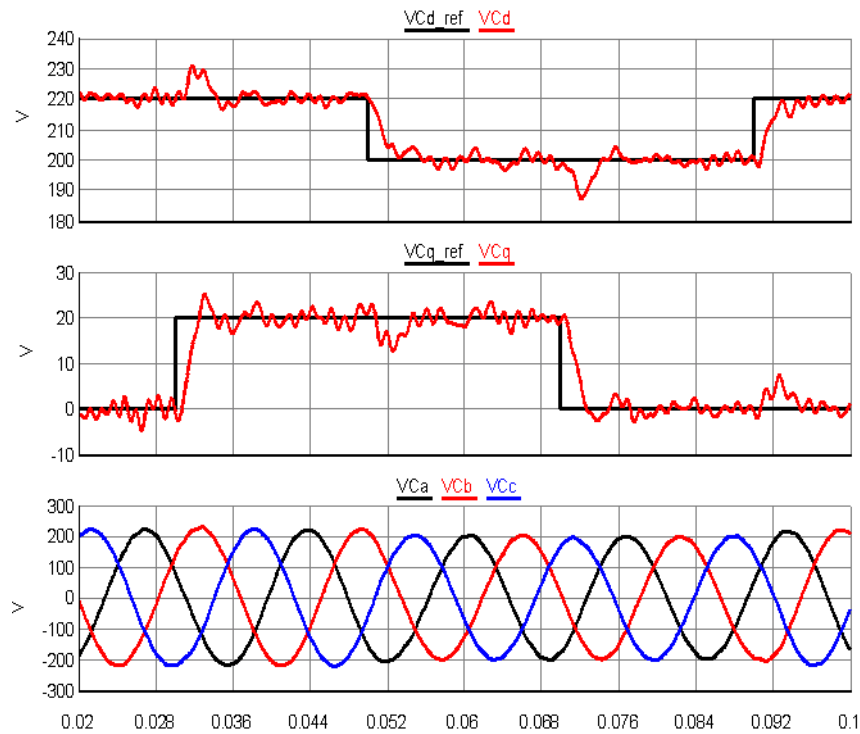


Figure 7.13 Standalone VSI: Output/load voltage in tracking performance test experiment.

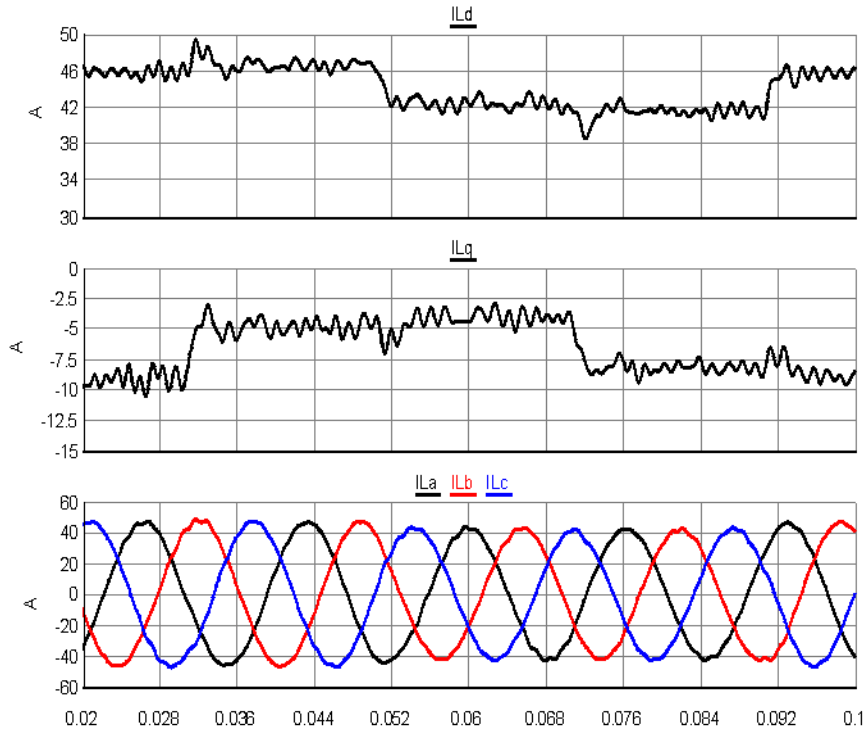


Figure 7.14 Standalone VSI: Output/load current in tracking performance test experiment.

7.4 Comparison of Simulation and Experimental Results

The figures to follow, Figure 7.17, Figure 7.16 and Figure 7.17 show the similarity of the results obtained by simulation and experimental work for each of the three cases in which the system was tested. Generally, the resemblance shown by the simulation and experimental responses is adequate and qualifies the validity of the results. One of the difference is in the initial transition period of v_{cq} where a high frequency transient is observed in simulation while an overshoot is observed in the experimental result. This is because in the experimental work, the step time is larger as compared to the step time of MATLAB simulations. RTDS has a time step of $50\mu\text{sec}$ for large time step blocks, and DS1103 is operated on $10\mu\text{sec}$. In MATABL the simulations are run at time step as low as $1\mu\text{sec}$. The profile of the signals in the simulation results seem smoother because of a smaller time step.

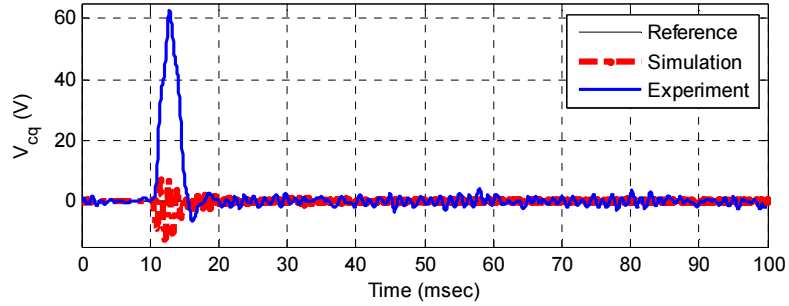
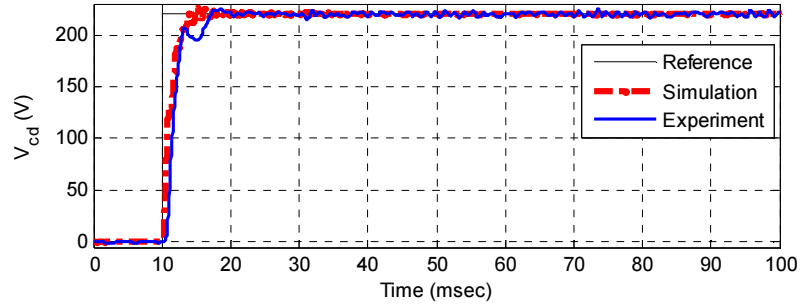


Figure 7.15 Robustness test: Comparison of output voltage in simulations and experiments.

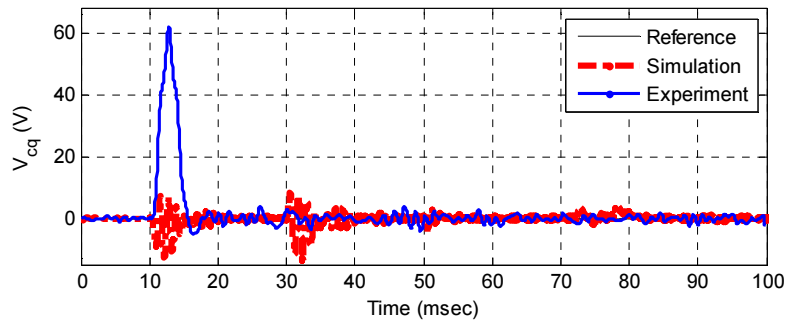
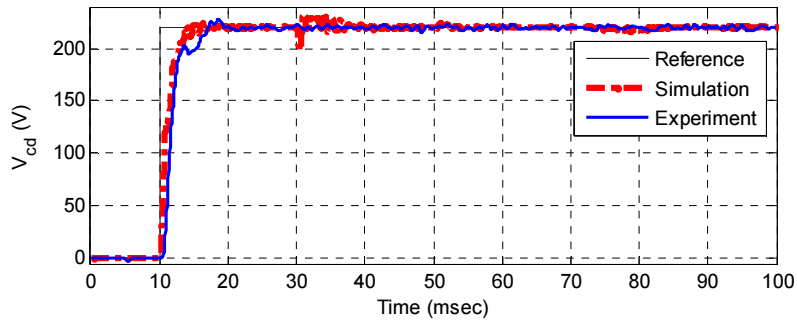


Figure 7.16 Disturbance test: Comparison of output voltage in simulations and experiments.

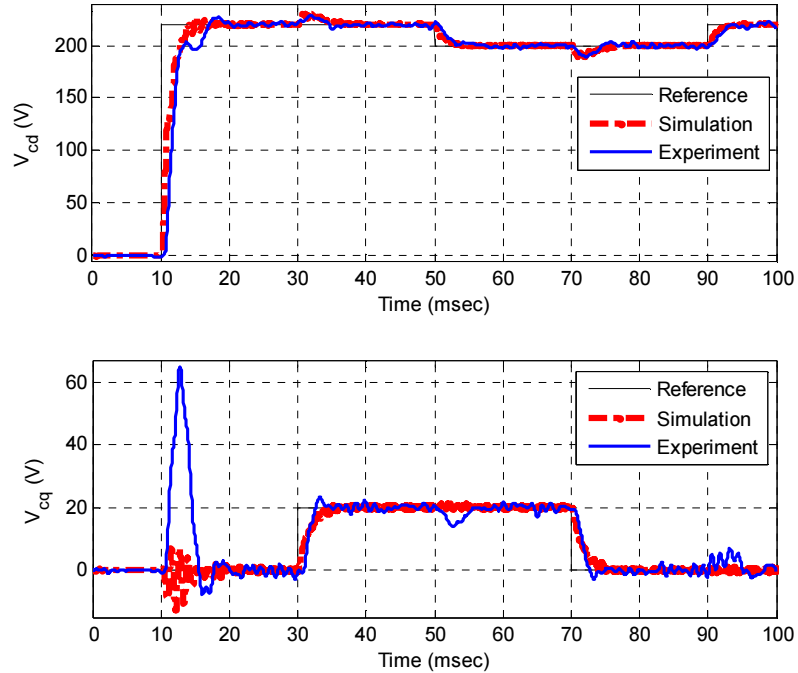


Figure 7.17 Tracking performance test: Comparison of output voltage in simulations and experiments.

7.5 Performance comparison of the proposed controller to existing methods in literature

For the standalone VSI, the results of proposed method are compared with the results of reference [48], as discussed in section 2.4. Similar to the test cases of [48], for comparison the system response is evaluated in the condition when load is applied and load is removed.

7.5.1 Comparison of transient behavior

To compare the transient performance of the proposed controller to that of the controller in [48], the waveform of the output voltage is analyzed when a load is applied to the system and when the load is removed. The response of the controller in [48], is shown in Figure 7.18, which is taken from the reference [48].

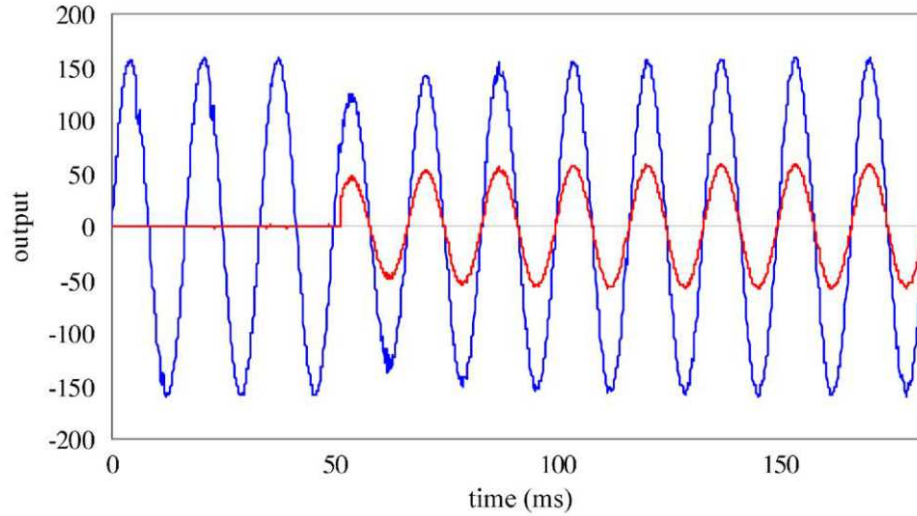


Figure 7.18 On-Load response of the controller in [48]. The voltage and current waveforms.

It is clearly seen that the amplitude of the voltage waveform appears to be reduced, as the load is applied. Also the voltage amplitude takes some time to build up back to its reference value (approximately 50 msec). Now a similar test is performed on the proposed controller to compare it with the results of Figure 7.18. The On-Load performance of the proposed controller is presented in Figure 7.19. As shown in the figure, the output voltage waveform is robustly regulated at the reference amplitude as the load current change. There is a very small spike in the waveform which disappears quickly thus there is no reduction in the voltage amplitude. This shows excellent robustness and improved performance as compared to the results of [48].

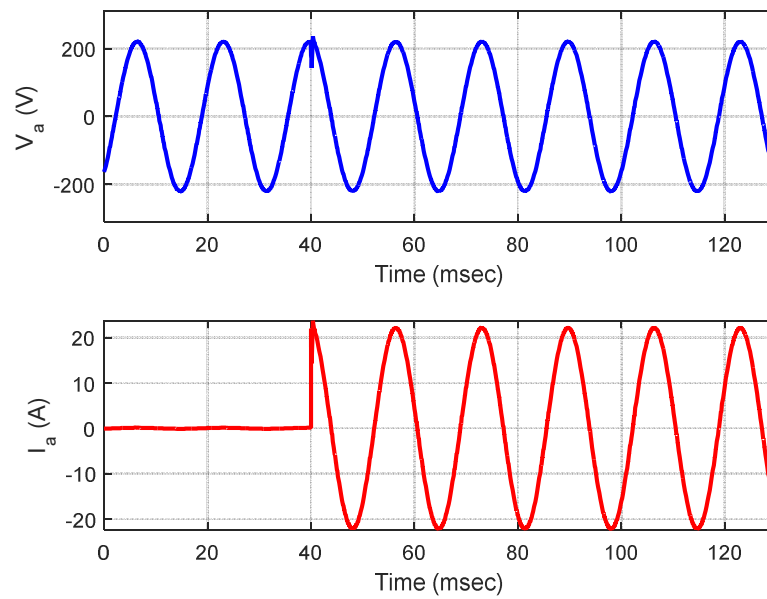


Figure 7.19 On-Load performance of the proposed controller.

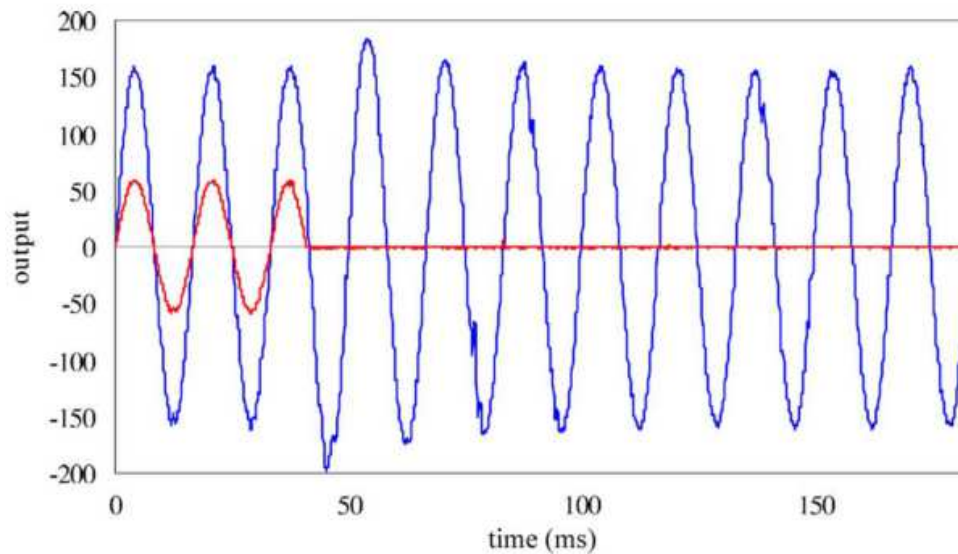


Figure 7.20 Off-Load response of the controller in [48]. The voltage and current waveforms

For the off-load case, the performance of the controller in [48], is shown in Figure 7.20, which is taken from the same reference. As seen in the figure, when the load is removed, the voltage amplitude rises and then settles back to the reference value in about 50 msec.

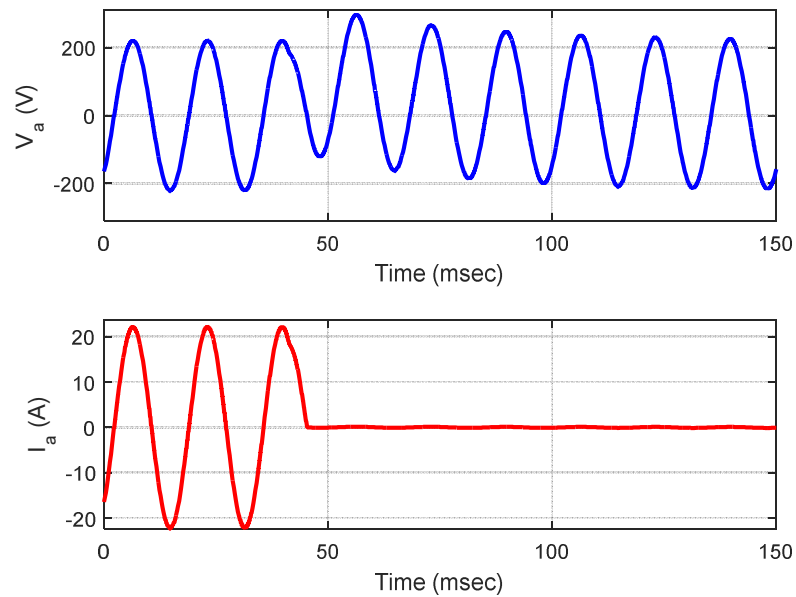


Figure 7.21 Off-Load performance of the proposed controller.

The off-load test performance of the proposed controller is shown in Figure 7.21. The performance is satisfactory although the overshoot in the amplitude is slightly higher. The voltage amplitude is regulated back to the reference level quickly in approximately 60 msec. Thus the results of the off-load test are comparable to [48].

7.5.2 Steady-state performance

For steady-state performance comparison, the THD values of output voltage waveform are compared for the two cases; one for small load current and other for large current. The results are shown in Table 7-6. Good performance is obtained for the proposed controller in the steady-state as well. The THD values are very small and also the voltage regulation at the reference level is very good. Thus an improved steady-state performance is obtained for the proposed controller.

Table 7-6: comparison of steady-state performance of the proposed controller with [48].

	Output voltage		Load current (A)
	THD	RMS value (V)	
Controller of ref. [48]	1%	110.3	0.1
Proposed Controller	0.91%	155.6	0.11
Controller of ref. [48]	0.9%	109.5	39.3
Proposed Controller	0.79%	155.5	22.2

7.6 Conclusion

The proposed reference tracking robust control method was implemented and tested on the VSI system with simulations and real time hardware in the loop experiments. It was observed to give remarkable results. The controller was designed by the proposed method with given uncertainty ranges of the load. The controller stabilized the system efficiently in presence of uncertainties and load disturbances and also demonstrated excellent reference tracking ability. The derived results have provided an efficient way for the application of control theory for norm-bounded uncertainties to VSIs and also enabled optimization of the controller for best performance. The performance comparison of the proposed method with the existing relevant methods in literature has shown that the VSI performance is improved with the proposed controller. This establishes the effectiveness of the method.

CHAPTER 8

RESULTS AND ANALYSIS: GRID-CONNECTED VSI

In this chapter the results of the proposed control design method for grid-connected VSI are described which include results of the algorithms for controller design, the results of simulations and the results of the RTHIL experimental work. The developed schematics of the system were provided in section 6.2.2 and 6.2.3 for the simulation and experimental work.

8.1 Results of the algorithms

The 3-phase, 3-leg inverter with LC filter of Figure 4.1 is considered. The constant parameters of the system are given in Table 8-1. The controller is design according to the algorithms discussed in section 5.3. The robust stabilizing controller is designed by the IRSD algorithm for grid-connected case using *theorem 4-2*. The freedom in choice of α and β is utilized to maximize the convergence rate of the system using the intelligent technique DE. For solving the LMIs, the MATLAB® LMI Toolbox and YALMIP [77] are used.

8.1.1 IRSD results

Starting with the IRSD results, the system constants were defined according to Table 8-1. Also the initial uncertainty bounds chosen are shown in this table. The parameters used to initialize DE in this step are shown in Table 8-2.

Table 8-1: System constants for grid-connected VSI.

Parameter	Symbol	Value
Frequency	f	60 Hz
DC voltage	V_{DC}	600 V
Filter capacitance	C_f	75 μ F
Filter inductance	L_f	0.8 mH
Nominal line resistance	R_0	0.4 Ω
Nominal line inductance	L_0	1 μ H
Chosen line resistance uncertainty	λ_R	80 m Ω
Chosen line inductance uncertainty	λ_L	0.02 μ H
Grid voltage	$[V_{GD} \ V_{GQ}]$	[220 0] V
Base voltage (phase-neutral)	V_B	220 V
Base 3 phase power	S_B	100 kVA
Carrier frequency	f_c	12 kHz

Table 8-2: DE parameters of IRSD algorithm for grid-connected mode.

Parameter	Symbol	Value
No. of parameters to be optimized	n	2
Population size	N_P	20
No. of generations	N_G	20
Crossover Factor	FC	0.6
Mutation Factor	FM	0.5
Desired cost	J_d	1e-3

The cost function minimization plot is given in Figure 8.1. The proposed controller settings other results are provided in Table 8-3.

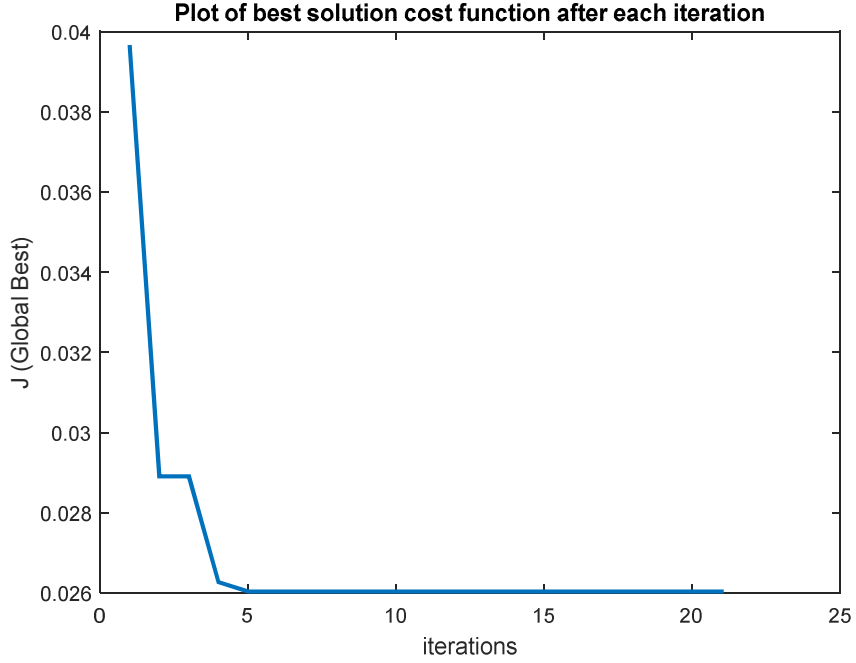


Figure 8.1 Cost minimization in grid-connected IRSD algorithm.

Table 8-3: Results of IRSD algorithm for grid-connected case.

Parameter	Symbol	Value
Tuning parameters	$[\alpha \ \beta]$	$[0.236 \ 0.99]$
Lower bound of α	$\underline{\alpha}$	0.0904
Stabilizing controller gain	\mathbf{K}	$\begin{bmatrix} 213 & 0 & 2.1 & 0 & -8 & 0 \\ 0 & 213 & 0 & 2.1 & 0 & -8 \end{bmatrix} \times 10^{-3}$
Observer gain	\mathbf{L}	$\begin{bmatrix} 3.1 & 0 & -26.4 & 0 & -5705 & 0 \\ 0 & 3.1 & 0 & -26.4 & 0 & -5705 \end{bmatrix}^T$
Convergence rate	h	38.413
Line impedance uncertainty bounds	$[\bar{\lambda}_R \ \bar{\lambda}_L]$	$[57.6m\Omega \ 0.085\mu H]$

The obtained convergence rate can be considered satisfactory. Also the line uncertain parameter bounds are reasonable. As discussed before in section 3.3.3, the actual bound for robustness are higher than these. The uncertainty bound for line inductance has increased considerably from the initially chosen value. Though the uncertainty bound for line resistance is decreased from its initial choice. If required this bound can be increased by modifying the optimization algorithm with a multi-objective cost function that maximizes the uncertainty bound along with the convergence rate. Next step is to design the tracking controller.

8.1.2 IRTD results

The tracking controller is designed using the DE based algorithm IRTD in section 5.3.3 for optimum tracking performance. The designed tracking controller also successfully passes the robustness test which is performed as mentioned in *remark 4-3*. This establishes guaranteed robustness of controller for the given uncertainty. The DE initialization parameters and resulting controller gains are provided in Table 8-4. The plot of the cost function minimized during the iterations of the algorithm is shown in Figure 8.2.

8.2 Simulation results

Following the same pattern as in the standalone case, the performance of the designed controller is tested in three cases and a different property is analyzed in each case. The tests are listed below and their specifications are given in Table 8-5.

Case I: Robustness test

Case II: Disturbance test

Case III: Tracking performance test

Table 8-4: DE parameters and results of IRTD algorithm for grid-connected mode.

Parameter	Symbol	Value
No. of parameters to be optimized	n	4
Population size	N_p	50
No. of generations	N_G	50
Crossover Factor	FC	0.6
Mutation Factor	FM	0.5
Desired cost	J_d	1e-6
Integral controller gain	K_I	$\begin{bmatrix} -1055.6 & 6081.8 \\ -42 & -8473.6 \end{bmatrix}$

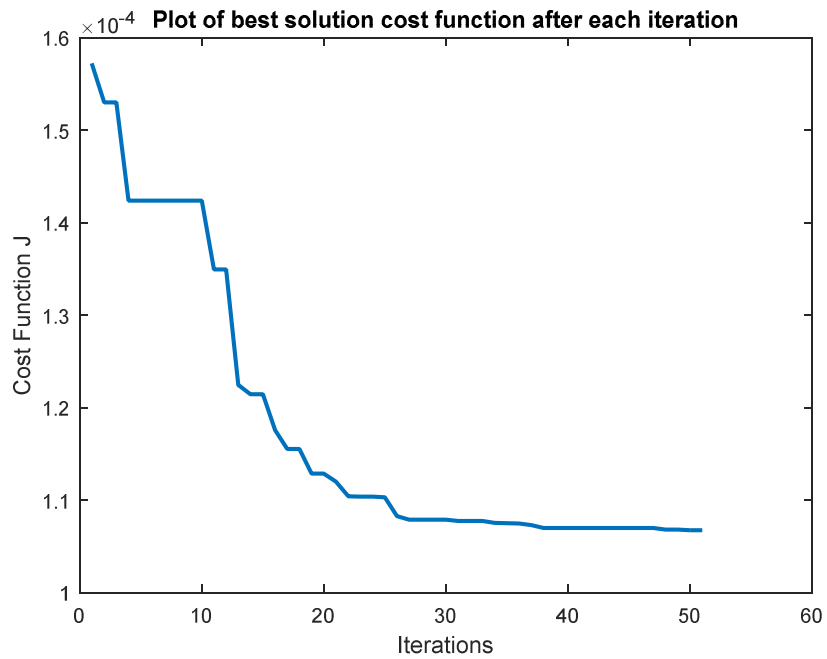


Figure 8.2 Cost function plot of IRTD algorithm for grid-connected mode.

The first case is the robustness test where the performance is observed in the presence of small variations in line resistance and inductance. In the second case the performance of

the system is observed for larger disturbances, when a relatively large change occurs in the line parameters. The third case is dedicated for the tracking performance of the system. Different reference inputs for real and reactive power are provided and results are analyzed. For all cases the system starts at an operating condition of real power output of 20 kW and unity power factor.

Table 8-5: Simulation and experimental tests variations.

Robustness Test					
Time (<i>msec</i>)	0	5	15	25	35
r_g (Ω)	0.4	0.45	0.45	0.4	0.4
l_g (μH)	1	1	1.08	1.08	1
Disturbance Test					
Time (<i>msec</i>)	0	5	25	45	65
r_g (Ω)	0.4	0.6	0.6	0.4	0.4
l_g (μH)	1	1	500	500	1
Tracking Performance Test					
Time (<i>msec</i>)	0	5	25	45	65
P_{ref} (<i>kW</i>)	20	20	15	15	20
Q_{ref} (<i>kVAR</i>)	0	1	1	0	0

Case I: Robustness Test

This purpose of this test is to see the effect of small line impedance variations on the performance of the system. The variations in the load are as given in Table 8-5. The changes in the resistance and inductance values are according to the results of the IRSD

algorithm for which robustness is guaranteed with the obtained convergence rate. Thus excellent performance of the system is expected in this test. As seen in Figure 8.3, the power output of the system is regulated at the desired value during the test. The magnitude of deviation is very small and the settling time is less than 5 msec. In Figure 8.4 the plot of current injected to the grid is shown. The robustness of the system for is clear from the three phase sinusoidal waves of the current signal as a very small spike is observed at the time the uncertainty acts. A very small deviation can be observed in i_{ld} as well and it settles back in less than 5 msec. Also the capacitor voltage signals can be seen in Figure 8.5.

Case II: Disturbance Test

In this case large disturbances are applied to the system by means of simulating big changes in the line impedance parameters as given in Table 8-5. The purpose is to observe if the system can maintain stability in the event of such huge variations. As the results show in the Figure 8.6, the system remain stable in face of the disturbances and the power output is regulated at the reference value, although the deviations are large which is expected. The settling time in each deviation is still impressive, around 5 msec. The same can be inferred from the plot of current and voltage signals in Figure 8.7 and Figure 8.8 respectively.

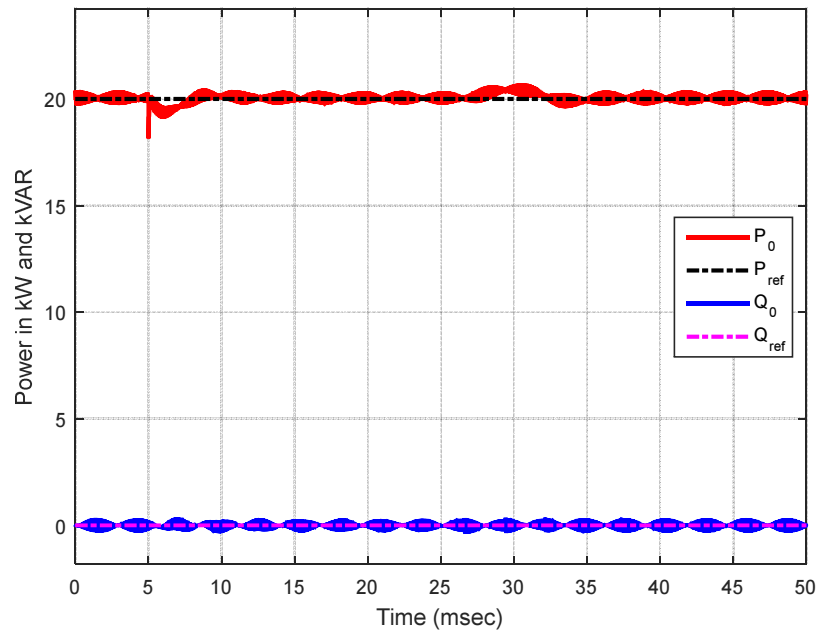


Figure 8.3 Grid-connected VSI: Output real and reactive power in robustness test simulation.

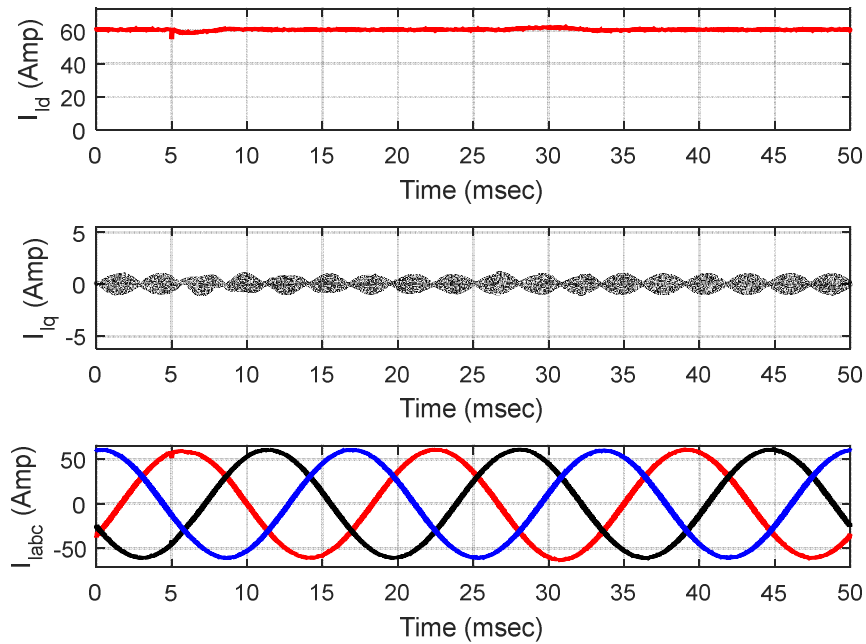


Figure 8.4 Grid-connected VSI: Output/load current in robustness test simulation.

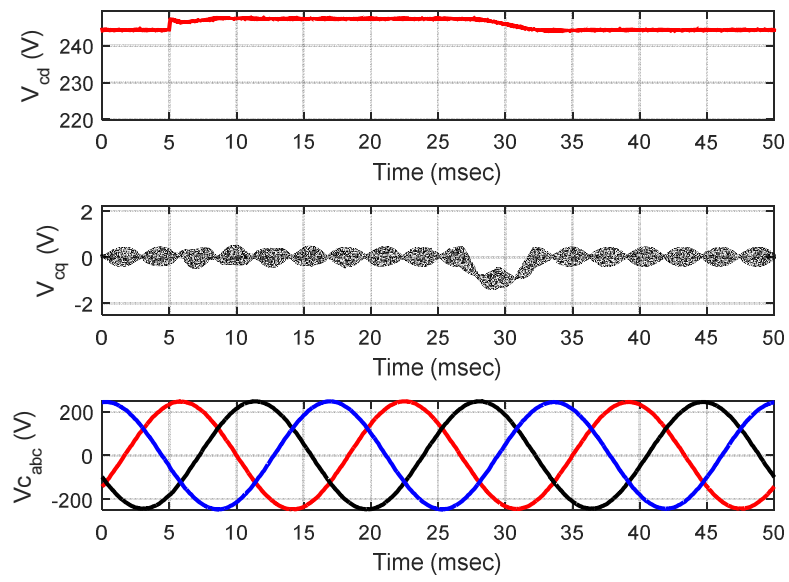


Figure 8.5 Grid-connected VSI: Capacitor voltage in robustness test simulation.

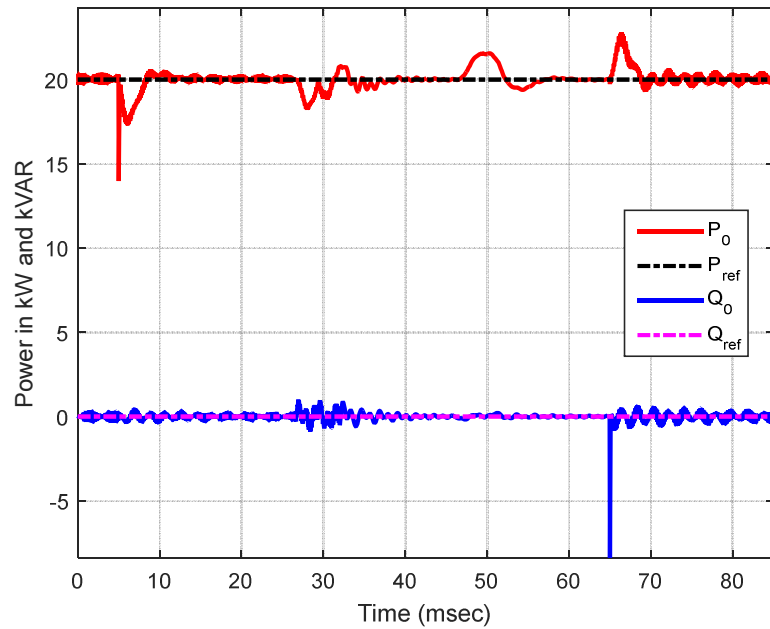


Figure 8.6 Grid-connected VSI: Output real and reactive power in disturbance test simulation.

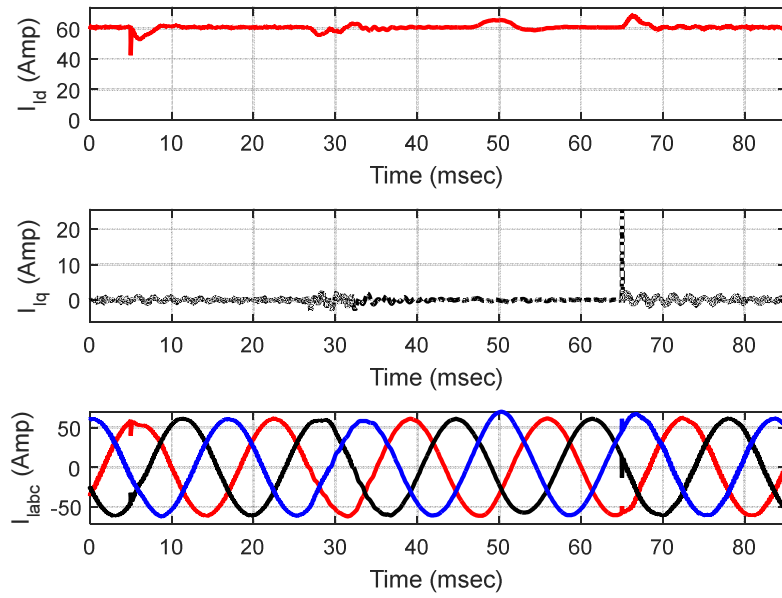


Figure 8.7 Grid-connected VSI: Output/load current in disturbance test simulation.

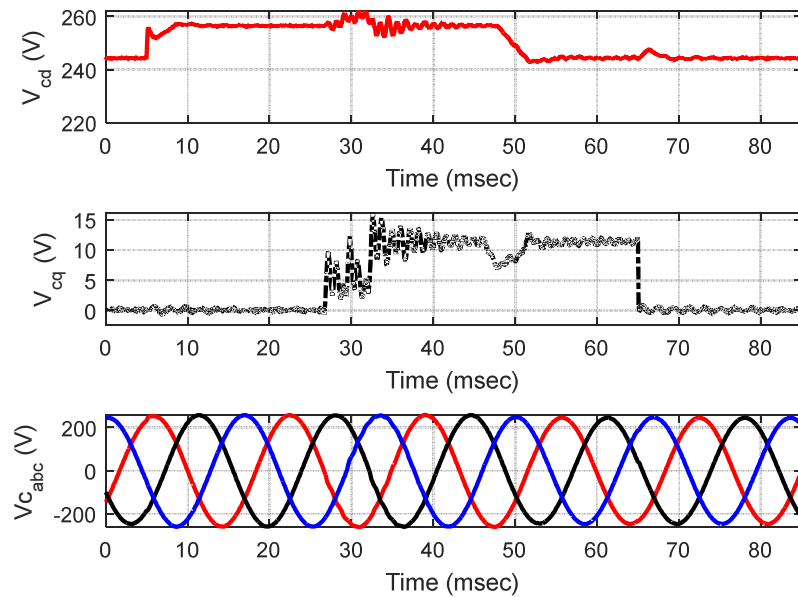


Figure 8.8 Grid-connected VSI: Capacitor voltage in disturbance test simulation.

Case III: Tracking Performance Test

In this case the output real and reactive power are given several reference inputs to follow to observe the tracking performance of the system. Figure 8.9 shows the result. The real and reactive power of system are successfully following the reference inputs which are according to Table 8-5. Few oscillations are observed in the response however they settle quickly. The output current behavior is shown in Figure 8.10, which shows smooth transitions are the reference power level changes. The capacitor voltage is shown in Figure 8.11 which decreases when the current reference decreases and later increases again back with the current, as per theoretical expectations.

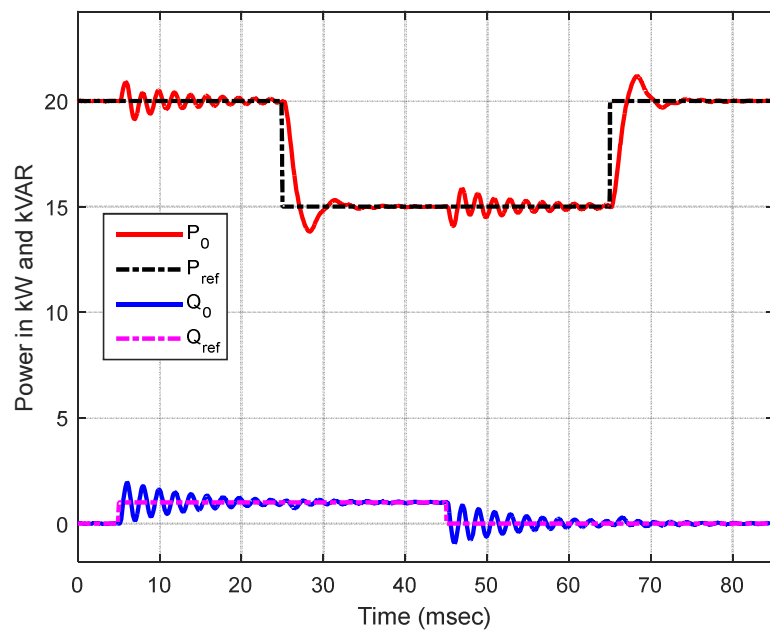


Figure 8.9 Grid-connected VSI: Output real and reactive power in tracking performance test simulation.

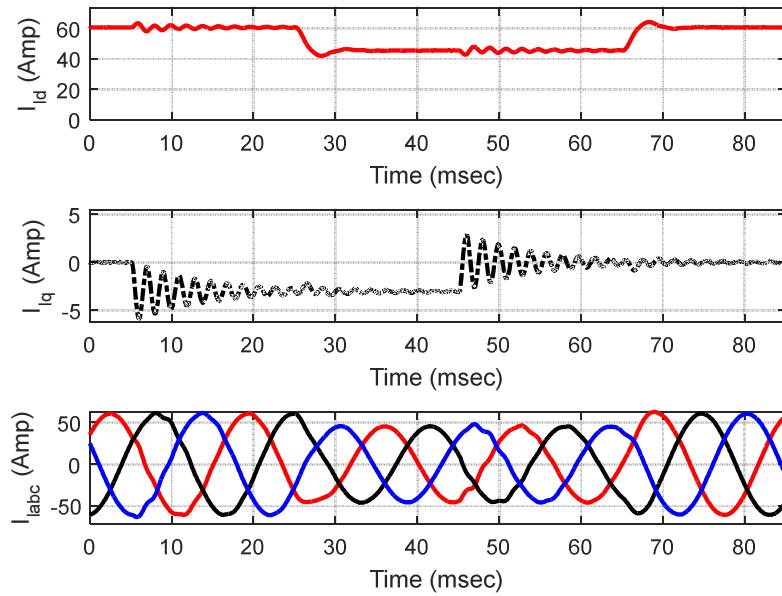


Figure 8.10 Grid-connected VSI: Output/load current in tracking performance test simulation.

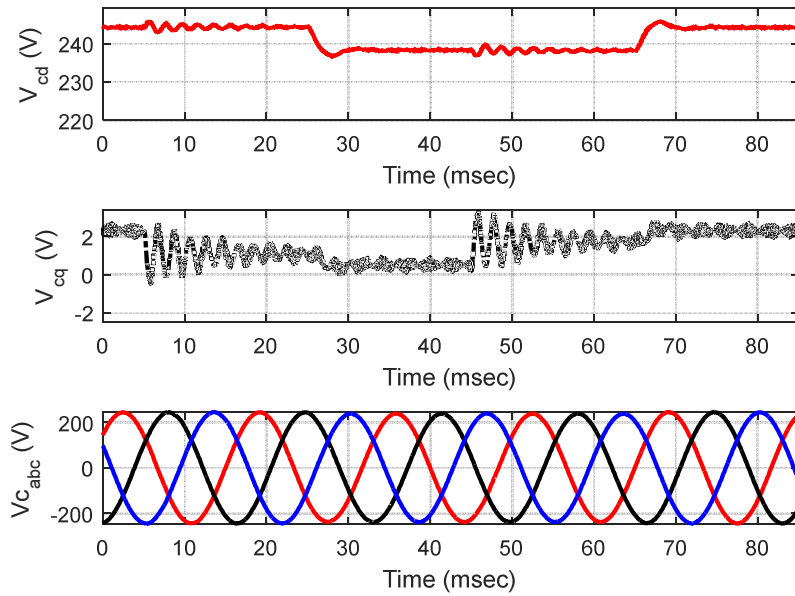


Figure 8.11 Grid-connected VSI: Capacitor voltage in disturbance test simulation.

8.3 Experimental results

The experimental results are presented in the figures to follow. The pattern followed is similar to that of simulation results

Case I: Robustness Test

The same uncertainties are applied as mentioned in Table 8-5 for robustness test. The resulting variations in the real and reactive powers are presented in Figure 8.12. Since the variations of line resistance and inductance are within the guaranteed robustness limit (see Table 8-3), the performance is excellent. Very small deviations are observed in the power signals which defuse within few milliseconds. Similarly very smooth profile dq and three phase signals are obtained for the output current which can be seen in Figure 8.13. The capacitor voltage signals can be observed in Figure 8.14.

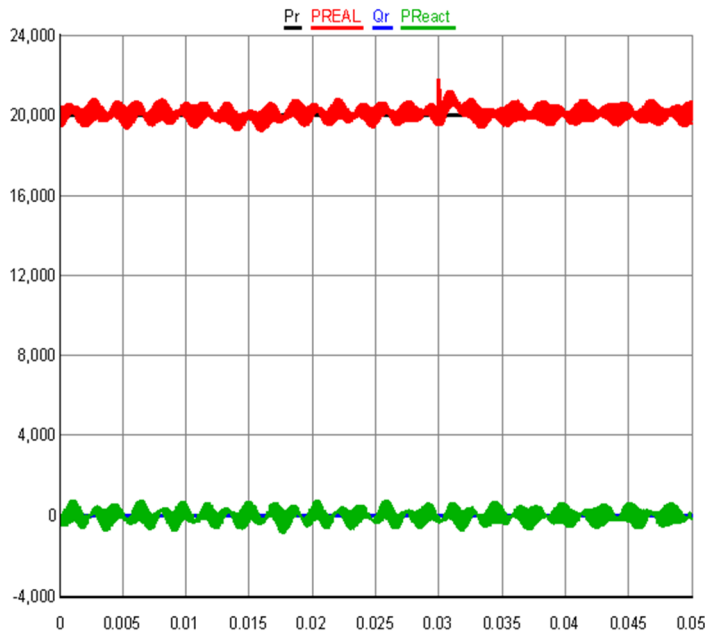


Figure 8.12 Grid-connected VSI: Output real and reactive power in robustness test experiment.

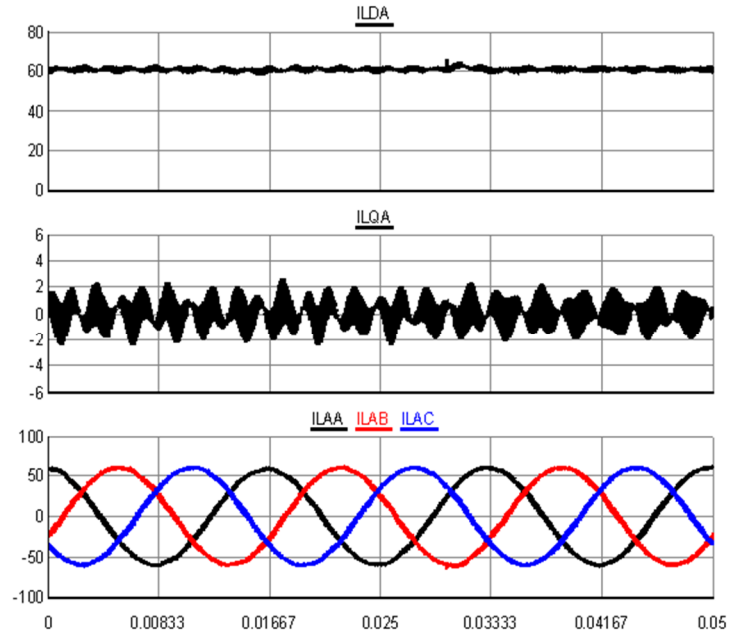


Figure 8.13 Grid-connected VSI: Output/load current in robustness test experiment.

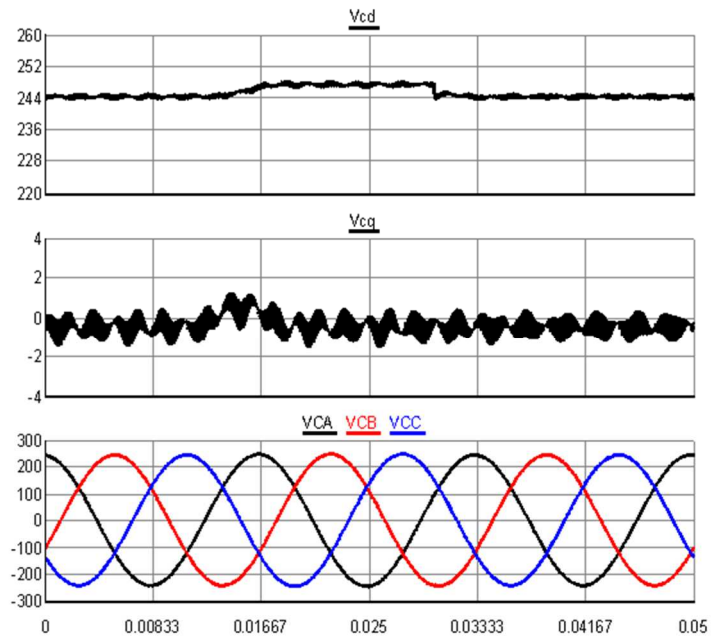


Figure 8.14 Grid-connected VSI: Capacitor voltage in robustness test experiment.

Case II: Disturbance Test

As given in Table 8-5 larger variations are created in the line resistance and inductance. As shown in Figure 8.15, the deviations in the output real and reactive power are larger. However, these deviations settle quickly and the magnitude of deviations can be considered acceptable. Figure 8.16 shows the profile of the current signal which is also more disturbed this time but it is quickly restored to the reference value after each disturbance. The capacitor voltage is changing accordingly with the output current as shown in Figure 8.17.

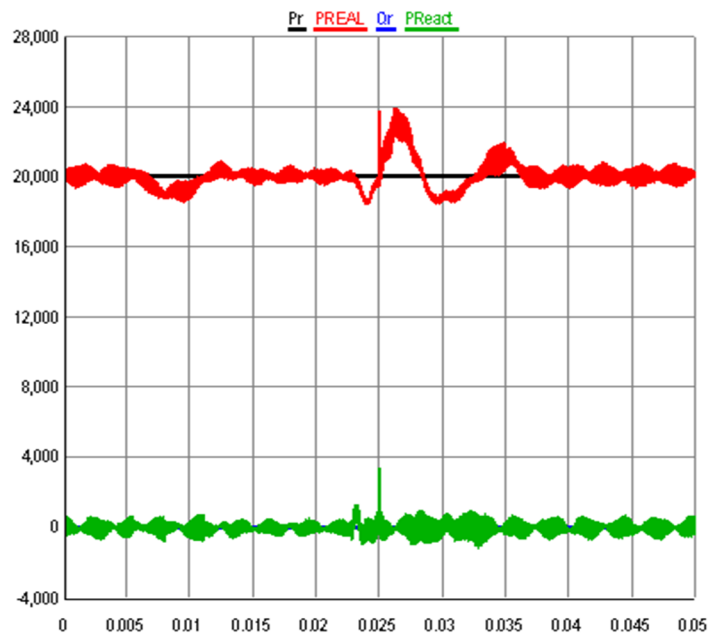


Figure 8.15 Grid-connected VSI: Output real and reactive power in disturbance test experiment.

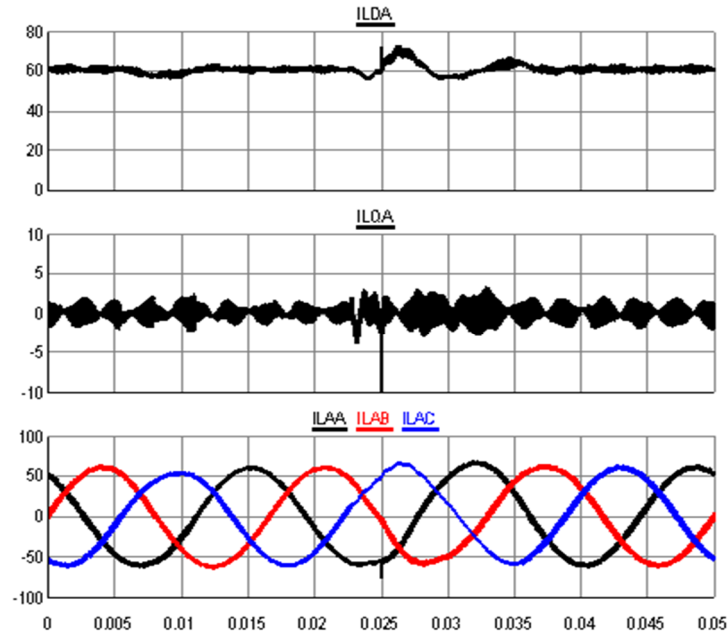


Figure 8.16 Grid-connected VSI: Output/load current in disturbance test experiment.

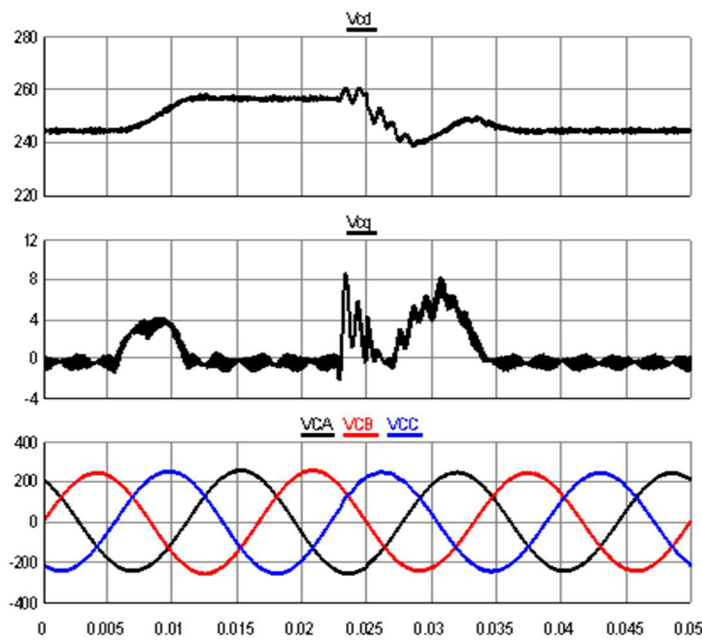


Figure 8.17 Grid-connected VSI: Capacitor voltage in disturbance test experiment.

Case III: Tracking Performance Test

Now the experimental tracking performance tests are performed. Various reference values of real and reactive powers are given as mentioned in Table 8-5. As the results show in Figure 8.18, the output real and reactive powers are able to follow the reference level. Some oscillations are observed in the reactive power response. But these oscillations die out fairly quickly. The current is also expected to show a similar behavior as power given in Figure 8.19. However these oscillations are decaying and after about 0.04 sec it disappear. The capacitor voltage profile is shown in Figure 8.20, which is changing according to the changing output current.

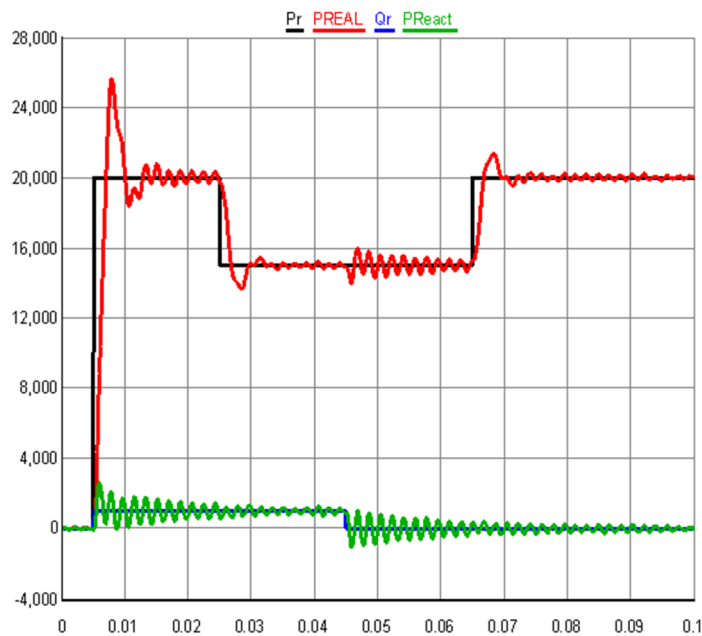


Figure 8.18 Grid-connected VSI: Output real and reactive power in tracking performance test experiment.

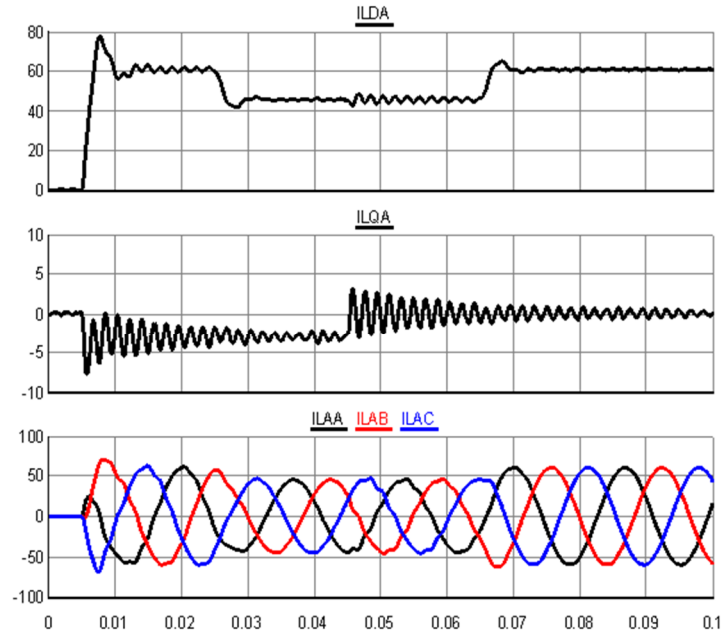


Figure 8.19 Grid-connected VSI: Output/load current in tracking performance test experiment.

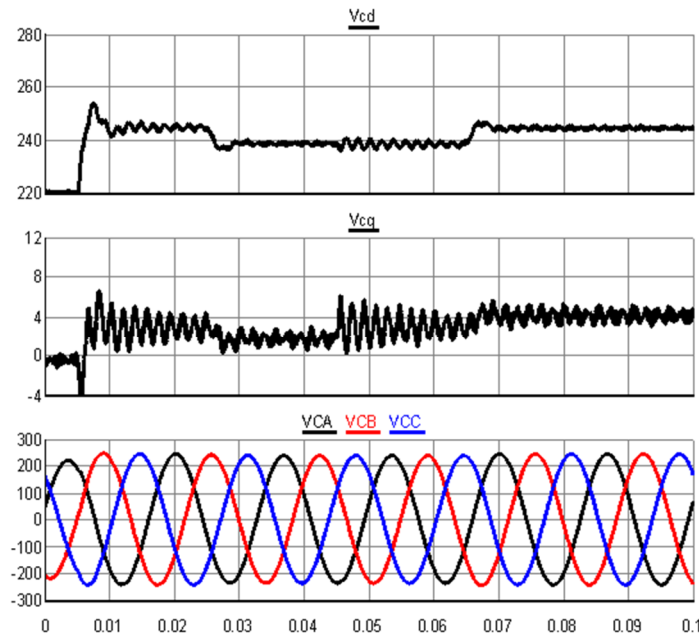


Figure 8.20 Grid-connected VSI: Capacitor voltage in tracking performance test experiment.

8.4 Comparison of Simulation and Experimental Results

To validate the results a comparison of the simulation and experimental results is presented in Figure 8.21, Figure 8.22 and Figure 8.23. The control variable, the output current is compared for the three cases of the results as mentioned in the previous section. The resemblance in the results is very good which validates the adequacy of the results.

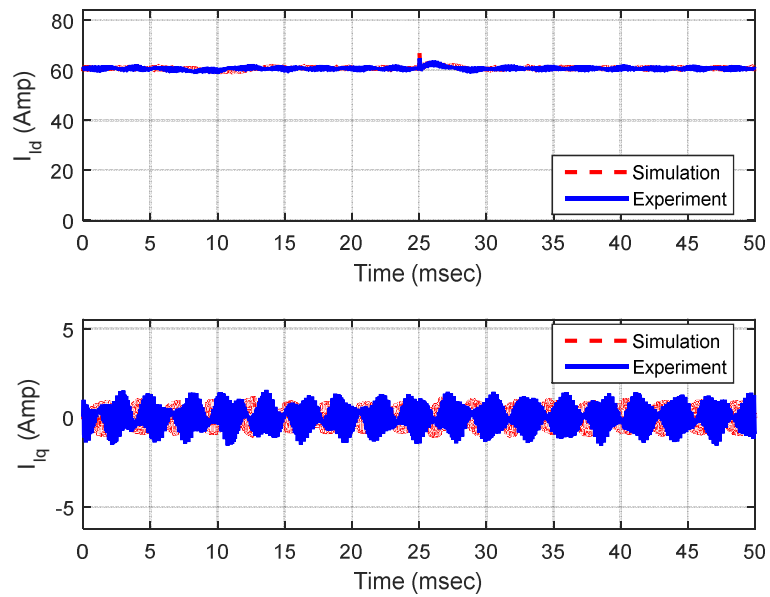


Figure 8.21 Robustness test: Comparison of output voltage in simulations and experiments.

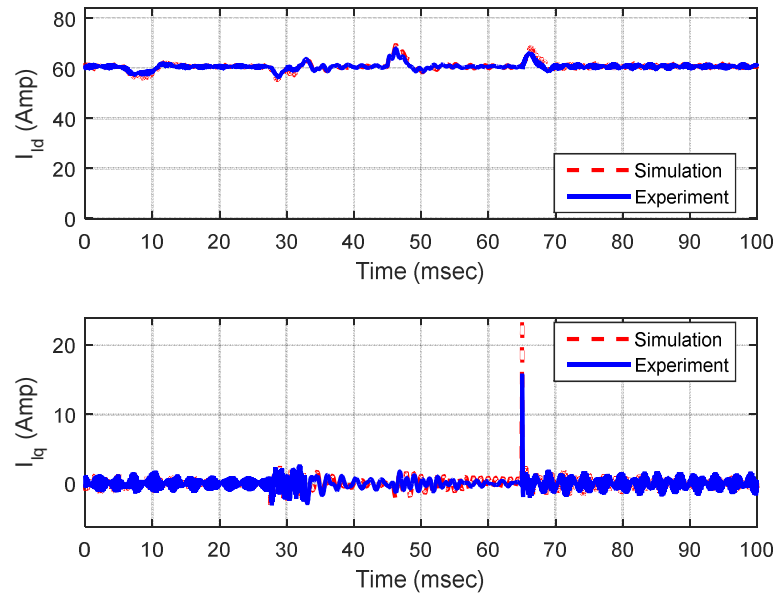


Figure 8.22 Disturbance test: Comparison of output voltage in simulations and experiments.

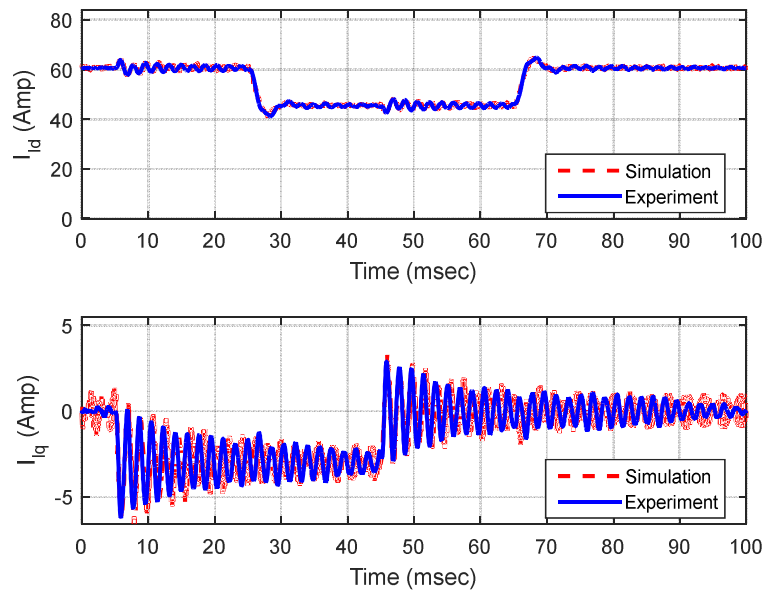


Figure 8.23 Tracking performance test: Comparison of output voltage in simulations and experiments.

8.5 Performance comparison of the proposed controller to existing methods in literature

As discussed in section 2.4, the results of proposed method for grid connected case are compared with the results of reference [30]. The comparison is done in the transient and steady state behavior of the system.

8.5.1 Comparison of transient behavior

To show the transient performance of the system under uncertain variation, Figure 12 is provided in reference [30]. The same figure is also presented in Figure 8.24.

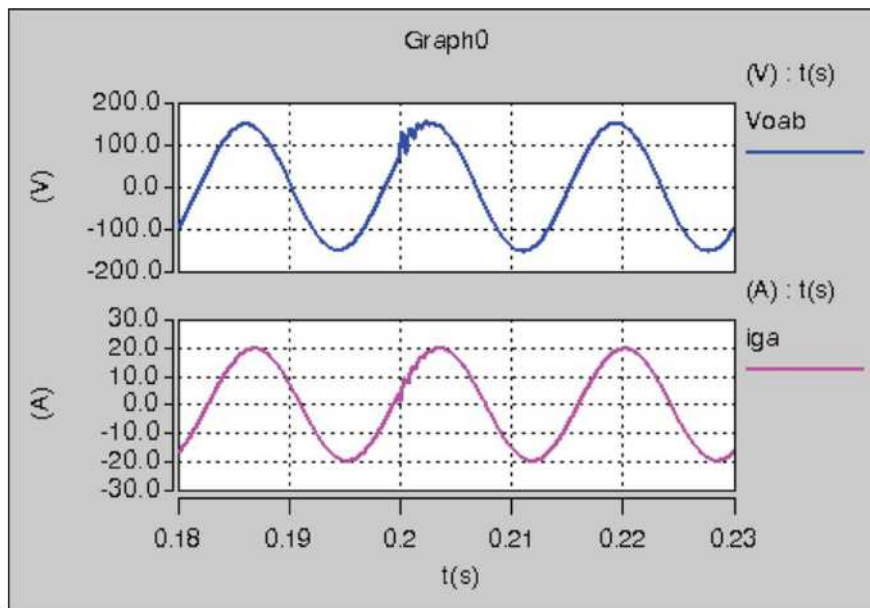


Fig. 12. Simulation results of the H_∞ controller with grid impedance $[r_g, L_g]$ changing from $[0.1 \Omega, 0.05 \text{ mH}]$ to $[0.2 \Omega, 0.3 \text{ mH}]$ at the instant $t = 0.2 \text{ s}$.

Figure 8.24 Transient performance of the controller proposed in [30].

The controller in [30] is designed for the nominal values $[r_g, L_g] = [0.2\Omega, 0.15mH]$. To show the transient performance of the system, the r_g value is changed from, half of the nominal value to the nominal value and the L_g value from one third of the nominal value to twice the nominal value.

Now the performance of the proposed controller in this work is shown. The nominal values for which the controller is designed are $[r_g, l_g] = [0.4\Omega, 1\mu H]$. To show the transient performance of the proposed controller the r_g value is changed from half of nominal value to the 1.5 times the nominal value and the l_g value is changed from $1/10^{\text{th}}$ of the nominal value to 50 times the nominal value, i.e. from $[0.2\Omega, 0.1\mu H]$ to $[0.6\Omega, 50\mu H]$. The changes occur at $t=20$ msec. The resulting response of the output current and the filter capacitor voltage is shown in Figure 8.25.

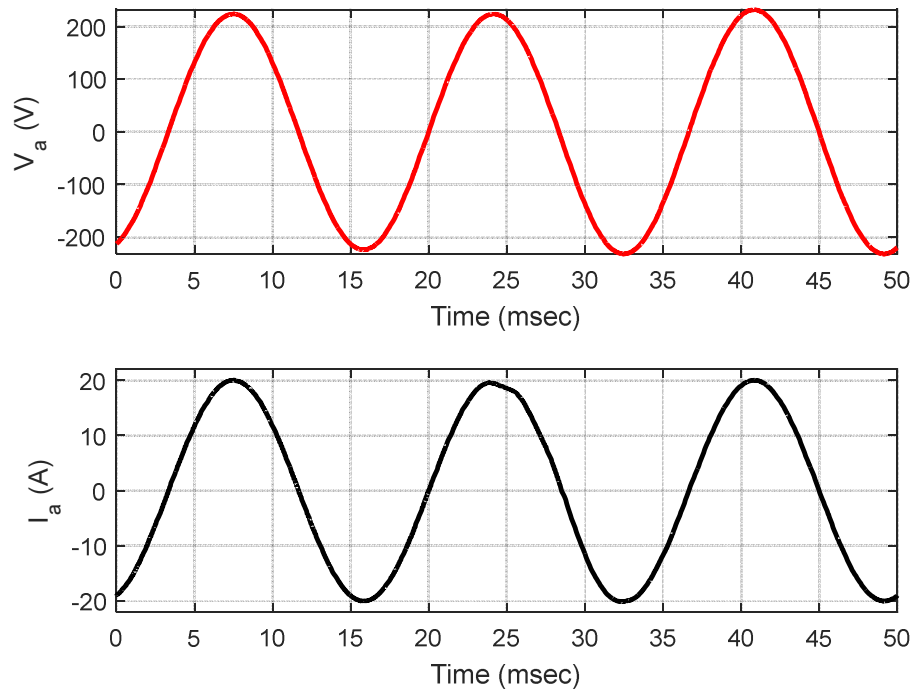


Figure 8.25 Simulation results of the proposed controller for grid-connected VSI, when $[r_g, l_g]$ change from $[0.2\Omega, 0.1\mu H]$ to $[0.4\Omega, 10\mu H]$

The signal profile of voltage and current in Figure 8.25 look smoother as compared to the one in Figure 8.24. Thus for larger or equal percentage variation from the nominal value, the performance of the proposed controller is improved.

To further establish the improvement by the proposed controller, another case is considered where the transient behavior is investigated in case of larger change in l_g only. The following figure shows the response of the proposed controller when l_g is changed from 0.05 mH to 0.3 mH , where r_g remain constant at 0.4Ω .

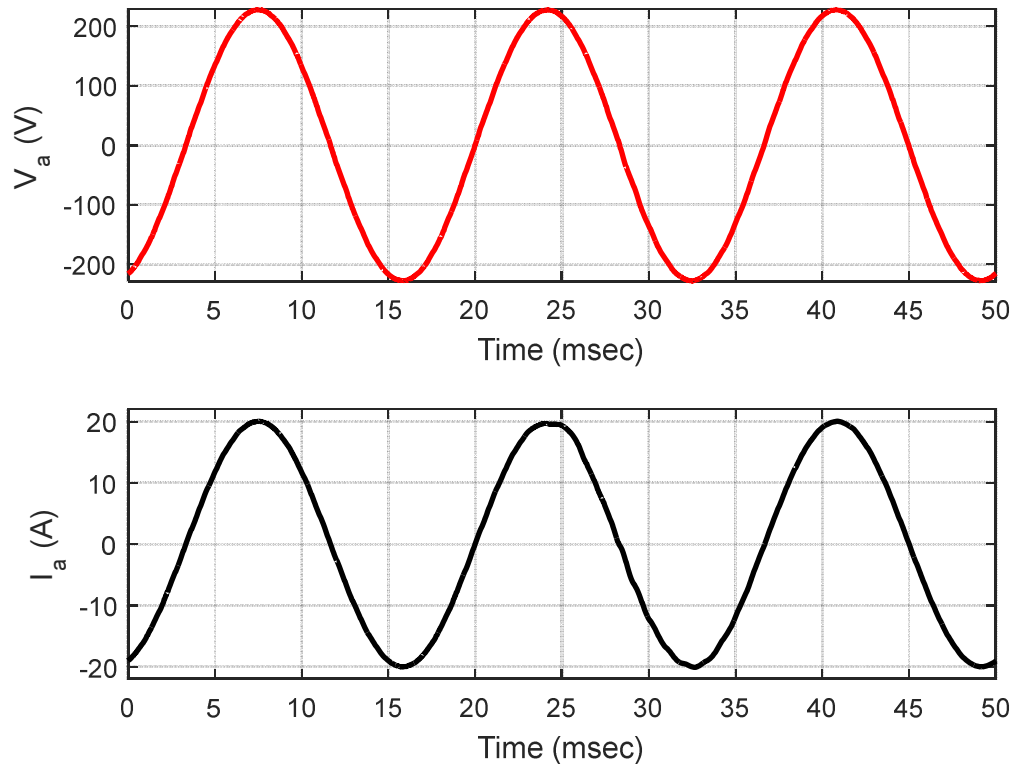


Figure 8.26 Transient performance of the proposed controller when l_g is changed from 0.05 mH to 0.3 mH .

This shows that the proposed controller can withstand very large amount of uncertainties and perform very smoothly.

8.5.2 Comparison of steady-state performance

For comparison of the steady-state performance, the THD values of current signal for different reference values and under uncertain values are collected as given in Table 8-6. The results for the H_∞ controller are obtained from Table II of reference [30].

The two cases presented in [30] are compared with similar cases of the proposed controller. As seen in Table 8-6, comparison case I is when the controllers are operating at the nominal values of the grid impedance. The comparison shows that the THD values for the three different reference inputs for the output current are improved by the proposed controller. Smaller THD values are obtained for all the three current levels.

In the comparison case II, for both controllers, an equal deviation is considered in the grid line inductance while the grid line resistance remains at nominal value. Again the proposed controller demonstrates improved performance over the H_∞ controller. The THD values for reference currents of 10A and 20A are considerably smaller with the proposed controller. For the 15A reference the THD value of the proposed controller is just slightly high. Therefore in this case as well, the proposed controller has shown improved performance.

Table 8-6: THD values of the H_∞ controller in reference [30] and the proposed controller.

	Controller	Grid impedance	Change from nominal value		i_{ldref} and P_{ref}		
					10 A	15 A	20 A
			Δr_g	Δl_g	3.3 kW	4.95 kW	6.6 kW
Comparison case I	H_∞ controller	$[r_g, L_g]$ = [0.2 Ω , 0.15mH]	0	0	3.398%	2.441%	2.385%
	Proposed controller	$[r_g, l_g]$ = [0.4 Ω , 1 μ H]	0	0	2.88%	2.15%	1.69%
Comparison case II	H_∞ controller	$[r_g, L_g]$ = [0.2 Ω , 0.3mH]	0	0.15mH	3.709%	2.401%	2.206%
	Proposed controller	$[r_g, l_g]$ = [0.4 Ω , 0.15mH]	0	0.15mH	3.01%	2.44%	1.65%
Additional cases	Proposed controller	$[r_g, l_g]$ = [0.4 Ω , 0.3mH]	0	0.3mH	3.03%	2.99%	2.23%
	Proposed controller	$[r_g, l_g]$ = [0.3 Ω , 0.15mH]	-0.1 Ω	0.15mH	3.42%	2.47%	2.24%
	Proposed controller	$[r_g, l_g]$ = [0.5 Ω , 0.15mH]	0.1 Ω	0.15mH	2.53%	2.24%	1.62%

Some additional cases are also presented in which the THD values are shown for the proposed controller. In one case l_g value is changed to 0.3mH, which is a big deviation from the nominal value. For this case as well, the proposed controller shows very good performance as the THD values remain under 3.5% for all the reference current levels. In the other two cases the THD values are shown for some deviations in the grid line

resistance. The results are satisfactory, as very low THD values are obtained especially for higher reference current values. This establishes that the performance of the grid-connected VSI, is improved by the proposed controller in comparison to the similar work in literature.

8.6 Conclusion

The results obtained for the grid-connected VSI are satisfactory. As demonstrated by the robustness test, the controller was able to robustly stabilize the system with excellent performance in terms of negligible deviation from the steady-state values, if the uncertain parameters stayed in the range of allowable limit. For higher deviations the performance would deteriorate, which is expected. However the controller was able to keep the system stable with fairly good performance during large disturbances too as the system converges back to the steady-state in a few milliseconds. The tracking controller was also effective as it was able to make the system's output power follow the reference value efficiently. Additionally the effectiveness of the controller was established by a comparison of its performance to one of the most recent and closely related work in [30]. The comparison showed that the proposed controller provided improved performance in both the transient and steady-state.

CHAPTER 9

CONCLUSIONS AND FUTURE WORK

In this chapter, the conclusions and inferences of the thesis are summarized. This mainly outlines the considered problem, the proposed solution and its application and analysis of the results. Also a discussion on the prospects of extending this work in future is presented at the end.

9.1 Standalone VSI: Conclusions

Conclusions related to the robust control design problem of VSIs for applications in standalone mode of microgrid are following:

- 1- The problem of robust control design for standalone VSI was considered which has application in the autonomous mode of microgrid.
- 2- The objective of control design was to robustly stabilize the VSI system for a given range of load uncertainties with regulation of the output voltage at the required reference level.
- 3- A time domain mathematical model of the system was developed using the dynamical equations of the system in the synchronous dq frame.
- 4- A novel approach was presented to design the robust controller by formulating system uncertainties in a fashion that enables application of robust control theory for systems with norm-bounded time varying uncertainties.

- 5- A new control design theorem (*theorem 3-1*) was derived using Sylvester's criteria which provided a systematic way of choosing the arbitrary uncertainty coefficient matrices and tune the controller for higher convergence rate.
- 6- On the grounds of the first theorem, a second theorem (*theorem 3-2*) was developed to design robust controller with a guaranteed convergence rate for certain bounds of the uncertainties.
- 7- Using an evolutionary optimization technique (DE), an algorithm (IRSD) was developed based on earlier presented theorems, to optimize the robust controller by maximizing the convergence rate of the system, for certain ranges of uncertainties.
- 8- For reference tracking of the output voltage, the control law was augmented with integral controller and a method to test the robustness of the system with the augmented controller was presented.
- 9- Another algorithm based on DE was presented to optimize the integral controller gain for good tracking performance.
- 10- Controller was designed for a standalone VSI system using the proposed algorithms and the results of the algorithms were presented.
- 11- Simulations of the system with the proposed controller were developed in MATLAB/SIMULINK. And the performance of the system was tested under different practical scenarios.
- 12- Real-time hardware-in-the-loop (RTHIL) experimental setup was developed using RTDS simulator and dSPACE DS1103 controller board. The system with the proposed controller was tested under several different disturbance cases on the RTHIL setup.

13- The performance of the systems was found to be excellent with the proposed controller. The results showed improvement in the transient behavior of the system. The system was able to sustain small uncertainties very well as their effect on the output voltage profile was negligible. For larger parameter variations as well the controller was able to keep the system stable with good performance. The controller also demonstrated very good tracking performance. Thus the efficacy of the proposed controller was illustrated.

9.2 Grid-connected VSI: Conclusions

The proposed control design method was extended for the grid-connected VSI case. The conclusions related to this work are presented now.

- 1- The problem of robust control design for VSI in the grid-connected mode of the microgrid was considered.
- 2- The objective of control design was to robustly stabilize the VSI system for a given range of line impedance uncertainties with regulation of the output real and reactive power at the required reference level.
- 3- A mathematical model of the grid-connected VSI system was developed in time domain using the dynamical equations of the system in the synchronous dq frame.
- 4- A novel approach to design the robust controller was presented by formulating system uncertainties in a manner that enables application of robust control theory for systems with norm-bounded time varying uncertainties.
- 5- A new control design theorem (*theorem 4-1*) was derived using Sylvester's criterions which provided a systematic way to tune the controller for higher convergence rate by rightly choosing the arbitrary uncertainty coefficient matrices.

- 6- Based on the first theorem, another theorem (*theorem 4-2*) was developed to design robust controller for certain bounds of the uncertainties with a guaranteed convergence rate.
- 7- An algorithm (IRSD) was developed using an evolutionary optimization technique (DE) to optimize the robust controller performance, based on formerly developed theorems. This algorithm maximizes the convergence rate of the system, for certain ranges of uncertainties.
- 8- For reference tracking of the real and reactive power to the grid, the robust stabilizing controller was augmented with integral controller and a test to establish the robustness of the system with the augmented controller was presented.
- 9- Another DE based algorithm was developed to optimize the integral controller gain for good tracking performance of the output power.
- 10- Using the proposed algorithms the controller was designed for the grid-connected VSI system and the results of the algorithms were presented.
- 11- Simulations were developed in MATLAB/SIMULINK for the grid-connected system with the proposed controller and the performance of the system was evaluated under different test cases.
- 12- The grid-connected system with the proposed controller was also tested under several different cases of uncertainties and disturbances, on the RTHIL setup.
- 13- The proposed controller showed excellent performance for the grid-connected system as well. The transient behavior of the system was improved as it demonstrated small magnitude of deviations and fast convergence to steady-state. Negligible effect was observed on the current and power signal profile due to small

uncertainties. Also, the controller was able to keep the system stable with good performance for larger variations in the uncertain parameters. Very good tracking performance was demonstrated by the controller as well. The effectiveness of the proposed controller was thus illustrated.

9.3 Future Work

There are several possibilities of extending this work in future as following:

- 1- The proposed control design scheme can be applied with other robust control design methods for linear systems with norm-bounded time varying uncertainties, such as [72], [73].
- 2- A robust control design toolbox can be developed in MATLAB in which several control design methods are available to the user. Providing the system constants, the user can design robust controller with any of these methods for VSI in both, the standalone or grid connected modes of the microgrid. The toolbox also provides the user with the simulation results of the system with the resulting controller. This way the user can apply several control design methods, compare their results and choose the best one for his case.
- 3- The proposed controller can be designed for a prototype inverter and hardware experimental results can be obtained. Controller implementation for this can be done on the existing DS1103 board.
- 4- The proposed method can be applied for control of microgrid where multiple VSIs are connected. Both Islanded and grid-connected mode can be considered.
- 5- Multi-objective optimization algorithms can be designed, where not only the convergence rate, but the uncertainty bounds are maximized.

- 6- The robust tracking controller can be designed with a different approach, where the integral controller is augmented in the system first and then the robust stabilizing controller is designed for the augmented system.
- 7- Other intelligent techniques can be used for implementation of the optimization algorithms, such as particle swarm optimization (PSO), simulated annealing etc.

APPENDIX

dSPACE DS1103 CONTROLLER BOARD: UTILITY AND APPLICATIONS

The DS1103 controller board is a product of dSPACE GmbH. It is a Programmable process controller (PPC) board which is used for numerous applications in engineering research. A brief overview regarding the applications and functionalities of DS1103 controller board is presented in this appendix.

1. Prominent features

- 1- It is a single board system, providing processing in real-time with an ample range of input/output connections.
- 2- High speed and precision of the input/output channels
- 3- Featuring CAN (controller area network) bus which allow communication between controllers and devices without requiring a computer in between.
- 4- Providing serial interfaces appropriate for automotive applications
- 5- With PLL-based UART (Universal asynchronous receiver transmitter) for high accuracy baud rate.

2. Major applications

The DS1103 controller board is an advanced rapid prototyping tool. Following are some of its major applications:

- 1- Automation and control systems
- 2- Control of power electronic converters
- 3- Variable speed drives
- 4- Robotics
- 5- Automotive control
- 6- Active vibration control

3. Input/output interfaces

The DS1103 controller board has a variety of input/ output interfaces to meet the needs in a wide range of applications. The details are as following:

- 1- 20 A/D channels with 16 bit resolution
- 2- 8 D/A channels with 16 bit resolution
- 3- 32 bit digital I/O channels
- 4- Digital incremental encoder interface (6 channels)
- 5- Analogue incremental encoder interface (1 channel)
- 6- Serial interface

7- CAN interface

8- To perform additional I/O task, a slave DSP can be interfaced

4. Controller programming with RTI Simulink blocks library.

Programming a controller on DS1103 is simplified by RTI (real-time interface) Simulink library. In a very convenient way Simulink models can be programmed on the controller board using the I/O blocks for external connections from this library. The Figure 1 shows the RTI Simulink library.

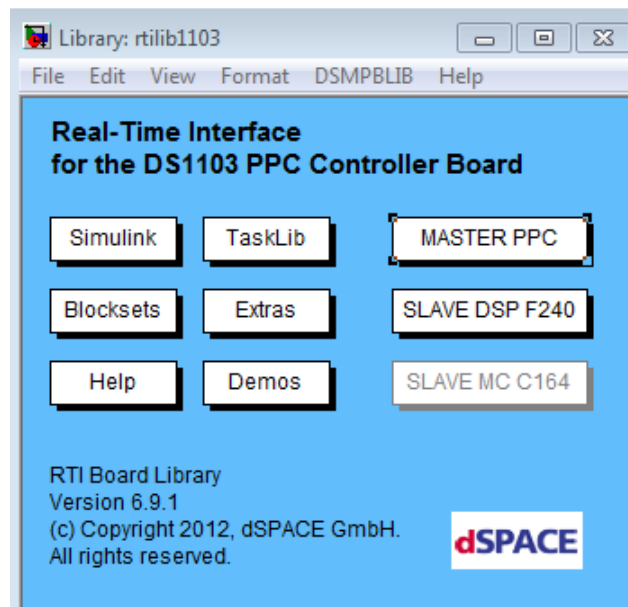


Figure 1 RTI Simulink Library.

The blocks available in the library enable the user to graphically configure all the I/O interfaces. The Figure 2 shows a view of the RTI master PPC library, which has all the real-time interfacing blocks for the DS1103 controller board.

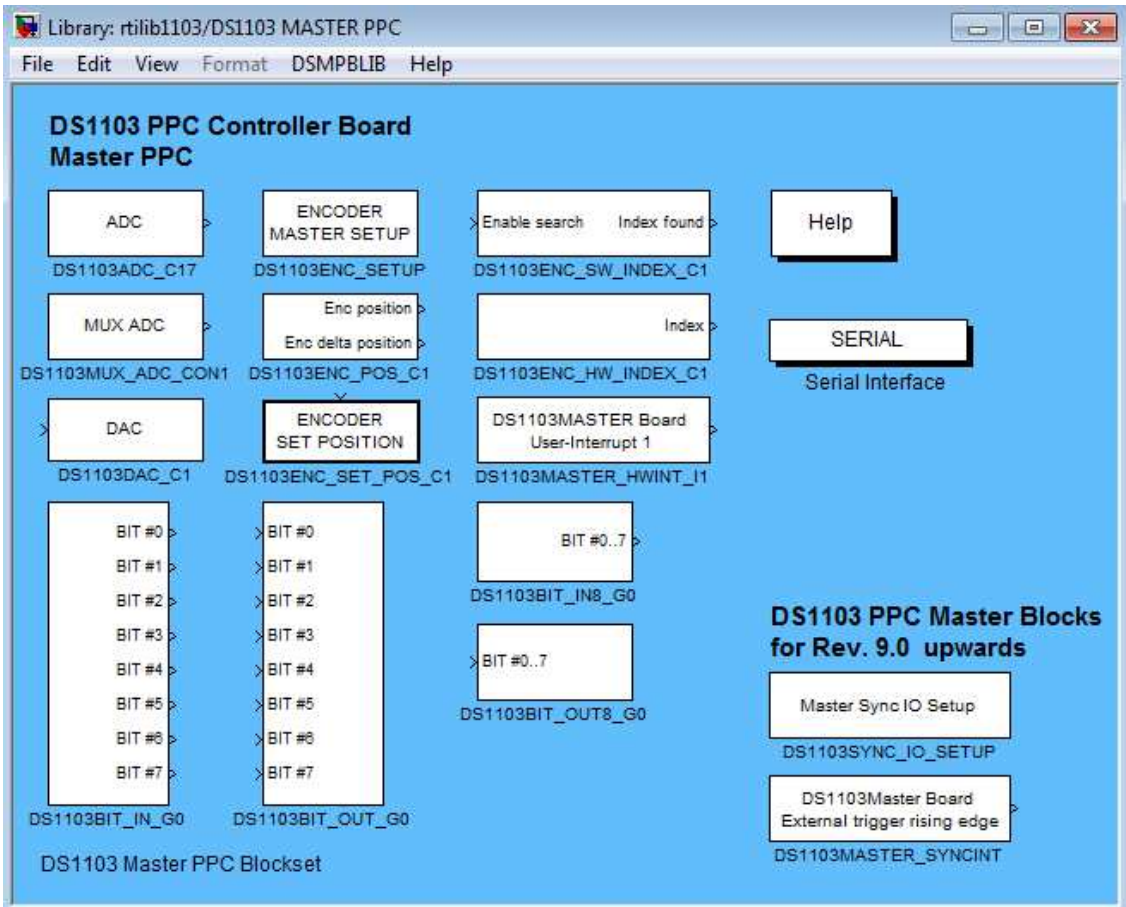


Figure 2 View of the RTI Master PPC library.

The various I/O blocks are visible in the figure, such as ADC for analogue input signals, DAC for analogue output signals, DS1103_BIT_IN block for digital input, DS1103_BIT_OUT block for digital output signals. The description of how to use these blocks is also provided. The help documentation can be accessed from the main RTI library as visible in Figure 1.

For the work done in this thesis, mainly the analogue I/O interfacing was required. Thus the ADC, MUX_ADC and DAC blocks were used. The implementation schematics are provided in chapter 6.

References

- [1] F. Blaabjerg, R. Teodorescu, M. Liserre, and A. V. Timbus, "Overview of Control and Grid Synchronization for Distributed Power Generation Systems," *IEEE Trans. Ind. Electron.*, vol. 53, no. 5, pp. 1398–1409, Oct. 2006.
- [2] M. Liserre, T. Sauter, and J. Hung, "Future Energy Systems: Integrating Renewable Energy Sources into the Smart Power Grid Through Industrial Electronics," *IEEE Ind. Electron. Mag.*, vol. 4, no. 1, pp. 18–37, Mar. 2010.
- [3] S. Alepuz, S. Busquets-Monge, J. Bordonau, J. Gago, D. Gonzalez, and J. Balcells, "Interfacing Renewable Energy Sources to the Utility Grid Using a Three-Level Inverter," *IEEE Trans. Ind. Electron.*, vol. 53, no. 5, pp. 1504–1511, Oct. 2006.
- [4] M. Prodanovic and T. C. Green, "High-Quality Power Generation Through Distributed Control of a Power Park Microgrid," *IEEE Trans. Ind. Electron.*, vol. 53, no. 5, pp. 1471–1482, Oct. 2006.
- [5] M. Davari and Y. A.-R. I. Mohamed, "Robust Multi-Objective Control of VSC-Based DC-Voltage Power Port in Hybrid AC/DC Multi-Terminal Micro-Grids," *IEEE Trans. Smart Grid*, vol. 4, no. 3, pp. 1597–1612, Sep. 2013.
- [6] J. He and Y. W. Li, "Generalized Closed-Loop Control Schemes with Embedded Virtual Impedances for Voltage Source Converters with LC or LCL Filters," *IEEE Trans. Power Electron.*, vol. 27, no. 4, pp. 1850–1861, Apr. 2012.
- [7] J. R. Fischer, S. A. Gonzalez, M. A. Herran, M. G. Judewicz, and D. O. Carrica, "Calculation-Delay Tolerant Predictive Current Controller for Three-Phase Inverters," *IEEE Trans. Ind. Informatics*, vol. 10, no. 1, pp. 233–242, Feb. 2014.
- [8] F. M. Serra, C. H. De Angelo, D. G. Forchetti, and G. O. Garcia, "Non-linear control of a three-phase front end converter," in *2012 IEEE International Conference on Industrial Technology*, 2012, no. Vdc, pp. 821–826.
- [9] J. Jung, N. T. Vu, D. Q. Dang, T. D. Do, Y.-S. Choi, and H. H. Choi, "A Three-Phase Inverter for a Standalone Distributed Generation System: Adaptive Voltage Control Design and Stability Analysis," *IEEE Trans. Energy Convers.*, vol. 29, no. 1, pp. 46–56, Mar. 2014.
- [10] M. A. Haj-ahmed and M. S. Illindala, "The influence of inverter-based DGs and their controllers on distribution network protection," in *2013 IEEE Industry Applications Society Annual Meeting*, 2013, pp. 1–9.

- [11] N. Bhugra and K. P. Detroja, "Sliding mode control based power balancing for grid connected PV system," *2013 IEEE Int. Conf. Control Appl.*, pp. 673–678, Aug. 2013.
- [12] D.-E. Kim and D.-C. Lee, "Inverter Output Voltage Control of Three-Phase UPS Systems Using Feedback Linearization," in *IECON 2007 - 33rd Annual Conference of the IEEE Industrial Electronics Society*, 2007, pp. 1737–1742.
- [13] S. Jiang, D. Cao, F. Z. Peng, Y. Li, and J. Liu, "Low THD, fast transient, and cost-effective synchronous-frame repetitive controller for three-phase UPS inverters," in *2011 IEEE Energy Conversion Congress and Exposition*, 2011, pp. 2819–2826.
- [14] G. S. G. Shen, D. X. D. Xu, L. C. L. Cao, and X. Z. X. Zhu, "An Improved Control Strategy for Grid-Connected Voltage Source Inverters With an LCL Filter," *IEEE Trans. Power Electron.*, vol. 23, no. 4, pp. 1899–1906, Jul. 2008.
- [15] Y. A.-R. I. Mohamed and E. F. El-Saadany, "A Robust Natural-Frame-Based Interfacing Scheme for Grid-Connected Distributed Generation Inverters," *IEEE Trans. Energy Convers.*, vol. 26, no. 3, pp. 728–736, 2011.
- [16] P. Cortes, M. P. Kazmierkowski, R. M. Kennel, D. E. Quevedo, and J. Rodriguez, "Predictive Control in Power Electronics and Drives," *IEEE Trans. Ind. Electron.*, vol. 55, no. 12, pp. 4312–4324, Dec. 2008.
- [17] K.-J. Lee, B.-G. Park, R.-Y. Kim, and D.-S. Hyun, "Robust Predictive Current Controller Based on a Disturbance Estimator in a Three-Phase Grid-Connected Inverter," *IEEE Transactions on Power Electronics*, vol. 27, no. 1, pp. 276–283, 2012.
- [18] M. A. Herran, J. R. Fischer, S. A. Gonzalez, M. G. Judewicz, and D. O. Carrica, "Adaptive Dead-Time Compensation for Grid-Connected PWM Inverters of Single-Stage PV Systems," *IEEE Trans. Power Electron.*, vol. 28, no. 6, pp. 2816–2825, 2013.
- [19] P. Cortes, J. Rodriguez, C. Silva, and A. Flores, "Delay Compensation in Model Predictive Current Control of a Three-Phase Inverter," *IEEE Trans. Ind. Electron.*, vol. 59, no. 2, pp. 1323–1325, 2012.
- [20] R. A. Mastromauro, M. Liserre, and A. Dell'Aquila, "Study of the Effects of Inductor Nonlinear Behavior on the Performance of Current Controllers for Single-Phase PV Grid Converters," *IEEE Trans. Ind. Electron.*, vol. 55, no. 5, pp. 2043–2052, May 2008.
- [21] M. P. Kazmierkowski, M. Jasinski, and G. Wrona, "DSP-Based Control of Grid-Connected Power Converters Operating Under Grid Distortions," *IEEE Trans. Ind. Informatics*, vol. 7, no. 2, pp. 204–211, 2011.

- [22] Y. Tang, P. C. Loh, P. Wang, F. H. Choo, and F. Gao, "Exploring Inherent Damping Characteristic of LCL-Filters for Three-Phase Grid-Connected Voltage Source Inverters," *IEEE Trans. Power Electron.*, vol. 27, no. 3, pp. 1433–1443, Mar. 2012.
- [23] J. Dannehl, M. Liserre, and F. W. Fuchs, "Filter-Based Active Damping of Voltage Source Converters With LCL Filter," *IEEE Trans. Ind. Electron.*, vol. 58, no. 8, pp. 3623–3633, Aug. 2011.
- [24] D.-E. Kim and D.-C. Lee, "Feedback Linearization Control of Three-Phase UPS Inverter Systems," *IEEE Trans. Ind. Electron.*, vol. 57, no. 3, pp. 963–968, Mar. 2010.
- [25] X. Bao, F. Zhuo, and B. Liu, "Feedback Linearization Control of Photovoltaic Inverter with LCL Filter," in *7th International Power Electronics and Motion Control Conference (IPEMC)*, 2012, pp. 2197–2201.
- [26] X. Bao, F. Zhuo, Y. Tian, and P. Tan, "Simplified Feedback Linearization Control of Three-Phase Photovoltaic Inverter With an LCL Filter," *IEEE Trans. Power Electron.*, vol. 28, no. 6, pp. 2739–2752, Jun. 2013.
- [27] B. Song, Y. Liu, and C. Fan, "Feedback linearization of the nonlinear model of a small-scale helicopter," *J. Control Theory Appl.*, vol. 8, no. 3, pp. 301–308, Jul. 2010.
- [28] J. S. Lim, C. Park, J. Han, and Y. Il Lee, "Robust Tracking Control of a Three-Phase DC–AC Inverter for UPS Applications," *IEEE Trans. Ind. Electron.*, vol. 61, no. 8, pp. 4142–4151, Aug. 2014.
- [29] Z. Chen and E. Spooner, "Voltage source inverters for high-power, variable-voltage DC power sources," *IEE Proceedings - Generation, Transmission and Distribution*, vol. 148, no. 5, p. 439, 2001.
- [30] S. Yang, Q. Lei, F. Z. Peng, and Z. Qian, "A robust control scheme for grid-connected voltage-source inverters," *IEEE Trans. Ind. Electron.*, vol. 58, no. 1, pp. 202–212, Jan. 2011.
- [31] J. M. Guerrero, L. G. de Vicuna, J. Matas, J. Miret, and M. Castilla, "Output impedance design of parallel-connected UPS inverters," in *2004 IEEE International Symposium on Industrial Electronics*, 2004, vol. 2, pp. 1123–1128 vol. 2.
- [32] Y. W. Li, "Control and resonance damping of voltage-source and current-source converters with LC filters," *IEEE Trans. Ind. Electron.*, vol. 56, no. 5, pp. 1511–1521, May 2009.

- [33] J. He and Y. W. Li, "Analysis, Design, and Implementation of Virtual Impedance for Power Electronics Interfaced Distributed Generation," *IEEE Trans. Ind. Appl.*, vol. 47, no. 6, pp. 2525–2538, 2011.
- [34] J. M. Guerrero, L. Hang, and J. Uceda, "Control of Distributed Uninterruptible Power Supply Systems," *IEEE Transactions on Industrial Electronics*, vol. 55, no. 8, pp. 2845–2859, 2008.
- [35] N. Pogaku, M. Prodanovic, and T. C. Green, "Modeling, Analysis and Testing of Autonomous Operation of an Inverter-Based Microgrid," *IEEE Trans. Power Electron.*, vol. 22, no. 2, pp. 613–625, Mar. 2007.
- [36] Z. W. Z. Wang and L. C. L. Chang, "A DC Voltage Monitoring and Control Method for Three-Phase Grid-Connected Wind Turbine Inverters," *IEEE Trans. Power Electron.*, vol. 23, no. 3, 2008.
- [37] S. Eren, A. Bakhshai, and P. Jain, "A CLF-based nonlinear control technique for a grid-connected voltage source inverter with LCL filter used in renewable energy power conditioning systems," in *4th International Conference on Power Engineering, Energy and Electrical Drives*, 2013, no. May, pp. 840–845.
- [38] F. Z. Peng, H. Akagi, and A. Nabae, "A new approach to harmonic compensation in power systems—a combined system of shunt passive and series active filters," *IEEE Trans. Ind. Appl.*, vol. 26, no. 6, pp. 983–990, 1990.
- [39] O. Vodyakho and C. C. Mi, "Three-Level Inverter-Based Shunt Active Power Filter in Three-Phase Three-Wire and Four-Wire Systems," *IEEE Trans. Power Electron.*, vol. 24, no. 5, pp. 1350–1363, May 2009.
- [40] L. Asiminoaei, P. Rodriguez, F. Blaabjerg, and M. Malinowski, "Reduction of Switching Losses in Active Power Filters With a New Generalized Discontinuous-PWM Strategy," *IEEE Trans. Ind. Electron.*, vol. 55, no. 1, pp. 467–471, Jan. 2008.
- [41] J. He, Y. W. Li, and M. S. Munir, "A Flexible Harmonic Control Approach Through Voltage-Controlled DG–Grid Interfacing Converters," *IEEE Trans. Ind. Electron.*, vol. 59, no. 1, pp. 444–455, Jan. 2012.
- [42] W. Zhao and G. Chen, "Comparison of active and passive damping methods for application in high power active power filter with LCL-filter," in *2009 International Conference on Sustainable Power Generation and Supply*, 2009, pp. 1–6.
- [43] J. Rodríguez, R. M. Kennel, J. R. Espinoza, M. Trincado, C. A. Silva, and C. A. Rojas, "High-performance control strategies for electrical drives: An experimental assessment," *IEEE Trans. Ind. Electron.*, vol. 59, no. 2, pp. 812–820, 2012.

- [44] R. R. Errabelli and P. Mutschler, "Fault-Tolerant Voltage Source Inverter for Permanent Magnet Drives," *IEEE Trans. Power Electron.*, vol. 27, no. 2, pp. 500–508, Feb. 2012.
- [45] J.-F. Stumper, S. Kuehl, and R. Kennel, "Predictive torque control for AC drives: Improvement of parametric robustness using two-degree-of-freedom control," *2013 IEEE Energy Convers. Congr. Expo.*, no. 3, pp. 1170–1175, Sep. 2013.
- [46] B. Tamyurek, "A High-Performance SPWM Controller for Three-Phase UPS Systems Operating Under Highly Nonlinear Loads," *IEEE Trans. Power Electron.*, vol. 28, no. 8, pp. 3689–3701, Aug. 2013.
- [47] G. Escobar, A. A. Valdez, J. Leyva-Ramos, and P. Mattavelli, "Repetitive-Based Controller for a UPS Inverter to Compensate Unbalance and Harmonic Distortion," *IEEE Trans. Ind. Electron.*, vol. 54, no. 1, pp. 504–510, Feb. 2007.
- [48] G. Willmann, D. F. Coutinho, L. F. A. Pereira, and F. B. Libano, "Multiple-Loop H-Infinity Control Design for Uninterruptible Power Supplies," *IEEE Trans. Ind. Electron.*, vol. 54, no. 3, 2007.
- [49] B. Hoff, W. Sulkowski, and P. Sharma, "Cascaded model predictive control of voltage source inverter with active damped LCL filter," *2013 IEEE Energy Convers. Congr. Expo.*, pp. 4119–4125, Sep. 2013.
- [50] N. Mendoza, J. Pardo, M. Mantilla, and J. Petit, "A comparative analysis of Direct Power Control algorithms for three-phase power inverters," in *2013 IEEE Power & Energy Society General Meeting*, 2013, pp. 1–5.
- [51] M. Salehifar, R. S. Arashloo, J. M. Moreno-Equilaz, V. Sala, and L. Romeral, "Fault Detection and Fault Tolerant Operation of a Five Phase PM Motor Drive Using Adaptive Model Identification Approach," *IEEE J. Emerg. Sel. Top. Power Electron.*, vol. 2, no. 2, pp. 212–223, Jun. 2014.
- [52] C. N. M. Ho, V. S. P. Cheung, and H. S. H. Chung, "Constant-frequency hysteresis current control of grid-connected VSI without bandwidth control," in *2009 IEEE Energy Conversion Congress and Exposition*, 2009, pp. 2949–2956.
- [53] Z. Yao and L. Xiao, "Two-Switch Dual-Buck Grid-Connected Inverter With Hysteresis Current Control," *IEEE Trans. Power Electron.*, vol. 27, no. 7, pp. 3310–3318, Jul. 2012.
- [54] J. C. Moreno, J. M. E. Huerta, R. G. Gil, and S. A. Gonzalez, "A Robust Predictive Current Control for Three-Phase Grid-Connected Inverters," *IEEE Trans. Ind. Electron.*, vol. 56, no. 6, pp. 1993–2004, Jun. 2009.

- [55] J. M. Espi, J. Castello, R. García-Gil, G. Garcera, and E. Figueres, "An Adaptive Robust Predictive Current Control for Three-Phase Grid-Connected Inverters," *IEEE Trans. Ind. Electron.*, vol. 58, no. 8, pp. 3537–3546, 2011.
- [56] G. Wenming, H. Shuju, and X. Honghua, "Robust current control design of Voltage Source Converter under unbalanced voltage conditions," in *2013 IEEE PES Asia-Pacific Power and Energy Engineering Conference (APPEEC)*, 2013, pp. 1–5.
- [57] Y. A.-R. I. Mohamed and E. F. El-Saadany, "An Improved Deadbeat Current Control Scheme With a Novel Adaptive Self-Tuning Load Model for a Three-Phase PWM Voltage-Source Inverter," *IEEE Trans. Ind. Electron.*, vol. 54, no. 2, 2007.
- [58] J. F. Stumper, S. Kuehl, and R. Kennel, "Robust deadbeat control for synchronous machines rejecting noise and uncertainties by predictive filtering," in *8th International Conference on Power Electronics - ECCE Asia: "Green World with Power Electronics"*, ICPE 2011-ECCE Asia, 2011, no. 1, pp. 1378–1385.
- [59] D. Mahinda Vilathgamuwa and F. Blaabjerg, "A Robust Control Scheme for Medium-Voltage-Level DVR Implementation," *IEEE Trans. Ind. Electron.*, vol. 54, no. 4, pp. 2249–2261, Aug. 2007.
- [60] J. Rodriguez, M. P. Kazmierkowski, J. R. Espinoza, P. Zanchetta, H. Abu-Rub, H. a Young, and C. a Rojas, "State of the Art of Finite Control Set Model Predictive Control in Power Electronics," *Ind. Informatics, IEEE Trans.*, vol. 9, no. 2, pp. 1003–1016, 2013.
- [61] Z. Chen, A. Luo, H. Wang, Y. Chen, M. Li, and Y. Huang, "Adaptive sliding-mode voltage control for inverter operating in islanded mode in microgrid," *Int. J. Electr. Power Energy Syst.*, vol. 66, pp. 133–143, 2015.
- [62] D. De and V. Ramanarayanan, "A proportional + multiresonant controller for three-phase four-wire high-frequency link inverter," *IEEE Trans. Power Electron.*, vol. 25, no. 4, pp. 899–906, 2010.
- [63] A. Hasanzadeh, C. S. Edrington, B. Maghsoudlou, F. Fleming, and H. Mokhtari, "Multi-loop linear resonant voltage source inverter controller design for distorted loads using the linear quadratic regulator method," *IET Power Electronics*, vol. 5, no. 6. p. 841, 2012.
- [64] L. F. A. Pereira, J. V. Flores, G. Bonan, D. F. Coutinho, and J. M. G. da Silva, "Multiple Resonant Controllers for Uninterruptible Power Supplies—A Systematic Robust Control Design Approach," *IEEE Trans. Ind. Electron.*, vol. 61, no. 3, pp. 1528–1538, 2014.

- [65] M. Jorge Rodrigo, M. J. Luiz Antonio, M. Vinicius Foletto, P. Humberto, R. Cassiano, and O. Ricardo C. L. F., “Robust state feedback current controller applied to converters connected to the grid through LCL filters,” in *Anais do XIX Congresso Brasileiro de Automática, CBA*, 2012, pp. 1039–1046.
- [66] A. Hajizadeh, “Robust Power Control of Microgrid Based on Hybrid Renewable Power Generation Systems,” *Iran. J. Electr. Electron. Eng.*, vol. 9, no. 1, pp. 44–57, 2013.
- [67] J. Liu and K. W. E. Cheng, “ μ -based robust controller design of LCLC resonant inverter for high-frequency power distribution system,” *IET Power Electron.*, vol. 6, no. 4, pp. 652–662, Apr. 2013.
- [68] I. R. Petersen and R. Tempo, “Robust control of uncertain systems: Classical results and recent developments,” *Automatica*, vol. 50, no. 5, pp. 1315–1335, May 2014.
- [69] C.-H. Lien, “Robust Observer-Based Control of Systems With State Perturbations Via LMI Approach,” *IEEE Trans. Automat. Contr.*, vol. 49, no. 8, pp. 1365–1370, Aug. 2004.
- [70] C.-H. Lien, “An efficient method to design robust observer-based control of uncertain linear systems,” *Appl. Math. Comput.*, vol. 158, no. 1, pp. 29–44, Oct. 2004.
- [71] H. Kheloufi, A. Zemouche, F. Bedouhene, and M. Boutayeb, “On LMI conditions to design observer-based controllers for linear systems with parameter uncertainties,” *Automatica*, vol. 49, no. 12, pp. 3700–3704, Dec. 2013.
- [72] J. Wang, L. Huang, and H. Ouyang, “Robust output feedback stabilisation for uncertain systems,” *IEE Proc. - Control Theory Appl.*, vol. 150, no. 5, pp. 477–482, Sep. 2003.
- [73] M. S. Mahmoud and S. A. Hussain, “Improved resilient feedback stabilisation method for uncertain systems,” *IET Control Theory Appl.*, vol. 6, no. 11, p. 1654, 2012.
- [74] S. Wang and Y. Jiang, “Comment on ‘On LMI conditions to design observer-based controllers for linear systems with parameter uncertainties [Automatica 49 (2013) 3700–3704],’” *Automatica*, vol. 50, no. 10, pp. 2732–2733, Oct. 2014.
- [75] A. Yazdani and R. Iravani, *Voltage-Sourced Converters in Power Systems*. Hoboken, NJ, USA: John Wiley & Sons, Inc., 2010.
- [76] M. A. Abido and N. A. Al-Ali, “Multi-Objective Optimal Power Flow Using Differential Evolution,” *Arab. J. Sci. Eng.*, vol. 37, no. 4, pp. 991–1005, 2012.

- [77] J. Lofberg, "YALMIP : a toolbox for modeling and optimization in MATLAB," *2004 IEEE Int. Conf. Robot. Autom. (IEEE Cat. No.04CH37508)*, 2004.
- [78] A. P. S. Mosek, "The MOSEK optimization software," *Online [http://www. mosek.com](http://www.mosek.com)*, vol. 54, 2010.
- [79] M. A. A. Hassan, "Dynamic analysis and control of microgrids," KING FAHD UNIVERSITY OF PETROLEUM AND MINERALS (SAUDI ARABIA), 2011.
- [80] A. H. Syed and M. A. Abido, "Differential Evolution based intelligent control for speed regulation of a PMDC motor," in *21st Mediterranean Conference on Control and Automation*, 2013, pp. 1451–1456.
- [81] A. A. Abou El Ela, M. A. Abido, and S. R. Spea, "Differential evolution algorithm for emission constrained economic power dispatch problem," *Electr. Power Syst. Res.*, vol. 80, no. 10, pp. 1286–1292, 2010.
- [82] M. A. Abido and N. A. Al-Ali, "Multi-Objective Differential Evolution for Optimal Power Flow," *2009 Int. Conf. Power Eng. Energy Electr. Drives*, pp. 101–106, 2009.

Vitae

Name	Syed Asim Hussain
Nationality	Pakistani
Date of Birth	July 4 th , 1984
Email	syedasimhussain@gmail.com
Address	R-83, Block-18, F. B. Area, Karachi 75950, Pakistan
Academic Background	Electrical Engineer

Publications

Journals:

- Asim H. Syed, M. A. Abido, 'A novel strategy to design enhanced performance robust controller for standalone VSI,' (submitted).
- Asim H. Syed, M. A. Abido, 'A New Scheme for Enhanced Performance Robust Control Design for Grid Connected VSI,' (submitted).
- Magdi S. Mahmoud, Asim H. Syed, 'Output Feedback Event-Based Stabilization over Networks with Varying Transmission Delays,' Int. J. of Systems, Control & Communications, pp. 97-120, doi: 10.1504/IJSCC.2014.064203, vol. 6, no. 2/2014.
- M.S. Mahmoud, S.A. Hussain, 'Improved resilient feedback stabilization method for uncertain systems,' IET Control Theory & Application, pp. 1-7, doi: 10.1049/iet-cta.2011.0388, 2012

Conferences:

- Asim H. Syed, M. A. Abido, 'An efficient intelligent robust control design method for grid connected VSI,' 23rd Mediterranean Conference on Control & Automation (MED), 2015, Torremolinos, Spain (accepted).
- Asim H. Syed, M. A. Abido, 'New Robust Controller Design for Voltage Source Inverters in Microgrids,' Proceedings of the 22nd Mediterranean Conference on Control & Automation (MED), 2014, pp. 734-739, doi: 10.1109/MED.2014.6961461, Palermo, Italy, June 2014.
- S. El-Ferik, A.H. Syed, H.M. Omar, M.A. Deriche, 'Anti-Swing Nonlinear Path Tracking Controller for Helicopter Slung Load System,' Proceedings of the 2nd IFAC Workshop on Research, Education & Development of Unmanned Aerial Systems, Compiègne, France, Nov 2013.
- A.H. Syed, M.A. Abido, 'Differential Evolution based intelligent control for speed regulation of a PMDC motor,' Proceedings of the 21st Mediterranean Conference on Control & Automation (MED), 2013, pp. 1451-1456, doi: 10.1109/MED.2013.6608912, Chania, Greece, June 2013.
- U. Gazder, A.H. Syed, 'Traffic Forecasting for King Fahd Causeway Using Artificial Neural Networks,' Proceedings of the 15th International Conference Computer Modelling & Simulation (UKSim), pp. 1-5, doi: 10.1109/UKSim.2013.9, April 2013.
- S. A. Hussain, "Controller design Model to stabilize a UAV helicopter system", Proceedings of the International Conference on Test & Measurement 2010, Phuket, Thailand, Dec, 2010.